Modeling Transient Three-dimensional Temperature Fields in Mountain Permafrost

---

Dissertation
zur
Erlangung der naturwissenschaftlichen Doktorwürde
(Dr. sc. nat.)

vorgelegt der

Mathematisch-naturwissenschaftlichen Fakultät

der

Universität Zürich

von

Jeannette Nötzli

von

Pfäffikon ZH

Promotionskomitee
Prof. Dr. Wilfried Haeberli (Vorsitz)
Dr. Stephan Gruber (Leitung der Dissertation)
Dr. Martin Hölzle

Zürich, 2008

Abstract

Permafrost is a common and important thermal phenomenon in the subsurface of high mountains. Its degradation due to climate change may lead to adverse effects, such as decreasing stability of infrastructure or an increase in rock falls from permafrost slopes. Research intensively deals with assessing and modeling mountain permafrost conditions, since they are not directly visible and extrapolation of measurements is difficult in steep and inhomogeneous terrain. So far, focus of mountain permafrost modeling studies was typically on the thermal conditions of the near-surface.

The objective of this thesis is to describe and analyze mountain permafrost in greater depths (i.e., below the active layer), with a main focus on its three-dimensional distribution and transient effects from past and possible future climate variations. We design a modeling procedure that includes the processes in the atmosphere, at the surface, and in the subsurface, and which is based on the combination of existing approaches. To calculate subsurface temperature fields we determine ground surface temperatures with a distributed surface energy balance model based on climate time series. The result is used as upper boundary condition in a heat conduction scheme. For the simulation of scenarios of future permafrost conditions, we use climate time series constructed from Regional Climate Model results. The modeling procedure is tested in a number of validation steps, namely sensitivity studies and comparisons with field data. Due to the complex situation in nature, we first apply the modeling procedure to a number of idealized test cases with simplified topography, typical surface and subsurface characteristics, and different climate scenarios. The subsequent application to real topography includes the characterization of permafrost conditions at borehole sites and rock fall starting zones.

The results indicate a three-dimensional distribution pattern of mountain permafrost, which is mainly influenced by topography and spatially and temporally variable surface temperatures. Isotherms incline steeply and strong lateral heat fluxes exist, which minimizes the influence of the geothermal heat flux. Transient signals from past climate variations in current permafrost temperatures derive mainly from the last glacial period and the major fluctuations during the past millennium. Temperature depressions in high mountains are smaller than in flat terrain, because multi-lateral warming in steep topography accelerates the pace of a surface temperature signal intruding into the subsurface. Simulations of future conditions point to subsurface temperature fields that substantially deviate from stationary conditions and are characterized by deep-reaching and long-term perturbations, generally

rising temperatures, and an increase in both volume and vertical extent of warm permafrost zones. In the European Alps, near-surface permafrost on steep south-exposed slopes will have disappeared even in the highest peaks within the next two centuries, but substantial permafrost volumes will remain at depth for centuries to millennia.

Three-dimensional and transient modeling tools are important for the comprehensive analysis of mountain permafrost conditions, since in complex mountain topography near-surface conditions do not provide sufficient information. For future research the influence of variable surface and subsurface characteristics on the subsurface thermal field, the interpretation of temperatures recorded in boreholes in mountain topography, and the re-analysis of past rock fall events from permafrost slopes are important topics.

Zusammenfassung

Permafrost ist ein wichtiges und weit verbreitetes thermisches Phänomen im Hochgebirge. Seine Degradation als Folge der Klimaerwärmung kann negative Auswirkungen haben, wie zum Beispiel abnehmende Stabilität von Hochgebirgsinfrastruktur oder eine zunehmende Anzahl von Felsstürzen aus steilen Felswänden. Ein wichtiger Teil der Permafrostforschung beschäftigt sich damit, seine Verbreitung und thermischen Eigenschaften zu modellieren, da diese nicht direkt sichtbar und Extrapolationen im steilen, inhomogenen Gelände schwierig sind. Zu diesem Zweck wurden bis heute in erster Linie die Bedingungen an der Oberfläche und in den obersten Metern erforscht.

Das Ziel der vorliegenden Arbeit ist es, Gebirgspermafrost in größerer Tiefe (unterhalb der Auftauschicht) zu analysieren und zu modellieren. Dabei stehen die dreidimensionale Verteilung und mögliche transiente Effekte von vergangenen und möglichen zukünftigen Klimaänderungen im Zentrum. Es wurde ein Modellierverfahren entwickelt, das die Prozesse in der Atmosphäre, an der Oberfläche sowie im Untergrund betrachtet und auf der Kombination von bestehenden Modellen basiert. Zur Berechnung von Temperaturfeldern im Innern steiler Berge werden basierend auf Klimazeitreihen mit einem Energiebilanzmodell Oberflächentemperaturen bestimmt, die anschließend in einem Wärmeleitungsschema als obere Randbedingung eingesetzt werden. Für die Simulation von zukünftigen Szenarien werden Klimazeitreihen aus den Resultaten Regionaler Klimamodelle (RCM) erstellt. Das Modellierverfahren wurde in verschiedenen Validierungsschritten getestet, darunter Sensitivitätsstudien und Vergleiche mit Messdaten. Aufgrund der komplexen Verhältnisse in der Natur wurden verschiedene numerische Experimente mit idealisierter Topographie, typischen Eigenschaften von Oberfläche und Untergrund, sowie verschiedenen Klimaszenarien durchgeführt. In einem zweiten Schritt wird das Modellierverfahren auf reale Topographien in Fallstudien angewandt, zum Beispiel zur Untersuchung der thermischen Bedingungen an Bohrlochstationen oder Anrisszonen von Felsstürzen.

Die Resultate zeigen ein dreidimensionales Verbreitungsmuster von Permafrost im Hochgebirge, das vor allem von der Topographie und räumlich und zeitlich variierenden Oberflächentemperaturen gesteuert wird. Die Isothermen im Untergrund sind steil und in den gipfelnahen Bereichen fast vertikal. Es sind starke laterale Wärmeflüsse vorhanden, was den Einfluss des geothermalen Wärmeflusses minimiert. In den heutigen Permafrosttemperaturen der Alpen lassen sich transiente Effekte nachweisen, die in erster Linie von der letzten Eiszeit und den größeren Schwankungen der letzten tausend Jahre ausgehen. Die Tem-

peraturdepressionen sind im Hochgebirge kleiner als in flachen Regionen, weil die steile Topographie das Eindringen einer Temperaturänderung von der Oberfläche in den Untergrund beschleunigt. Simulationen von zukünftigen Szenarien deuten auf Temperaturfelder, die stark vom Gleichgewichtszustand abweichen und langfristig und tief greifend gestört sind. Generell erwärmt sich der Untergrund, und die warmen Permafrostzonen nehmen an Volumen und vertikaler Ausdehnung zu. Die Simulationen deuten darauf, dass der Permafrost in den Alpen in den oberflächennahen Schichten von süd- und ostexponierten Gebirgsflanken in den nächsten 200 Jahren verschwinden wird. In der Tiefe bleiben Permafrostvorkommen dagegen noch während Jahrhunderten bis Jahrtausenden bestehen.

Dreidimensionale und zeitabhängige Modellierverfahren sind wichtig, um die Verteilung und Bedingungen von Gebirgspermafrost umfassend beurteilen zu können, da in der steilen Topographie von Hochgebirgen die Betrachtung von oberflächennahen Bedingungen nicht ausreicht. In Zukunft sind der Einfluss von unterschiedlichen Oberflächen- und Untergrundeigenschaften auf die thermischen Bedingungen im Untergrund, die Interpretation von gemessenen Temperaturprofilen in Bohrlöchern im Gebirge und die Re-analyse von Felssturzanrisszonen im Permafrost wichtige Forschungsthemen.

Table of Contents

Abstract i

Zusammenfassung iii

Table of Figures vii

List of Abbreviations ix

Part I – Synopsis 1

1 Introduction 3

1.1 Motivation and Problem Statement 3
1.2 Objective and Research Questions 4
1.3 Approach 5
1.4 Organization of Thesis 6

2 Scientific Background 9

2.1 Mountain Permafrost 9
2.1.1 Definition 9
2.1.2 Relevance 10
2.1.3 Characteristics and Governing Factors 13
2.1.4 Thermal Conditions at the Surface 15
2.1.5 Subsurface Thermal Regime 15
2.1.6 Response to Climate Change and Slope Stability 18
2.2 Modeling Mountain Permafrost 21
2.2.1 Empirical and Statistical Models 21
2.2.2 Surface Energy Balance 22
2.2.3 Subsurface Heat Transport 22
2.2.4 Driving Meteo Data 23

3 Modeling Procedure 25

3.1 Overview of the Modeling Procedure 25
3.2 Atmosphere Surface Interface: RCM – Distributed Surface Energy Balance 27
3.2.1 Construction of RCM-based Climate Time Series 28
3.2.2 The Energy Balance Model TEBAL 29
3.3 Surface Subsurface Interface: Surface Energy Balance – Subsurface Heat Transport 29
3.3.1 TEBAL and Upper Boundary Condition 29
3.3.2 Subsurface Heat Conduction 29
3.4 Validation of the Modeling Approach 31
3.4.1 Energy Balance Model for Steep Topography 31
3.4.2 Subsurface Temperatures at Borehole Locations 32
3.4.3 Sensitivity Studies 33

4 Modeled Temperature Fields in Mountain Permafrost....35
4.1 Equilibrium Temperature Fields....36
4.2 Transient Temperature Fields....37
4.2.1 Effects of Past Climatic Conditions....38
4.2.2 Effects of Future Warming....38
4.2.3 Effects of Topography....40
4.3 Borehole Sites....41
4.3.1 Zugspitze: Planning of a Permafrost Borehole....41
4.3.2 Schilthorn: Current and Future Subsurface Temperatures....44
4.4 Case Study Matterhorn....45

5 General Discussion....49
5.1 Modeling Approach....49
5.2 Interpretation of Results....51
5.3 Implications for Permafrost Research....52
5.3.1 Mapping of Mountain Permafrost....52
5.3.2 Interpretation of Borehole Profiles....52
5.3.3 Slope Stability....53

6 Summary, Outlook, and Conclusion....55
6.1 Summary of Progress....55
6.2 Major Results....56
6.3 Future Research....58
6.4 Conclusion....60

Bibliography....61

Part II – Publications....69

I Three-dimensional Distribution and Evolution of Permafrost Temperatures in Idealized High-mountain Topography....71

II Ground Surface Temperature Scenarios for Complex High-Mountain Topographies Based on Regional Climate Model Results....99

III Transient Thermal Effects in Alpine Permafrost....119

IV Comparison of Simulated 2D Temperature Profiles with Time-Lapse Electrical Resistivity Data at the Schilthorn Crest, Switzerland....145

Appendix....143

Personal Bibliography....155

Curriculum Vitae....159

Acknowledgements....161

Table of Figures

Figure 1.1. Schematic structure of the thesis and its two main parts *Synopsis* and *Publications*. 7

Figure 2.1. Mountain permafrost is relevant for (i) construction practices, (ii) natural hazards, (iii) alpine landscape evolution, and (iv) climate observation.. 11

Figure 2.2. Energy fluxes at and below the surface of a steep mountain and schematic evolution of a warming permafrost body inside the mountain. 14

Figure 2.3. The thermal memory of the subsurface for changes in GST. 17

Figure 2.4. Schematic evolution of a permafrost temperature profile after a rise in surface temperature from T_0 to T_1.. 19

Figure 2.5. Massive ice visible in the starting zone of a rock fall on the Matterhorn south face, immediately after the event in July 2003 20

Figure 2.6. FE mesh of a simplified ridge cross section as used for modeling in this thesis 23

Figure 3.1. The modeling approach designed in the scope of this thesis combines a surface energy balance model with three-dimensional subsurface heat conduction.. 26

Figure 3.2. Unfrozen water content curves for different freezing intervals 31

Figure 4.1. The most prevalent features of mountain topography are ridges and peaks. 35

Figure 4.2. The equilibrium temperature field of a cross sections through a simplified mountain ridge with 60° steep slopes and corresponding distribution of heat fluxes 36

Figure 4.3. Equilibrium temperature fields of two cross sections through a simplified mountain peak. 37

Figure 4.4. The evolution of different isotherms as caused by linearly increasing surface temperatures is displayed together with the schematic evolution of an equilibrium permafrost body 40

Figure 4.5. Percentage of a temperature signal at the surface that has penetrated to depth for a one-, two-, and three-dimensional situation after 100 and 200 years 40

Figure 4.6. Drilling on the Zugspitze in August 2007 and completed western borehole 42

Figure 4.7. North-south cross section through the modeled temperature field of the Zugspitze crest at the borehole location.. 43

Figure 4.8. T(z) profiles measured in the western borehole in the Zugspitze crest compared to profiles extracted from modeled temperature fields. 43

Figure 4.9. Modeled temperature distribution in the Schilthorn crest, Switzerland for today and in 100 years. 45

Figure 4.10. North-south and east-west cross section through the temperature field of the Matterhorn. 46

Figure 4.11. Slices through the temperature field at the rock fall starting zone on the Hörnligrat 47

List of Abbreviations

BTS	Bottom Temperature of the Snow Cover
DEM	Digital Elevation Model
ERT	Electrical Resistivity Tomography
FD / FE	Finite Difference / Finite Element
FRACTure	Flow, Rock and Coupled Temperature Effects
GCM	General Circulation Model (also: Global Climate Model)
GCOS	Global Climate Observation System
GST	Ground Surface Temperature
GTN-P	Global Terrestrial Network for Permafrost
IPCC	Intergovernmental Panel on Climate Change
LfU	Bayerisches Landesamt für Umwelt (Bavarian State Ministry for the Environment)
LIA	Little Ice Age
LTF	Load Time Function
MGST	Mean Ground Surface Temperature
MW	Medieval Warmth
PACE	Permafrost and Climate in Europe
PERMOS	Permafrost Monitoring Switzerland
RCM	Regional Climate Model
TEBAL	Topography and Energy Balance
TTOP	Temperature at the Top of Permafrost
UBC	Upper Boundary Condition
y BP	Years Before Present (conventional ^{14}C, uncalibrated)
ZAA	Zero Annual Amplitude

Part I – Synopsis

Chapter 1

Introduction

Permafrost is a common and important thermal phenomenon in high mountain areas and its degradation following climate change may lead to adverse effects. Contrary to glaciers and their changes, it is invisible to us because it is purely defined based on ground temperatures. A major part of mountain permafrost research therefore deals with assessing and modeling its distribution and thermal conditions. Despite vast research on its near-surface characteristics, the distribution and thermal conditions of mountain permafrost below the uppermost meters are barely known at present. The objective of this thesis is to investigate mountain permafrost at greater depth and to explore and describe its three-dimensional nature as well as its evolution over time. For this purpose, a procedure to model subsurface temperatures in steep mountains is designed, which is based on the combination of existing approaches. The modeling procedure will be applied for numerical experimentation as well as for selected case studies.

1.1 Motivation and Problem Statement

In alpine environments such as the European Alps, permafrost is a widespread thermal subsurface phenomenon. As such, permafrost is largely controlled by climatic conditions and reacts sensitively to their changes. In the past decades, alpine permafrost in Europe has warmed by 0.5–1.0 °C in the upper tens of meters (Harris et al. 2003, PERMOS 2007, Vonder Mühll 2001). This trend is expected to continue or even accelerate based on climate simulations (IPCC 2007). Moreover, atmospheric warming is generally more pronounced for high elevation sites than for global or hemispherical average (Beniston et al. 1997).

Warming permafrost can change the stability of perennially frozen mountain slopes consisting of bedrock or non-consolidated sediments (Davies et al. 2001, Haeberli 1992a, Haeberli et al. 1997) and lead to increasing problems with human infrastructure (Gruber

and Haeberli 2007, Haeberli 1992a, Harris et al. 2001a, Romanovsky et al. 2007) or rock fall (Deline 2001, Noetzli et al. 2003). The exceptional rock fall activity in the Alps (Keller 2003) in the hot summer of 2003 (Schaer et al. 2004), for example, has pointed to the fast and serious response of perennially frozen mountain slopes to increasing air temperatures. The rock fall events of 2003 were presumably connected to enlarged active layer thickness (Gruber et al. 2004a) and included only smaller volumes of rock (i.e., thousands of cubic meters). In terms of permafrost thickness, however, which ranges up to several hundreds of meters in the Alps (Haeberli et al. 1993), this is only scratching the surface. A temperature rise over long time periods of centuries, such as the recent warming since the end of the 19th century (e.g., Luterbacher et al. 2004) or projected future warming (IPCC 2007), will affect temperatures at great depth. Corresponding deep-seated instabilities may include large volumes of material (Haeberli et al. 1997).

In view of growing human activity in cold mountain areas (e.g., tourism, telecommunication networks, hydropower production) sound knowledge concerning the occurrence and the thermal conditions of permafrost, as well as their evolution over time is essential. It can help to reduce installation and maintenance costs of infrastructure and to increase the safety of people in such areas. Yet, so far mountain permafrost has been studied intensively for the near-surface layer. Its three-dimensional distribution and thermal conditions at depth inside mountains are barely understood. This is mainly due to the following reasons: 1) The extreme topography of high mountains leads to spatially highly variable surface conditions and distortions of heat flow density in the subsurface. As a result, complex three-dimensional patterns of temperature distribution exist (Kohl et al. 2001); 2) Temperature profiles measured in boreholes in mountains cannot be used for an extrapolation in space or time in a simple and straightforward way (Gruber et al. 2004c). Their interpretation needs correction in order to separate topographical effects and climate signals; 3) Existing experimental models for the assessment of mountain permafrost distribution typically focus on near-surface temperatures (Gruber 2005, Lehning et al. 2002, Stocker-Mittaz 2002) and consider neither the thermal conditions at greater depth nor a three-dimensional heat flow in the underground. Corresponding modeling tools, however, are essential when addressing the previous two aspects.

1.2 Objective and Research Questions

The main goal of this thesis is the analysis of the three-dimensional character of permafrost in mountains, particularly the influence steep topography has on its distribution, thermal conditions, and evolution over time. The main research question addressed is the following:

- *What is the thermal state of permafrost inside steep mountains today and in the future?*

This question can be further split into the following sub-questions:

- *How does steep topography influence the distribution of subsurface temperatures?*

The basis for the understanding of the three-dimensional character of mountain permafrost is the assessment of the influence of topography (e.g., ridges, peaks, or spurs) on the pattern of permafrost distribution. This is also a prerequisite for the differentiation of topographical and climate-related effects in borehole temperature profiles.

- *How big is the influence of past climate variations on present-day mountain permafrost conditions?*

For a realistic assessment of current thermal conditions at depth, transient effects caused by past temperature variations have to be taken into account. For this purpose, we need to identify past climate periods that have a significant effect on current subsurface temperatures in high mountains and we need to quantify this effect.

- *How will permafrost in high mountains react to projected future changes in atmospheric conditions?*

Because surface temperatures largely influence subsurface temperatures, we are first interested in the possible range of surface temperature changes, which are then further propagated into the subsurface. Steep topography modifies the energy balance at the surface and changing atmospheric conditions may affect locations of varying topographic settings differently. Based on estimated changes in surface temperatures, we estimate the resulting changes in the subsurface temperature field, and analyze what time and depth scales are involved in mountain permafrost degradation.

The focus of this thesis is on permafrost conditions below steep topography and on their long-term evolution. That is, the near-surface layer (i.e., the uppermost meters) and short term variations (i.e., seasonal, diurnal), as well as material other than bedrock are not specifically considered.

1.3 Approach

The simulation of transient ground temperatures in mountain permafrost has to account for the processes at the interface atmosphere and surface as well as for those in the subsurface. That is, it requires a model for the energy balance at the surface and heat transfer in the underground (Gruber et al. 2004c). For simulations of future climate conditions, Regional

Climate Models (RCMs) are currently most suitable (Salzmann et al. 2007a). Well-planned coupling of such models can provide the tool needed to address the above stated research questions, and serve as a basis for numerical experimentation with idealized test cases. Even if single model components have been tested, their combination and application to research areas require validation to gain confidence in the results (Rykiel 1996). Here, we validate the modeling procedure by sensitivity studies and comparison with field data.

Owing to the complex and highly variable conditions found in nature, the application of the modeling procedure first concentrates on numerical experimentation with simplified topography, typical values of surface and subsurface conditions, and different warming scenarios. In this way, we investigate general questions related to mountain permafrost and its degradation, for example, the temperature regime inside east-west or north-south trending ridges, the reaction of the permafrost base at depths of tens to hundreds of meters to warming under such topographies, or the effect of thermo-physical properties and subsurface ice on the pace of permafrost degradation. Subsequent results are easier to interpret and a step towards assessing natural and more complex situations. Finally, the application of the modeling procedure to real topography includes characterization of permafrost conditions at borehole sites and rock fall starting zones.

As a brief summary, the research approach in this thesis concentrates on 1) the development of a modeling procedure by combining RCMs, surface energy balance in steep topography, and three-dimensional subsurface heat transfer, 2) the validation of the modeling procedure, 3) the analysis of topographical effects on permafrost and its degradation by numerical experimentation, and 4) the transfer of experimental results to real situations.

1.4 Organization of Thesis

This thesis is divided into two complementary parts (Figure 1.1).

Part I provides a synopsis of the research conducted in the scope of this thesis, along with some unpublished results, and aims at putting it into a larger scientific context. It consists of six chapters: Following this introduction, the second chapter creates the link between previous research and our work by reviewing the main characteristics of mountain permafrost, its reaction to climate change, and existing approaches to model these. Chapter three is concerned with the modeling procedure, which combines three different types of models with two main interfaces. The chapter includes the combination of RCM output with the energy balance at the surface, the subsequent heat transfer from the surface into the underground, and the validation steps taken. In the fourth chapter, we present the resulting sub-

surface temperature fields for both, idealized and real topographies. Chapter five critically discusses the work presented, including the possibilities and limitations of the chosen modeling procedure and the interpretation and implications of the research results. Finally, the Chapter six concludes *Part I* of the thesis with a progress summary and the presentation of the major results as related to the research questions raised in Chapter 1. The chapter also provides an outlook on possible future research based on application and enhancement of the modeling procedure, as well as the conclusion.

Part II contains full versions of the four journal papers, which comprise the main scientific work of this thesis. Additionally, for each of the papers the research conducted is briefly summarized and the major findings are listed.

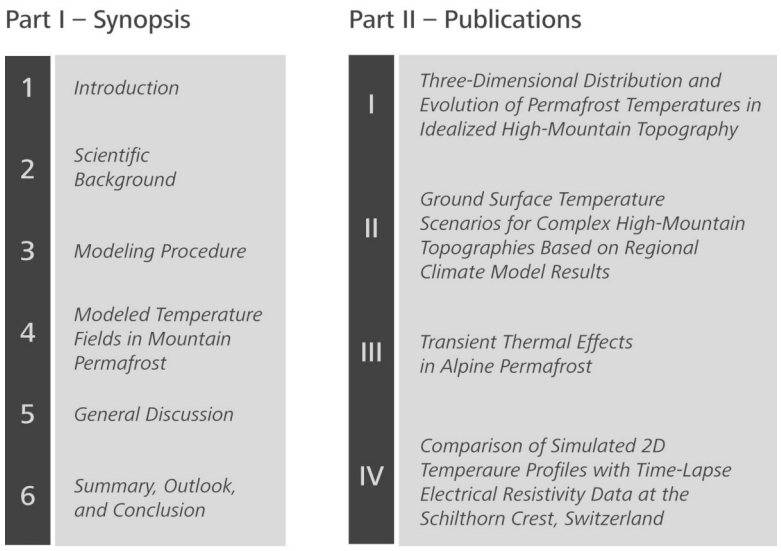

Figure 1.1. Schematic structure of the thesis and its two main parts *Synopsis* and *Publications*.

Chapter 2

Scientific Background

In this chapter, the scientific background of the research conducted in this thesis is outlined. Firstly, we set the context by discussing the main characteristics of mountain permafrost, its relevance, governing factors, and reaction to climate change. In the second part, we describe existing approaches to approximate or simulate the processes that govern the ground thermal regime in steep mountains.

2.1 Mountain Permafrost

2.1.1 Definition

Permafrost, or perennially frozen ground, is defined as material of the lithosphere that remains at or below 0 °C throughout the year (Brown and Péwé 1973, Washburn 1979). That is, permafrost is defined purely on the basis of temperature irrespective of the presence or absence of ice. The difference to non-frozen ground and the practical relevance of permafrost, however, comes with the ice contained in the underground (e.g., pore ice, ice-filled fractures, ice lenses), which can significantly change its characteristics (geotechnical properties, water permeability, etc.). *Mountain Permafrost*, or alpine permafrost, simply is permafrost in high-mountain areas and is characterized by the influence of mountain topography on its properties. For high mountains, numerous definitions exist, which generally relate to elevation, steep slopes, rocky terrain, and the presence of snow and ice (e.g., Barsch and Caine 1984). A detailed overview is given by Roer (2007).

The uppermost ground layer in permafrost typically thaws during summer due to seasonal variations in ground surface temperatures. The actual *Permafrost Body* is located below this so-called *Active Layer* and reaches from the *Permafrost Table* down to the *Permafrost Base* (a detailed description of permafrost-related terms can be found in, e.g., French 2007, Williams and Smith 1989). The *Permafrost Thickness* is the distance between the per-

mafrost table and the permafrost base. In mountain areas, permafrost thickness is not clearly defined, since permafrost extent in the underground is difficult to describe by only using the vertical dimension. Here, we consider permafrost thickness perpendicular to the surface.

Early permafrost research was conducted in high-latitude lowlands, mainly motivated by the expansion of infrastructure and with considerable financial interest involved (e.g., mining, pipeline construction, petroleum exploration). A wealth of basic and engineering knowledge is therefore available from polar and arctic permafrost studies (see French 2007). Only in the 1970s did geomorphologists begin systematic studies on mountain permafrost in Europe, mainly provoked by the distinct landform of rock glaciers (Barsch 1969, 1971, Haeberli 1973, 1975). Since then, mountain permafrost has become a research discipline of its own, dealing with its specific characteristics and problems, which for the most part are related to steep topography and high spatial variability. This complexity is the major challenge for the interpretation of observations and measurements, as well as for the design, parameterization, and validation of models.

In recent years, mountain permafrost studies focused more and more on steep rock slopes. On the one hand this was motivated by an increase in rock fall observations from permafrost areas (e.g., Deline 2001, Dramis et al. 1995, Keller 2003, Noetzli et al. 2003, Ravanel 2006) and rising scientific as well as public awareness of the relation of permafrost degradation and slope stability (Davies et al. 2001, Gruber and Haeberli 2007, Haeberli et al. 1997, Harris et al. 2001a). On the other hand, corresponding measurement strategies and modeling tools have been developed (Gruber et al. 2004b, Gruber et al. 2003, Wegmann 1998), which made permafrost research in steep bedrock slopes possible in the first place. So far, studies primarily concentrate on the European Alps. Here, considerable infrastructure exists, which facilitates access and, at the same time, increases the vulnerability of the area. However, phenomena and problems related to mountain permafrost are similar for all mountain regions and start to be recognized in other areas, such as the Canadian Rocky Mountains (Gertseema et al. 2006, Lewkowicz and Ednie 2004), the Southern Alps in New Zealand (Allen et al. 2008), Iceland (Etzelmüller et al. 2007), or the Kazbek massif in the eastern Caucasus (Haeberli et al. 2004, Huggel et al. 2005).

2.1.2 Relevance

The relevance of mountain permafrost relates to four main fields (Figure 2.1): 1) Construction and maintenance of infrastructure, 2) natural hazards, 3) climate observation, and 4) forming of the alpine landscape. While the latter two fields are mainly scientifically investigated, the first two also relate to practical problems and economical interests. In this section, we briefly summarize the four fields.

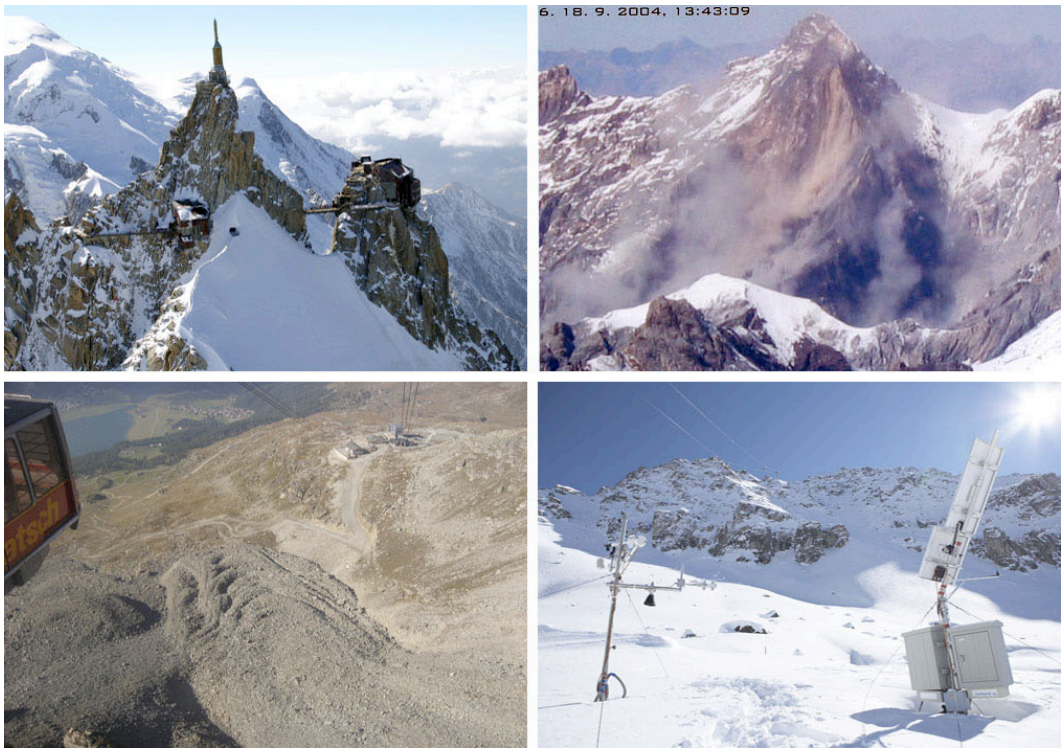

Figure 2.1. Mountain permafrost is relevant for (i) construction practices, (ii) natural hazards, (iii) alpine landscape evolution, and (iv) climate observation. The photos show the top station on the Aiguille du Midi (ca. 3,700 m a.s.l.; photo: S. Gruber), the rock fall event at Punta Thurwieser on September 18, 2004 (ca. 3,500 m a.s.l.; photo: Rozman et al. (2004)), the rock glacier Murtèl near Corvatsch (ca. 2,500 m a.s.l.), and the measurement station on the rock glacier Murtèl (photo: G. Nitsch).

1) Construction in Permafrost Environment

Engineering of infrastructure in alpine environments (mountain huts, cable car foundations, snow supporting structures, etc.) requires special adaptation of construction practices to the frozen ground (e.g., Haeberli 1992a, Keusen and Haeberli 1983, Phillips 2000). Possible problems include unstable foundations due to permafrost creep or degradation (induced by infrastructure through thaw settlement or changed snow accumulation patterns, or by climate change), or freezing water in pipes for water supply or waste water.

2) Natural Hazards

Although the geological and geometrical conditions are the decisive factors controlling slope stability, warming or thawing of ice in cracks and crevices of rock can lead to slope instabilities and may provoke failure (for more details on possible mechanisms see Section 2.1.6).

Similarly, permafrost bonds unconsolidated sediments in steep debris slopes. Thawing of previously frozen material can lead to a loss of cohesion, an increase in pore-water

pressure in originally ice-rich material, and reduced resistance to erosion by running water (Haeberli and Burn 2002). As a result, frequency and magnitude of debris flows may increase. In addition, slope failure can be caused by thaw consolidation in ice-supersaturated fine-grained material (Harris et al. 2001c).

3) Climate Information

Temperatures in the subsurface record the surface temperature history of the past. Unlike air or surface temperatures, which can change within very short time scales (i.e., minutes or hours), subsurface temperatures represent a systematic running mean of the variations at the ground surface. This information is used to invert past climate conditions from temperature profiles measured in deep boreholes (e.g., Huang et al. 2000, Isaksen et al. 2000, Lachenbruch and Marshall 1986, Pollak and Huang 2000, a list of early works on this subject is provided by Wang 1992). In mountain permafrost, the interpretation of borehole temperature profiles is a complicated task, because topography affects subsurface heat fluxes, which need to be determined exactly in order not to misinterpret three-dimensional effects as climate signals (Gruber et al. 2004c, Kohl et al. 2001).

The monitoring of current and future thermal conditions of mountain permafrost relies mainly on temperature data from boreholes, as only they provide direct permafrost measurements. The most prominent scientific monitoring networks for mountain permafrost are the European PACE transect (Harris et al. 2001b) and PERMOS in Switzerland (PERMOS 2007, Vonder Muehll et al. 2008). These networks are integrated into the Global Terrestrial Network for Permafrost (GTN-P) within the Global Climate Observation System (GCOS) (WMO 1997).

4) Forming of the Alpine Landscape

Many distinct geomorphological features of the alpine landscape are bound to the existence of permafrost. For example, rock glaciers evolve from creep of ice-supersaturated permanently frozen debris (Barsch 1971, Haeberli et al. 2006). After permafrost has disappeared within a rock glacier, it remains as a relict form, which, in turn, can be used for reconstruction of paleoclimatic conditions (e.g., Frauenfelder et al. 2001). Hanging glaciers and ice faces, although not considered permafrost themselves, indicate the occurrence of permafrost at their base, where bedrock temperatures cannot exceed 0 °C. The reverse conclusion, however, is not valid. The absence of hanging glaciers or rock glaciers does not necessarily indicate the absence of permafrost. Further, alteration of sediment transfer systems (i.e., rate and intensity) and mass movements form the alpine landscape.

2.1.3 Characteristics and Governing Factors

In Switzerland, approximately 5% of the area is within permafrost (Keller et al. 1998), which corresponds to roughly twice the area covered by glaciers in the year 2000 (Paul 2003). Permafrost thickness in the European Alps ranges from a few meters to several hundreds of meters (e.g., Haeberli 1992b, Luethi and Funk 2001). Detailed knowledge of permafrost thickness, and correspondingly of its actual extent inside mountains, is hardly available for mountain permafrost and restricted to the immediate surroundings of borehole locations in permafrost of smaller thickness (i.e., a few decameters). Maximum active layer thickness in the Alps ranges from a few meters for ice rich material (e.g., rock glaciers) to more than 10 m in bedrock slopes (PERMOS 2007).

As a very first approximation, in the European Alps permafrost can be expected in areas without closed vegetation cover above ca. 2,500 m a.s.l. (Haeberli 1975, Hoelzle et al. 1993). Permafrost distribution in mountains, however, is patchy (Etzelmüller et al. 2001, Hoelzle et al. 2001). It is governed by a number of factors ranging from continental to local scale (Gruber 2005, Hoelzle et al. 2001): On a *continental scale* (e.g., the Alpine region), climatic conditions influence the distribution of permafrost (e.g., the first approximation stated above relates to this scale). On a *regional scale* (e.g., the Monte Rosa massif) topography modifies the distribution pattern significantly. On a *local scale* (e.g., the borehole location on the Stockhorn) controlling factors are surface and subsurface properties, as well as snow distribution. This three-step scheme relates to the main energy fluxes that determine the subsurface thermal field (Figure 2.2) with topography and surface energy balance acting as the interface between atmosphere and permafrost in the underground. The major energy fluxes are directed from the atmosphere to the surface, and from there into the subsurface. A smaller energy flux exists from the interior of the Earth, as well as in the opposite direction. The latter is of relatively minor importance for this study and is therefore not considered.

Bedrock builds the most clearly defined surface and, in steeps slopes with no thick snow or debris cover, interacts unfiltered and immediately with the atmosphere (Gruber et al. 2004b). For less steep terrain, this straightforward system can be complicated by a number of factors, such as snow pack or various surface cover types. A snow cover has two main effects: 1) increase of the surface albedo, and 2) thermal insulation of the ground from the atmosphere. Depending on the thickness, duration, and timing of the snow pack, the ground can be either cooled or warmed compared to atmospheric temperatures (e.g., Hoelzle et al. 2003, Keller and Gubler 1993, Zhang et al. 2001). Alpine topography influences the distribution of the snow cover through the surface energy balance, wind drift, and avalanche formation. Surface cover types and materials exist in a wide range in high

mountain areas. For example, layers of coarse blocks exert a cooling influence on the subsurface through complex interactions of conduction through snow and advection, convection, and effects of latent heat in the voids (e.g., Gruber and Hoelzle 2008, Hanson and Hoelzle 2004, Harris and Pedersen 1998, Hoelzle and Gruber 2008, Humlum 1997), and, thus, favor permafrost conditions.

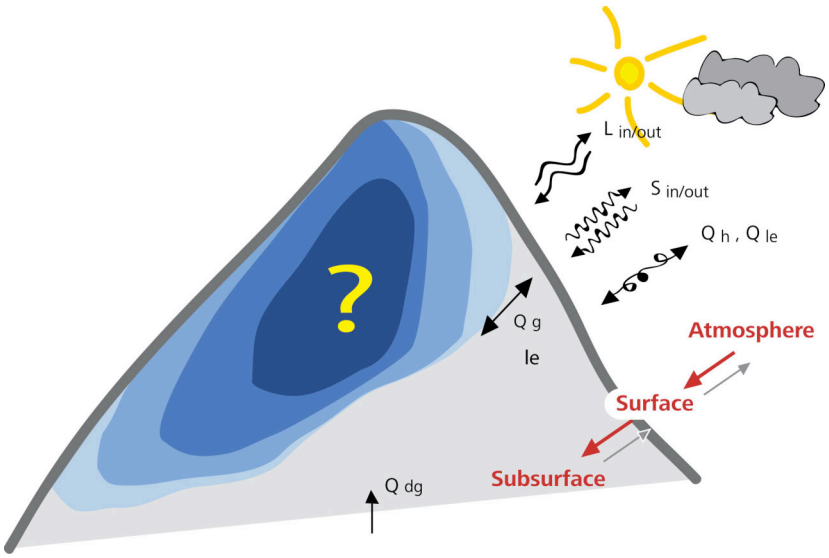

Figure 2.2. Energy fluxes at and below the surface of a steep mountain. The main energy fluxes are directed from the atmosphere to the surface, and from there into the subsurface. The schematic evolution of a warming permafrost body inside the mountain is depicted in blue colors.

In terms of subsurface material properties, primarily the thermo-physical properties (thermal conductivity, heat capacity), porosity (for bedrock this relates to the maximum ice/water content of the underground), and freezing characteristics are important for the thermal regime. These factors dominate conductive heat transport and phase change processes (cf. Section 2.1.4). In mountain permafrost, ice content is generally much lower than in high-latitude permafrost soils, but can vary significantly between sites and layers: debris slopes and rock glaciers can have high ice contents or even be ice super-saturated (e.g., the Murtèl rock glacier, Swiss Alps) (Haeberli et al. 2006). Finer debris material (e.g., on the Schilthorn, Swiss Alps) or bedrock (e.g., on the Stockhorn, Swiss Alps), in contrast, contains smaller amounts of ice. Often, a two-layer system is observed: the uppermost weathered layer has a considerable ice content, whereas the lower part of the subsurface does not contain significant amounts of ice (e.g., Schilthorn, Hauck 2001, Noetzli et al. 2008). Contrary to the implication of the name, a certain quantity of unfrozen water is usually pre-

sent in permafrost, since transition of ice to water occurs over a range of temperatures depending on the freezing characteristics of the material (see Section 2.1.5).

2.1.4 Thermal Conditions at the Surface

The ground surface temperatures (GST) result from the surface energy balance, which consists of the sum of all energy fluxes. According to the principle of energy conservation, this sum must balance at all times (Williams and Smith 1989):

$$Q^* + Q_H + Q_{LE} + Q_G + Q_M = 0 \text{ , where} \quad (1)$$

$$Q^* = S_{in} + S_{out} + L_{in} + L_{out} \quad (2)$$

with Q^* = radiation balance, S_{in} = incoming shortwave radiation, S_{out} = reflected shortwave radiation, L_{in} = incoming longwave radiation, L_{out} = outgoing longwave radiation, Q_H = sensible heat flux, Q_{LE} = latent heat flux, Q_G = ground heat flux, and Q_M = latent heat.

Mountain topography causes high spatial variability of GST. Air temperature changes with elevation and influences the sensible heat flux and incoming long wave radiation at the surface. The elevation gradient of air temperature for the Alps is around –0.6 °C /100 m. Aspect, slope, and horizon modify the amount of direct solar radiation received. For climates with a high proportion of incoming solar radiation (e.g., the European Alps) this can cause GST differences of about 7 °C between north- and south-exposed slopes having otherwise identical conditions (cf. *Publication I*, Noetzli et al. 2007b). This is in the same dimension as a change in elevation of about 1,000 m (cf. Haeberli 1975). The GST difference between steep east- and west-facing slopes is about 2.5 °C and is mainly caused by convective clouding due to diurnal fluctuations in cloud cover (cf. *Publication I*, Noetzli et al. 2007b). Comprehensive and detailed descriptions of the components of the surface energy balance in mountain terrain are given by Oke (1987), Plüss (1997), Hoelzle (1994), and Stocker-Mittaz (2002).

2.1.5 Subsurface Thermal Regime

The previous section points to the high spatial variability of surface temperatures in mountain areas, which is the major factor influencing the subsurface temperature pattern. In addition, the deep-seated upward heat flow from the Earth's interior, which varies only over much longer time scales than climatic conditions and is therefore considered as constant in this study, variations of the GST in the past, subsurface material properties, and topography modify the subsurface thermal field.

Conduction is the dominating heat transport process in the subsurface in bedrock permafrost. Heat conduction is the transfer of thermal energy through matter, from a region of higher temperature to a region of lower temperature. The three-dimensional transient temperature field in an isotropic and homogeneous medium is described by the heat conduction equation (Carslaw and Jaeger 1959):

$$\frac{\delta T}{\delta t} = \kappa \nabla^2 T, \text{ with} \tag{3}$$

$$T = T(t,x,y,z), \quad \nabla^2 T = \left(\frac{\delta^2 T}{\delta x^2}, \frac{\delta^2 T}{\delta y^2}, \frac{\delta^2 T}{\delta z^2}\right)$$

where T (K) is the temperature at time t (s), and κ (m^2 s^{-1}) is the thermal diffusivity. The thermal diffusivity is defined as the ratio of thermal conductivity λ (W m^{-1} K^{-1}) to volumetric heat capacity ρc_p (J m^{-3} K^{-1}). Thermal conductivity describes the rate of heat transfer, whereas heat capacity relates to the temperature change experienced by the ground due to a given energy input, but without undergoing phase change. Thermal diffusivity, hence, describes the pace at which a signal propagates into the subsurface. For Alpine bedrock, thermal conductivity ranges from about 1.5 and 4.5 W m^{-1} K^{-1} (Cermák and Rybach 1982), with most values between 2.5 and 3.0 W m^{-1} K^{-1} (Gruber et al. 2004b, Kohl 1999, Wegmann et al. 1998). Heat capacity typically ranges from 1.8 to 2.5 10^6 J m^{-3} K^{-1} (Cermák and Rybach 1982).

The thermal diffusivity of rock is relatively low causing changes in GST to propagate slowly into the subsurface, which leads to a high thermal inertia of the system. The deeper the temperatures are measured, the further back in time are the surface temperature conditions they represent, and the smoother is the signal because the GST variations attenuate with depth (cf. Figure 2.3, Lachenbruch et al. 1988). Variations in GST 10, 100, and 1,000 years ago produce maximum temperature anomalies in the present-day subsurface temperature field at depths of about 25, 80, and 250 m, when considering one-dimensional vertical heat transfer (Harris and Chapman 1997).

Ice contained in the pore spaces and crevices delays the response to surface warming by consumption of latent heat, which can influence the time and depth scales of permafrost degradation by orders of magnitude even in low porosity rock (Kukkonen and Safanda 2001, Romanovsky and Osterkamp 2000, Wegmann et al. 1998). Porosity prescribes the volume available for ice or water. The melting of ice takes place progressively over several degrees of temperature, while the unfrozen water content raises exponentially towards 0 °C (cf. Figure 3.2). The steepness of the unfrozen water content curve depends on the ground

material, any particular temperature being associated with a particular quantity of water present (Williams and Smith 1989). Relationships between unfrozen water content and temperature have been established for many types of soils (cf. Nicolsky et al. 2007, cf. Romanovsky and Osterkamp 2000). For frozen bedrock in high mountains, however, information on porosity and freezing characteristics is sparse. Wegmann (1998) found that most of the interstitial ice in the rock of the Jungfrau East Ridge, Switzerland, freezes at –0.3 °C and the porosity is in the order of 3%.

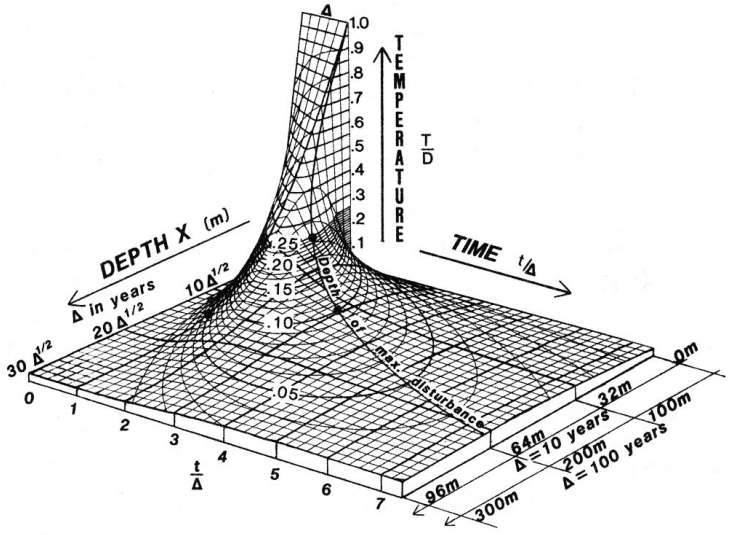

Figure 2.3. The thermal memory of the subsurface for changes in GST: Contours show the temperature anomaly at time t and depth x caused by a GST variation D of duration Δ. Depth axes give the depth for events of 10 y and 100 y (right), or for an arbitrary duration Δ (left). Considering the time 2 Δ after an event of duration Δ (i.e., t = 3Δ), the maximum temperature anomaly only amounts to 10% of the GST variation, and it occurs at a depth of about 38 m for Δ =10 y and 120 m for Δ = 100 y. Immediately after an event of duration Δ, the temperature anomaly has only penetrated down to about 50 m for Δ =10 y and 150 m for Δ = 100 y. From Lachenbruch et al. (1988).

Topography leads to converging heat flow below valleys and diverging heat flow towards the top of mountain peaks (for a review see Kohl 1999). Kohl (1999) further showed that the influence of topography on transient effects is observable down to depths of more than 1,000 m. First case studies in the Swiss Alps, taking into account surface temperatures that vary with elevation and aspect, demonstrate substantial lateral heat fluxes and temperatures that do not simply increase with depth (Gruber et al. 2004c, Wegmann et al. 1998). A review of available modeling studies on the effect of topography on subsurface temperatures is given in *Publication I* (Noetzli et al. 2007b).

Water circulation and corresponding advective heat transfer along the joint system of bedrock can contribute to subsurface heat transfer, and may lead to thaw corridors in permafrost, which substantially modify a purely conductive system. For example, the timing of many rock fall events in summer 2003, which occurred before the maximum active layer thickness would have been expected from one-dimensional heat conduction, points to an influence of heat transfer in bedrock permafrost other than conductive (Gruber et al. 2004a, Handschin 2007). Recently, thawed cleft systems influenced by moving water have also been identified by geophysical monitoring in solid rock walls (Krautblatter and Hauck 2007). Understanding of these processes, however, is limited and their contribution to subsurface heat transport has not yet been quantified. Convective heat transfer in the voids between coarse blocks plays a major role for the subsurface thermal regime of rock glaciers, but can be neglected for bedrock permafrost as a first approximation.

Further, the subsurface thermal field is modified by surface conditions that are inhomogeneous (e.g., lakes, buildings, etc.) (Gold and Lachenbruch 1973, Lachenbruch and Marshall 1986) or change with landscape and climate evolution (e.g., glacier coverage, sediment accumulation, geometry changes due to rock fall).

2.1.6 Response to Climate Change and Slope Stability

The principles of a surface temperature signal entering into the subsurface have been described in the previous section. An idealized sketch of a warming temperature profile is depicted in Figure 2.4: After a rise in GST from T_0 to T_1, the active layer thickens as a first and immediate reaction. Following further penetration of the temperature signal, the temperature profile bends towards warmer temperatures (intermediate reaction), before the permafrost base begins to rise, and, eventually, the temperature profile reaches a new equilibrium. Depending on subsurface properties and permafrost thickness, time scales to reach a new equilibrium are in the order of centuries to millennia. In mountain topography, equilibrium temperature profiles can deviate considerably from the linear form known from flat terrain and shown in Figure 2.4. It is therefore difficult to identify from a single point in time what transient effects influence the temperature profile (Gruber et al. 2004c).

In recent years, many rock falls have had their starting zones in permafrost areas, some of them involving large volumes of material (i.e., >1 mio m^3). Events have occurred in the European Alps (e.g., Fischer et al. 2006, Keller 2003, Noetzli et al. 2003, and references therein, Ravanel 2006, Sosio et al. 2008) and elsewhere (e.g., Chinn et al. 1992, Evans and Clague 1988, Gertseema et al. 2006, Haeberli et al. 2004, Korup 2005, Plafker and Ericksen 1978). Massive ice was visible in many starting zones immediately after the event (e.g., the events on the Matterhorn south face and Hörnligrat, or below the Marco e

Rosa Hut, Bernina, all in summer 2003). A first approach to determine thermal conditions in rock fall starting zones from permafrost areas points to a concentration of events from warm permafrost slopes (Noetzli et al. 2003).

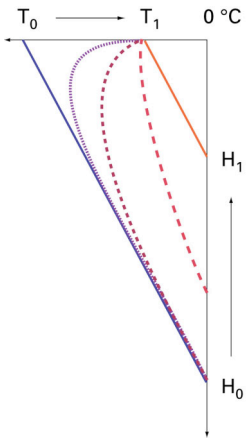

Figure 2.4. Schematic evolution of a permafrost temperature profile after a rise in surface temperature from T_0 to T_1. The permafrost thickness H_0 relates to an equilibrium profile for T_0, H_1 relates to T_1.

The interpretation of observations is difficult (Gruber and Haeberli 2007), because 1) they are biased due to better observation in recent times and often do not allow for a reconstruction of exact timing and pre-failure conditions, 2) permafrost degradation is only one important factor that determines slope stability and other mechanisms may have contributed considerably to failure, which, moreover, are different for each of the events, and 3) understanding of the processes and knowledge of the thermal conditions under which such instabilities develop are limited. Frequency and magnitude of a possibly resulting event are likely to correspond to the time and depth scales of permafrost degradation. Active layer thickening may lead to small events as an immediate reaction to an increase in surface temperatures (e.g., events in 2003), whereas permafrost degradation at depth may lead to large events delayed by decades or centuries (e.g., Brenva rock avalanches in winter 1997).

A detailed review of the connection of permafrost ice contained in fractures and the stability of rock slopes is given by Gruber and Haeberli (2007). They list five main physical processes that alter the geotechnical conditions in fractures and, eventually, may lead to slope instability and failure:

Figure 2.5. Massive ice was visible in the starting zone of a rock fall on the Matterhorn south face, immediately after the event in July 2003. The starting zone is located at approx. 3,600 m a.s.l. and is about 100 m high. Photo: L. Trucco.

(1) Thawing permafrost can lead to a loss of bonding in ice-filled fractures, which is often referred to as «ice cement».

(2) Ice segregation has the potential to slowly widen fractures and fissures. Ice segregation is caused by the movement of unfrozen water along temperature gradients towards a freezing front. This effect is known from frost heave processes, but has also been shown for rock (Akagawa and Fukuda 1991, Murton et al. 2001).

(3) Volume expansion of water during freezing (by 9%) can exert pressure in crack systems. In perennially frozen material, this can only occur when water is transported to a confined location with cold temperatures.

(4) Permafrost thaw and consecutive flowing water can lead to strong hydrostatic pressures, e.g., in fractures where ice is thawing, in areas impermeable due to ice, or in areas where ice is thawing above.

(5) The shear strength of ice-filled fractures decreases with warming ice. A stability minimum between –1.5 and 0 °C was demonstrated in laboratory experiments (Davies et al. 2001).

Further, permafrost developing in previously glacier-covered bedrock has the potential to intensify rock destruction through ice formation (Wegmann et al. 1998), which, in turn, can reduce the permeability and affect hydraulic pressures inside the fissured rock (Haeberli and Burn 2002).

Mass movements such as rock-ice avalanches can reach considerably longer travel distances in glacial than in non-glacial environments due to possible interactions with ice, snow and water (Huggel et al. 2004, Noetzli et al. 2006b). The mobility of rock falls in glacial environments has been observed to increase by about 25% compared to non-glacial environments (Deline 2001, Evans and Clague 1988). Hazard assessment and discernment of sensitive zones is traditionally based on historical observations, and hazard probabilities are calculated based on what happened in the past. However, this approach does not account for developments related to ongoing and projected climatic changes and needs to be complemented by possible effects of rapidly changing permafrost conditions.

2.2 Modeling Mountain Permafrost

Due to the invisibility of the phenomenon, the complexity of its distribution, and the high costs of measurements in steep terrain, the development of modeling tools to describe mountain permafrost is an important branch of research. Further, the assessment of future permafrost conditions is only possible based on appropriate modeling tools. The most promising approaches for the assessment of possible changes in mountain permafrost are downscaling and coupling strategies of *Global Circulation Models* (GCM), *Regional Climate Models* (RCMs), and regional to local *Permafrost Models*, forming a chain from global to local scale. The calculation of permafrost thermal conditions requires the coupling of the *Surface Energy Balance* together with a *Snow Pack Model* and *Three-dimensional Heat Transfer* in the subsurface (Gruber 2005). Here, we focus on energy balance and subsurface heat transfer models. A number of models that simulate the development of and heat transfer through an alpine snow pack exist (e.g., Bader and Weilenmann 1992, Brun et al. 1989, cf. also Frey 2007, Jordan 1991, Lehning et al. 2002, Luetschg 2004). For steep rock slopes as in the focus of this thesis, however, they are not of primary importance.

2.2.1 Empirical and Statistical Models

First attempts to estimate the distribution of mountain permafrost were published by Haeberli (1975). These so-called rules of thumb were based on proxies of the surface energy balance and calibrated by various data, such as the bottom temperature of the snow cover (BTS) and geophysical measurements. They include a topographical key, which describes the permafrost distribution as a function of altitude (sensible heat), aspect (incoming solar radiation), and topology (snow redistribution). With the development of *Geographical Information Systems* (GIS) this topographical key was implemented in a computer program (Keller 1992), which enabled the first permafrost distribution map of Switzerland (Keller et

al. 1998). In the following, modeling was enhanced by considering statistical relationships of air temperature and direct solar radiation, rather than topographical attributes. Such an approach was originally developed for the Upper Engadine, Switzerland (Hoelzle 1994) and consecutively adapted for use in other regions (Etzelmüller and Hoelzle 2001, King and Kalisch 1998, Mustafa et al. 2003) or for incorporation of additional data (e.g., Gruber and Hoelzle 2001). Since such models are locally calibrated and assume equilibrium conditions, they are only of limited use for application in other regions (cf. also Lewkowicz and Bonnaventure 2008) or for extrapolation to the future. Their main advantage is their robustness, easy applicability, and the small amount of input data required.

2.2.2 Surface Energy Balance

Following the above-described empirical and statistical approaches, *physics-based* or *process-oriented* mountain permafrost models concentrate on *surface energy balance* and *near-surface heat transport*. The modeling of surface energy fluxes is typically based on hourly or daily climate time series and requires robust parameterization to extrapolate over large horizontal and vertical distances in complex terrain (e.g., Mittaz et al. 2002, e.g., Plüss and Ohmura 1997). Energy balance models allow for transient modeling, use in any area where corresponding input data is available, and interaction or feedback with other models. Yet, these models are limited to the near-surface layer, require computational capacity, and quantitative input data (e.g., continuous climate time series). Therefore, models of reduced complexity are often deducted from key parameters and results gained from energy balance modeling (Gruber and Haeberli 2007, Smith and Riseborogh 2002). For example, rock wall temperature distribution modeled with a surface energy balance model (Gruber et al. 2004b) was parameterized and incorporated into an empirical GIS-based model to estimate rock temperatures in a case study of the Monte Rosa east face (Switzerland) (Fischer et al. 2006), or for the new permafrost distribution map of Switzerland (FOEN 2006).

2.2.3 Subsurface Heat Transport

The modeling of temperatures in the subsurface of high mountains especially needs a robust integration of topography, a three-dimensional formulation of subsurface heat transfer, and a temperature-dependent parameterization of the unfrozen water content and latent heat effects. For the solution of the transient three-dimensional heat conduction equation (Eq. 3) of two or three dimensions with variable boundary conditions numerical methods are required. In numerical solutions, differential equations are transformed into a solvable system of equations by discretization of the subsurface (Figure 2.6). Thereby, changes between nodes need to be adequately small and nodes should build a mesh that sufficiently represents the geometry modeled. The common approaches used for numerical solutions are *Finite*

Differences (FD) and *Finite Element* (FE) Methods. For three-dimensional heat conduction in mountains, FE approaches are preferred, because of their better ability to handle complex geometries (e.g., Haenel et al. 1988).

A great number of transient numerical heat transfer models and corresponding studies exist from high-latitude permafrost research (Goodrich 1978, Guymon and Hromadka 1977, Guymon et al. 1984, Lunardini 1991, Romanovsky et al. 1997, Seregina 1989), but they typically consider vertical heat transfer or flat terrain and do not integrate a three-dimensional formulation of heat transfer or steep topography. For permafrost studies in complex alpine terrain only a few examples exist. For the solution of the heat conduction equation (Eq. 3) in steep terrain, e.g., the simulators FRACTURE (Kohl and Hopkirk 1995) or MARC/MENTAT (Luethi and Funk 2001, Wegmann 1998) have been used.

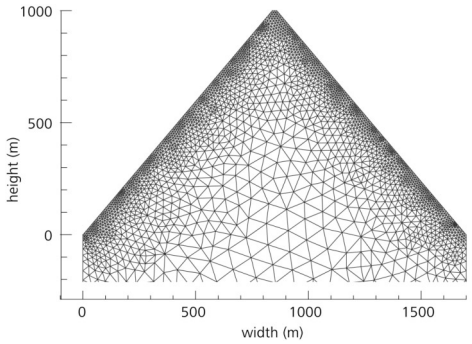

Figure 2.6. FE mesh of a simplified ridge cross section as used for modeling in this thesis.

2.2.4 Driving Meteo Data

Permafrost scenarios are often calculated based on incremental scenarios (e.g., Hoelzle and Haeberli 1995, Stocker-Mittaz et al. 2002). For incremental scenarios, particular climate elements are changed by plausible but arbitrary amounts (e.g., plus 3 °C in air temperature). This approach is easily applicable and its results are reproducible, but it actually simulates sensitivities and does not necessarily produce a realistic and physically plausible set of changes in atmospheric conditions (Salzmann et al. 2007b).

RCMs are promising tools to provide quantitative estimates of future regional climate scenarios on a physically consistent basis (IPCC 2001). In principal, RCMs are downscaled limited area models with initial conditions as well as lateral and surface boundary conditions taken from a run of a GCM. RCMs resolve horizontal grids of 10–50 km for continuous simulations of time slices of several decades. That is, an area as big and topographically complex as the Matter Valley, Switzerland, would be represented by one single

RCM grid cell having one average elevation value. The main challenge to use output from RCM's for impact studies in high mountain research is therefore the downscaling to finer spatial resolution. Corresponding dynamical approaches have recently been developed (Salzmann 2006, Salzmann et al. 2007a). A detailed account of the RCM principles, available downscaling methods, and possibilities and limitations of their application to high mountain research is given by Salzmann (2006).

Chapter 3

Modeling Procedure

The four research papers that comprise the main part of this thesis are based on the modeling procedure outlined below. The papers, however, typically apply and focus on only a part of the modeling procedure, whereas in this chapter, we intend to give a comprehensive overview. The steps taken to validate the modeling procedure are also compiled and described here.

3.1 Overview of the Modeling Procedure

A *Model* is a conceptual or mathematical representation of a phenomenon, process, or system. It provides an idealized or conceptual framework for logical reasoning, mathematical or computational evaluation, and hypothesis testing. It is idealized in the sense that it does not exactly represent the real world system, but explicitly makes assumptions and simplifications. In the scope of this thesis, we use the term *Modeling* in the sense of using computer models to describe the thermal conditions in the subsurface of high mountains. The implementation of a model over time is generally referred to as *Simulation*. In order to answer the research questions raised in Chapter 1, modeling can be used in two complementing ways: 1) Models represent a quantitative formulation of the system under consideration and, hence, can be used for reasoning about selected aspects by numerical experiments (e.g., idealized test cases, sensitivity studies) or for hypothesis testing. 2) Models can be applied for predictive simulations, that is, they are used for extrapolation to places or times where no information is available, namely past or future times and inaccessible or unknown areas. For both tasks, confidence in the model needs to be established by verification and validation (see Chapter 3.4).

Our modeling approach is based on the process domains outlined in the previous chapter (i.e., atmosphere–surface–subsurface) and combines three different types of models:

climate time series are used to drive a distributed *Surface Energy Balance Model* for steep topography (Topography and Energy BALance (TEBAL), Gruber 2005) to calculate mean ground surface temperatures (MGST). In this work, we use the term MGST when GST are calculated and averaged for a certain period of time, whereas we use GST when it is generally referred to ground surface temperatures. Computed MGST are used as the upper boundary condition (UBC) in a *Three-dimensional Heat Conduction Scheme* (Figure 3.1). We neglect the snow pack and do not consider other heat transfer processes than conduction, because this work focuses on steep bedrock slopes. We couple the energy balance and heat conduction models directly at the surface. This further implies that we assume the thermal offset (i.e., the temperature difference between the ground surface, GST, and the top of permafrost, TTOP) to be negligible in bedrock. The thermal offset is a result of seasonally varying thermal properties in the active layer and is mainly important in highly porous material.

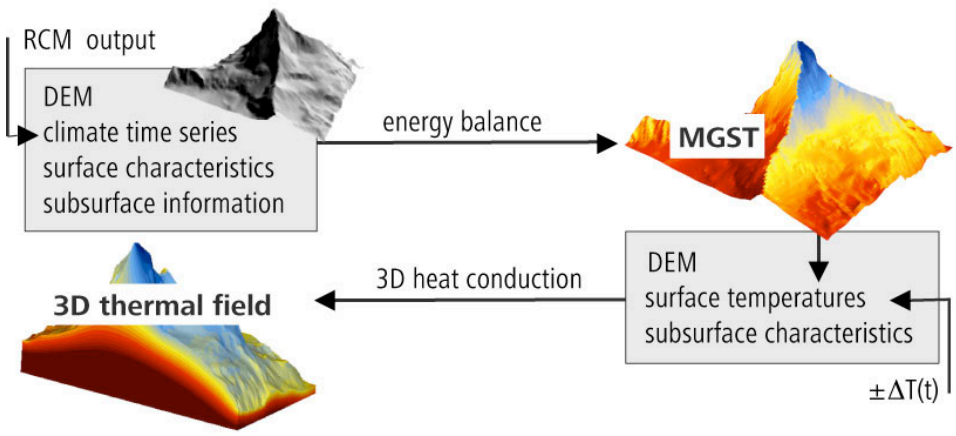

Figure 3.1. The modeling approach designed in the scope of this thesis combines a surface energy balance model, which calculates mean ground surface temperatures (MGST) in steep topography, with three-dimensional subsurface heat conduction. The surface energy balance model is driven by climate time series, which are measured or, for future simulations, downscaled from Regional Climate Model (RCM) results. In addition, the main input data required are a digital elevation model (DEM) and information on surface and subsurface characteristics. The function ΔT(t) prescribes the evolution of the ground surface temperature (GST) in simulations based on the heat conduction scheme.

Climate time series to drive the energy balance model are taken from Alpine measurement stations or, for simulations of possible future conditions, are based on results from *Regional Climate Models (RCMs)* using corresponding application procedures (Salzmann et al. 2007a).

The three model types as applied in this thesis involve different spatial and temporal resolutions (Table 1, cf. Section 2.1.2). While RCM data used comes in daily resolution

for grid cells of about 10–50 km, surface energy balance models in mountain permafrost are typically solved for hourly time steps and are designed for regional scale resolution of the topography (about 10–25 m). Numerical heat transport models can be adapted to diverse scales of time and space, depending on their scope of application and computational resources. In this study, the spatial extent and horizontal resolution of the FE mesh for the heat conduction scheme matches the surface energy balance model. The resolution of the FE mesh decreases with distance from the surface, and temporal variations in GST are adapted to the depths of interest or vice-versa.

Table 3.1. Temporal and spatial resolution of the three model types as applied in the scope of this thesis. The values indicate the approximate scale, rather than exact limits.

	Spatial Resolution	Temporal Resolution
Regional Climate Models	continental/regional 10–50 km	daily
Surface Energy Balance in Steep Topography	regional/local 5–50 m	minutes–daily
Subsurface Heat Conduction	local 5–50 m (horizontal) 0.5–100 m (vertical)	daily–100 years

The input required depends on the model (surface energy balance *EB* or heat conduction scheme *HC*) and mode (stationary *st* or transient *tr*) used and is the following:

- continual hourly or daily climate time series of the calculated period to drive the energy balance model (*EB, tr*) (i.e., air temperature, air pressure, relative humidity, wind speed and direction, precipitation, and global radiation),
- a digital elevation model (DEM) of the topography under consideration (*EB/HC, st/tr*),
- information on surface characteristics (for bedrock i.e., albedo, emmissivity, roughness length) (*EB/HC, st/tr*),
- information on subsurface characteristics (i.e., thermal conductivity, volumetric heat capacity, porosity, freezing characteristics) (*EB/HC, st/tr*), and
- the evolution of the GST (cf. $\Delta T(t)$ in Figure 3.1) in the past or the future (*HC, tr)*.

3.2 Atmosphere Surface Interface: RCM – Distributed Surface Energy Balance

The first step in our modeling procedure is to describe the interaction between atmosphere and surface, which includes the modeling of the surface energy balance driven by climate time series. Climate time series are either taken from high-alpine measurement stations

(e.g., Corvatsch or Jungfraujoch from MeteoSwiss), or – for future scenarios – constructed based on results from RCMs using special application techniques. The modeling described here mainly relates to *Publication II* (Salzmann et al. 2007b) in *Part II* of this thesis. In this section, we will first deal with the construction of future climate time series for alpine terrain and, in the second part, we will describe the energy balance model applied, which is especially designed for use in steep terrain.

3.2.1 Construction of RCM-based Climate Time Series

For the application of RCM results to an impact model, the use of a single scenario is not sufficient because uncertainties associated with modeling scenario climate conditions are high (Salzmann et al. 2007b). They include uncertainties in forcing emission scenarios, in model limitations of GCMs and RCMs, and in possible future changes in climate variability. In addition, uncertainties arise from the impact model itself (here, the surface energy balance model). To calculate possible changes in GST in steep mountain slopes, we therefore used a multi model approach including different emission scenarios, RCMs, and application procedures and constructed twelve different scenario climate time series with daily resolution (i.e., ten RCM-based and two incremental scenario time series). Details on the RCMs and scenarios applied are given in *Publication II* (Salzmann et al. 2007b).

The results of the RCM control (CTRL, 1961–1990) and scenario runs (SCEN, 2071–2100) were adapted for high-mountain situations using the so-called *Delta* and *Bias Approaches* (Salzmann et al. 2007a). The main difficulty thereby is the spatial mismatch between RCMs and complex mountain topography (cf. Section 3.1, Table 3.1). As a basis and site specific reference, observed meteorological data from a high Alpine station are used (here: Corvatsch, Switzerland). The *Delta Approach* calculates scenario climate time series by adjusting the observed climate data by the difference (e.g., temperature) or ratio (e.g., precipitation) between the SCEN and CTRL time slices. The *Bias Approach*, in contrast, uses debiased output of the scenario simulations, that is, it accounts for possible changes in climate variability. In addition, we created two incremental scenarios by simply increasing air temperature by +2 and +3 °C throughout the entire period, without changing any of the other climate variables.

RCM data available to our study are in daily resolution. Therefore, the scenario climate time series and the consecutive TEBAL runs were in daily resolution also. Based on the two application procedures, seven climate variables were obtained: 2 m temperature, air temperature, precipitation, global radiation, air pressure, vapor pressure, and wind speed.

3.2.2 The Energy Balance Model TEBAL

The surface energy balance model TEBAL (Gruber 2005) simulates time series of surface energy fluxes and near-surface temperatures in complex topography for each point of an input surface grid. The model contains algorithms for the mountain-specific extrapolation and parameterization of climate time series and surface energy fluxes, which are described in *Publications I and II* (Noetzli et al. 2007b, Salzmann et al. 2007b) and references therein (e.g., Corripio 2003, Erbs et al. 1982, Gruber 2005, Gruber et al. 2004b, Konzelmann et al. 1994, Plüss 1997, Plüss and Ohmura 1997, Stocker-Mittaz 2002). The ground heat flux is calculated based on ground heat conduction solved in a one-dimensional FD Crank-Nicholson scheme (Gruber 2005).

3.3 Surface Subsurface Interface: Surface Energy Balance – Subsurface Heat Transport

The second step in the modeling procedure is to describe the interaction between the surface and subsurface, which involves the modeling of the subsurface heat transfer below steep topography with spatially highly variable surface temperatures. Based on the surface energy balance model described in the previous section, we compute spatially distributed ground surface temperatures, which define the UBC in the heat conduction scheme. Here, the robust integration of the terrain geometry, the evolution of the UBC, and phase change processes are specifically addressed in the scope of this thesis. This section principally refers to *Publications I* and *III* (Noetzli and Gruber in review, Noetzli et al. 2007b).

3.3.1 TEBAL and Upper Boundary Condition

For use with the subsurface heat transport scheme, TEBAL was run with hourly time steps, which allows for simulations of the effect of diurnal fluctuations (e.g., the influence of convective clouding). Such diurnal fluctuations are the cause for differing surface temperatures of east- and west-facing slopes and, hence, are important for the simulation of GST variability in mountain topography. To obtain UBCs for the heat conduction scheme, we ran TEBAL over a ten-year period and averaged calculated GST time series to a single value for each grid cell of the input DEM.

3.3.2 Subsurface Heat Conduction

Herein, the simulator FRACTure (Flow, Rock And Coupled Temperature effects, Kohl and Hopkirk 1995) and the commercial modeling package COMSOL were used for the simulation of heat transport processes (cf. Section 2.3.3) in a forward FE modeling scheme. Both models include a full three-dimensional formulation of heat transport processes and enable

an easy integration of topography and varying upper boundary conditions. FRACTure was broadly applied and tested in the past for temperature calculations below complex topography (Kohl 1999, Kohl et al. 2001). COMSOL has been extended by an import routine for gridded elevation data describing complex geometries (Noetzli et al. 2007a) by request of and in collaboration with this study (COMSOL Script by S. Friedel, FEMLAB AG, Zurich, Switzerland).

The calculated MGST (see Section 3.3.1) serve as UBC for the computation of a stationary subsurface temperature field according to Equation (3) and the left term being zero. For transient forward simulations, the evolution of the UBC is prescribed by so called *Load Time Functions* (LTFs). That is, starting from an initial stationary solution of the prescribed UBC_i, UBC is changed according to the LTF during the simulation:

$$UBC(t) = UBC_i + LTF(t) \tag{4}$$

where t is time. LTFs consist of piecewise linear functions. Their level of detail and corresponding time steps taken by the solver determine the temporal resolution of the model run. Transient simulations are required for 1) modeling current temperature fields accounting for GST variations in the past, and 2) simulations of future temperature fields as a result of projected warming. An initialization procedure (i.e., the procedure to find starting values for the variables the model simulates) based on a simplified GST history for the Alps was developed and is described in *Publication III* (Noetzli and Gruber in review).

The latent heat effect (i.e., the effect of energy consumption during the phase change from ice to water) can be considered by an apparent heat capacity in numerical heat transport models. We used the approach described by Mottaghy and Rath (2006): The apparent heat capacity ρc_{app} substitutes the volumetric heat capacity ρc_p in the heat transfer equation within the freezing interval ω, where phase transition takes place (Figure 3.2):

$$\rho c_{app} = \rho c_p + \rho_i L_f \Phi \frac{\delta \Theta}{\delta T} \tag{5}$$

where ρ_i is the density of ice (i.e., 917 g m^{-3}), L_f is the specific latent heat of fusion of ice (i.e., 3.36 10^5 J kg^{-1}), Φ is the porosity, and Θ is the volumetric unfrozen water content. The unfrozen water content Θ is typically described by an exponential function (Anderson and Tice 1972, cf. also Nicolsky et al. 2007, Williams and Smith 1989) for the freezing interval ω, which depends on the material. Here, only the deviation of Θ needs to be incorporated into Equation 5:

$$\frac{d\Theta}{dT} = \begin{cases} \frac{2(T - T_L)}{\omega^2} \exp\left(\frac{T - T_L}{\omega}\right)^2 & \text{if } T \le T_L \\ 0 & \text{if } T > T_L \end{cases} \quad (6)$$

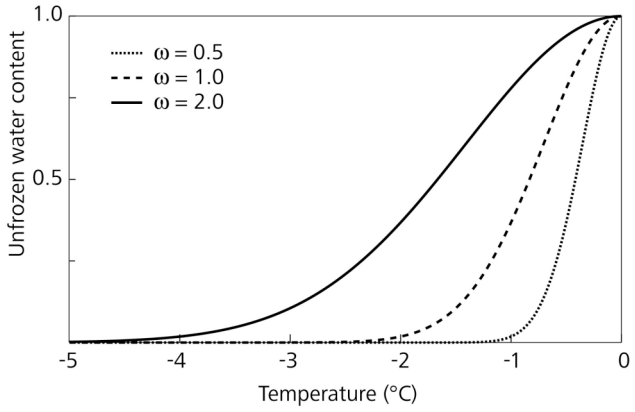

Figure 3.2. Unfrozen water content curves for different freezing intervals ω.

3.4 Validation of the Modeling Approach

According to Rykiel (1996), validation describes a testing process on which to base an opinion of how well a model performs. Based on the validation, the user can decide whether the model is acceptable for its intended purpose, which in this thesis is the calculation of three-dimensional subsurface temperature fields in mountain permafrost for the time and spatial scales described above (Table 3.1).

Measurements of entire three-dimensional temperature fields in mountains for comparison with modeling results do not exist and are hardly feasible. In order to gain confidence in the model results, we conducted three different validation steps, which include 1) testing the performance of the surface energy balance model by comparison with measured time series of near-surface rock temperatures, 2) evaluation of modeling results for borehole sites, and 3) sensitivity studies. Here, we outline and compile the steps taken, while detailed results are described in *Publications II–IV* and in the following chapter. Based on the steps taken, the performance of the model is assessed in a qualitative manner, rather than quantitatively. For our purpose, the correct representation of value ranges and patterns of subsurface temperatures, as well as the influence of estimated parameters are of primary importance.

3.4.1 Energy Balance Model for Steep Topography

The surface energy balance TEBAL has been validated for both, hourly (*Publication I*, Noetzli et al. 2007a) and daily (Gruber et al. 2004b) time steps. For this purpose, 14 log-

ger-measured temperature time series in steep rock walls in the Swiss Alps for the hydrological year 2001/2002 were compared to results from model runs where only the topographic attributes of the logger sites (i.e., slope, aspect, and elevation) were adjusted. The overall simulation of mean daily rock surface temperatures with hourly time steps for a one year period resulted in a mean coefficient of determination (R^2) of 0.78 (for daily time steps: 0.88) and in a mean absolute difference of 1.7 °C (for daily time steps: 1.2 °C).

For our work, it is particularly important to correctly model the spatial differences in surface temperatures as related to slope exposition, since they are the main cause for lateral subsurface heat fluxes. In order to double check, we compared the temperature offset for modeled and measured data: For a location at an elevation of 3,000 m a.s.l. and with a 60° slope it is approximately 7 °C between north and south exposition and 2.5 °C between east and west, respectively. These values correspond well with the rules of thumb mentioned earlier (Haeberli 1975) as well as with measured data of rock temperatures (Gruber et al. 2004b).

3.4.2 Subsurface Temperatures at Borehole Locations

In the scope of this thesis, we modeled the subsurface temperature fields of two permafrost borehole sites: Schilthorn (Swiss Alps) and Zugspitze (Germany). For both locations, modeling results were compared to measurements. The Schilthorn crest in the Bernese Alps, Switzerland, is one of the most prominent permafrost research sites in the Alps and the three boreholes are part of the monitoring networks PACE and PERMOS. The thermal field in the Zugspitze was modeled before a borehole was drilled in August 2007. First temperature data is now available and can be compared with modeling results.

In the Schilthorn study (see *Publication IV*, Noetzli et al. 2008), we analyzed whether subsurface heat transfer by conduction alone allows a realistic simulation of both, pattern and values of subsurface temperatures. We only applied the heat conduction scheme for this purpose and did not calculate the surface energy balance, but used near-surface temperatures measured during the hydrological year 2006/2007 as UBC instead. Since we assumed any north-south cross section to be similar, we measured near-surface temperatures along a cross crest profile through the two 100 m boreholes. The measured thermal offset between the ground surface and TTOP is small on the Schilthorn (about 0.3 °C, cf. Hoelzle and Gruber 2008) and was, hence, neglected in the simulations. Because surface temperatures in the year measured were warmer than in the previous decades, the simulation was performed with an initialization of 150 years. For simplicity, we assumed an isotropic and homogeneous medium (for details see *Publication IV*, Noetzli et al. 2008). Extracted temperature profiles from the modeled temperature field were then compared with T(z) profiles from the

two 100 m boreholes. Here, the temperature difference relates to the accuracy of the modeled temperature values, whereas the temperature gradient relates to the pattern of the temperature field. In addition, the subsurface thermal field was compared with data gained from *Electrical Resistivity Tomography* (ERT) monitoring along the same cross-crest profile (Hilbich et al. 2008).

On the Zugspitze, Germany, a permafrost monitoring borehole was planned based on simulations of the subsurface thermal field using our modeling approach (Noetzli et al. 2006a). The modeling involved both, the calculation of present-day MGST based on TEBAL and subsequent subsurface heat transport. We computed MGST based on climate time series from the Zugpitze (data source: Deutscher Wetterdienst) for the years 2000–2006. The subsurface thermal field was calculated for stationary, homogeneous, and isotropic conditions. Boreholes were drilled in August 2007, and first measured data are now available and can be compared with modeling results. Model output that is generated before the data are collected is the strongest case for validation with measured data according to Rykiel (1996).

3.4.3 Sensitivity Studies

Sensitivity studies were conducted to assess the influence of the major uncertainties we deal with when modeling transient permafrost temperatures in high mountains. Possible errors (other than from the representation of relevant processes in the model itself, e.g., phase change processes) mainly emerge from 1) the subsurface properties assumed in the model runs, 2) the reconstruction of the GST history in the past and the initialization procedure, and 3) projected future atmospheric conditions.

Uncertainties caused by the lack of information on subsurface properties in steep mountains were assessed in *Publication III* (Noetzli and Gruber in review). Additionally, we analyzed different past climate variations and their effect on subsurface temperatures. Uncertainties due to erroneous assumptions of future scenarios, RCM limitations, and application procedures were calculated and are described in *Publication II* (Salzmann et al. 2007b). These effects were additionally compared with those from incremental scenarios as well as with those from topography. Results from the sensitivity analyses are summarized in Section 4.2.

Chapter 4

Modeled Temperature Fields in Mountain Permafrost

Detailed results of the research conducted in this thesis are published in the four papers of *Part II*. This chapter summarizes these results facilitating a comprehensive overview, understanding and integration. We first focus on results from idealized test cases for equilibrium conditions, and secondly, on transient temperature fields for both, present-day climate and future scenarios. Finally, three case studies for real topography (i.e., Schilthorn, Zugspitze, and Matterhorn) are presented, for which some unpublished results are included.

As a basis for the numerical experiments, we used idealized geometries representing the most prevalent topographic forms that comprise high-mountain topography. As such, we identified ridges and peaks and simplified them to triangular prisms and pyramid geometries (Figure 4.1). In addition, we added a simple spur for some of the simulations, since irregularities often modify the surface of rock walls.

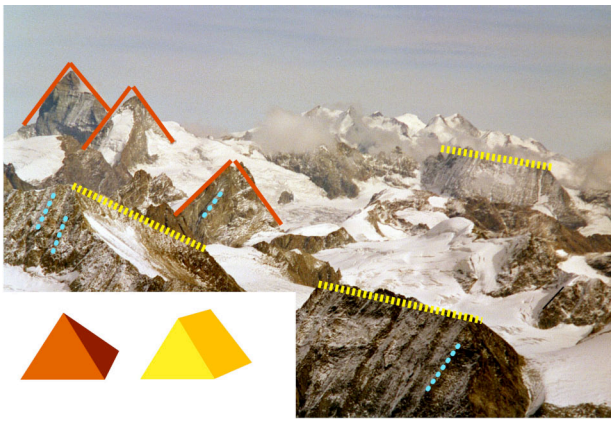

Figure 4.1. The most prevalent features of mountain topography are ridges (dashed yellow lines) and peaks (red lines). They were simplified to triangular prisms and pyramids. Inhomogeneities on rock wall surfaces, such as spurs (blue dots), are also considered. Photo: C. Rothenbühler.

4.1 Equilibrium Temperature Fields

Results presented in this section are taken from *Publication I* (Noetzli et al. 2007b) and describe the sole influence of mountain topography and spatially variable surface temperatures on the equilibrium subsurface temperature distribution. Model runs were performed on the basis of the geometries described above and typical values of surface and subsurface properties. Topographic attributes of the geometries (i.e., slope, elevation, and aspect) were varied in the simulations.

Combined effects of topography and spatially variable surface temperatures substantially influence the subsurface thermal and cause lateral heat fluxes in the underground (Figure 4.2). That is, a strong heat flux is directed from north to south faces and a smaller one from east to west faces. This heat flux is strongest near the top of a ridge or peak, where the influence of the geothermal heat flux becomes minimal. Isotherms incline steeply and are nearly vertical in the top parts. The steeper the mountain, the more the isotherms incline and the less important is the geothermal heat flux. Since isotherms are not horizontal, elevation and size of the topography do not only alter the volume but also the shape of the permafrost body.

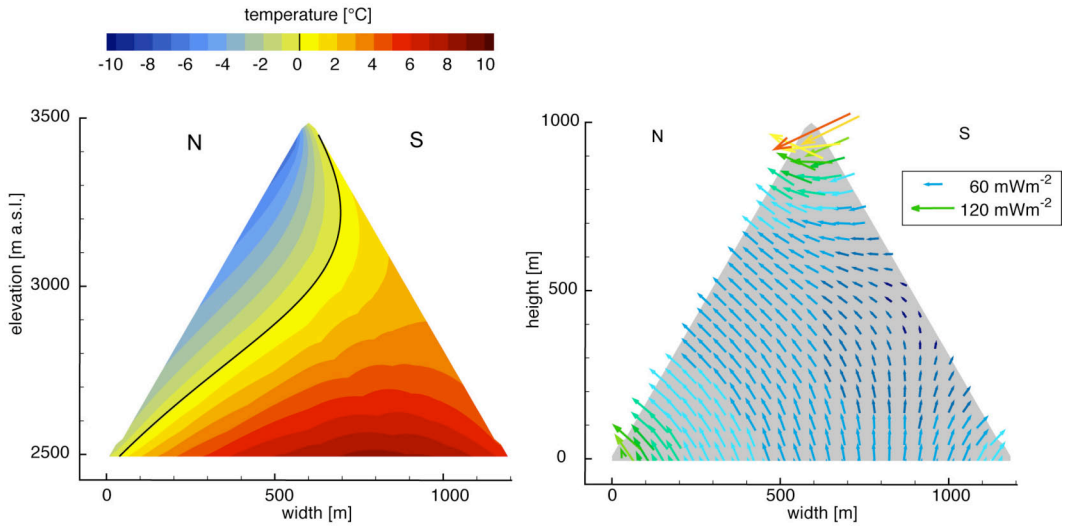

Figure 4.2. The equilibrium temperature field of a cross section through a simplified mountain ridge with 60° steep slopes is shown on the left. The corresponding distribution of heat fluxes is depicted on the right.

Combined effects of topography and spatially variable surface temperatures complicate the subsurface thermal field in such as way as to make it impossible to sufficiently describe it based on surface temperatures alone. Permafrost can occur at shallow depths below locations where GST is clearly positive, for example, on the southern side of a ridge

or below the edges of a pyramid (Figure 4.3). Further, inhomogeneities, such as a spur with a north-exposed part, can locally influence the subsurface temperature field and induce permafrost in an otherwise permafrost-free rock wall. Temperature profiles taken vertically in subsurface temperature fields below mountains considerably deviate from the linear temperature profiles known from flat terrain. The direction of the deviation is influenced by the location of the profile in the topography (e.g., middle or top part, warmer or colder side), whereas the size of the deviation is influenced by the steepness and complexity of the topography.

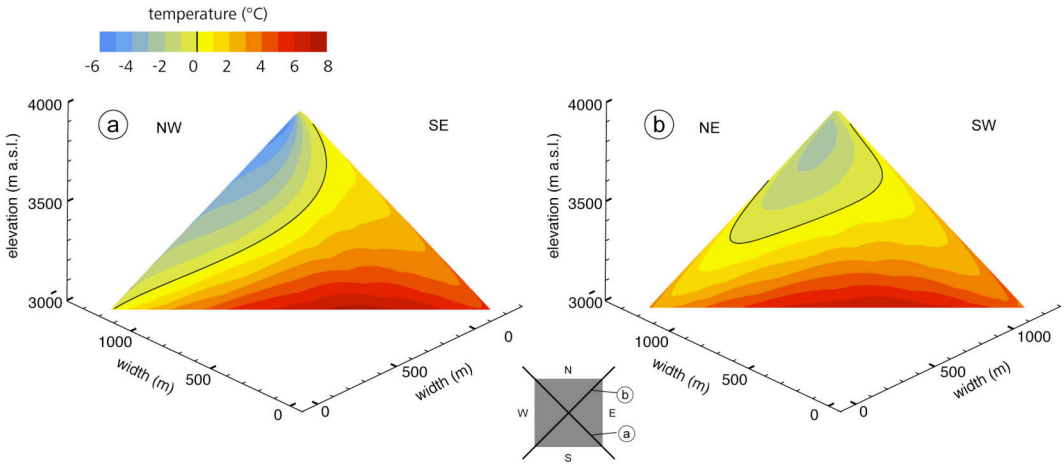

Figure 4.3. Equilibrium temperature fields of two cross sections through a simplified mountain peak (pyramid). Cross sections are taken diagonally along the edges of the pyramid: the left cross section is taken along the south-east and north-west ridges (a), the one on the right along the south-west and north-east ridges (b). From *Publication I* (Noetzli et al. 2007b).

4.2 Transient Temperature Fields

The results presented in this section are based on *Publications II* (Salzmann et al. 2007b) and *III* (Noetzli and Gruber in review) and describe combined transient and topographical effects in the subsurface thermal field. That is, simulations are not conducted stationarily as for temperature fields presented in the previous section, but time-dependently. As before, model runs were performed with simplified topographies and typical values of surface and subsurface properties. Results from sensitivity analyses as described in Section 3.4.3 are also presented here.

4.2.1 Effects of Past Climatic Conditions

Based on systematic model experiments, which use climate reconstruction data, we identified the last glacial period (ca. 18 ky BP) and the variations in the past millennium, namely the Medieval Warmth (MW), the Little Ice Age (LIA), and the recent warming, as the most important climate variations that influence present-day permafrost temperatures in the Alps. The temperature depression caused by the LIA is present in roughly the top 100 m and is less than 1 °C. Maximum temperature depressions exist in the innermost part of a large mountain. It amounts to about –3 °C (computed for a mountain of 1,000 m height) compared to present-day stationary conditions, and it reflects temperature conditions of the past ice age. From this it follows that for a reasonable simulation of current permafrost temperatures at depth it is necessary to account for past GST variations in a model initialization procedure. The effects of the past glacial period are negligible for mountain geometries such as ridges of only a few 100 m height, where mainly the LIA and subsequent recent warming are important. For larger mountains, such as the Matterhorn, however, the cold GST of the last Ice Age have to be taken into account.

Uncertainties in climate reconstruction are higher for the absolute amplitude than for relative climate fluctuations (Esper et al. 2005). That is, absolute values of modeling results are less reliable than patterns of transient present-day temperature fields. Modeled absolute temperature differences are around 1–2 °C at depth for the different GST histories considered. Calculations, however, were based on the assumption that GST variations closely follow air temperatures. In addition, the effect of different warming of, e.g., north- and south-exposed locations, has not been considered. These limitations are addressed in *Publication II* (Salzmann et al. 2007b) and in the following section.

In terms of subsurface properties, we found that mainly thermal conductivity (and correspondingly anisotropy) have a significant effect on the temperature depression at depth, which can amount to up to additional 2 °C for extreme values. In general, errors induced by uncertain assumptions of thermal conductivity, heat capacity, anisotropy, and heat production increase with depth and length of the simulation (but are mostly below 1 °C and do not exceed 3 °C), whereas errors caused by uncertainties in subsurface ice decrease (i.e,. about 0.2 °C at depth for long time scales, and up to 2 °C for short time scales in the uppermost decameters).

4.2.2 Effects of Future Warming

Possible changes in GST between the periods 1982–2002 and 2071–2100 calculated based on the different scenario climate time series reach from 1.2 to 4.7 °C, with a mean of 3.5 °C. For the same climate time series used, the difference in GST change between north

and south-facing slopes is in the range of 1 °C. This means that the range of resulting GST changes is significantly larger for different scenario climate time series used than for varying topographic settings.

Based on the above results from experimentation with the surface energy balance model and different scenario climate time series, we assumed a linear and uniform warming of GST of +3 °C/100 y for the next 200 years. We ran transient simulations of the subsurface heat conduction scheme with UBC evolving based on corresponding LTF. Results show that surface warming during the next two centuries affects ground temperatures in roughly the top 250 m of a mountain, whereas temperatures at greater depth still remain unchanged. Only about 50% of the GST change at the surface has penetrated to more than 100 m. For a larger mountain such as the Matterhorn (cf. Section 4.4), this is only the uppermost layer, but in smaller ridges the entire temperature field is warming.

Future subsurface temperature fields as calculated in our simulations significantly deviate from stationary conditions and can be characterized as follows: Isotherms are bent upwards to lie more or less parallel to the surface (Figure 4.4, left). Then, they move rather uniformly towards the inner part of the mountain. Heat fluxes near the surface drastically increase and change their direction on the colder side of the mountain. This leads to a zone inside the mountain where heat flows towards it from two sides. For all scenarios and case studies (i.e., idealized and real topographies in the European Alps), no permafrost remains at the surface on south faces after 200 years. A significant frozen part, however, remains only a few decameters below the surface. These remaining permafrost bodies constantly warm up and the volume of warm permafrost (i.e., temperatures between about –2 and 0 °C) increases both in size and vertical extent. New equilibrium conditions (Figure 4.4, right) will only be reached after time periods of centuries to millennia, depending primarily on the geometry and size of the mountain.

As opposed to the results from simulations over long time periods of millennia (cf. previous section), the effect of energy consumption during phase change of ice contained in pore spaces is visible in these subsurface temperature fields and can amount up to 1 °C for a 200 year model run. Changes to the freezing characteristics assumed do not alter the size of the permafrost body but the temperature distribution of its warmer part (i.e., where phase transition takes place). A steeper unfrozen water content curve (or a smaller freezing range) leads to more homogenous temperature fields, smaller temperature gradients with depth, and hence, steeper temperature profiles (cf. *Publication IV*, Noetzli et al. 2008).

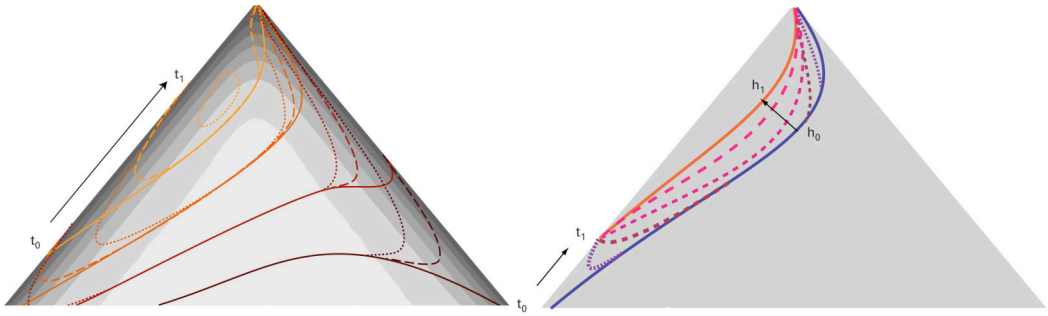

Figure 4.4. The evolution of different isotherms as caused by linearly increasing surface temperatures is displayed (or permafrost boundaries, when considering the different colors to be 0 °C isotherms for ridges of different elevation) (left). Gray shadings indicate the depth to which the signal penetrated and the temperature change experienced: the darker, the larger the change. On the right, the schematic evolution of an equilibrium permafrost body with the thickness h_0 is shown for a rise in surface temperature from t_0 to t_1 until it has reached a new equilibrium with the thickness h_1.

4.2.3 Effects of Topography

Although calculated future changes in GST do not vary to a large degree between locations of different topographic settings, two aspects are remarkable: 1) North faces generally react stronger to projected changes in atmospheric conditions, which can result in stronger warming of about 1 °C compared to south faces. 2) Sensitivity (i.e., ranges of GST changes) to the different scenario climate time series is higher for locations exposed to the south than for locations exposed to the north. Both aspects are mainly attributed to changes in global radiation and could, hence, not be demonstrated using incremental scenarios, where the only climate variable modified was air temperature.

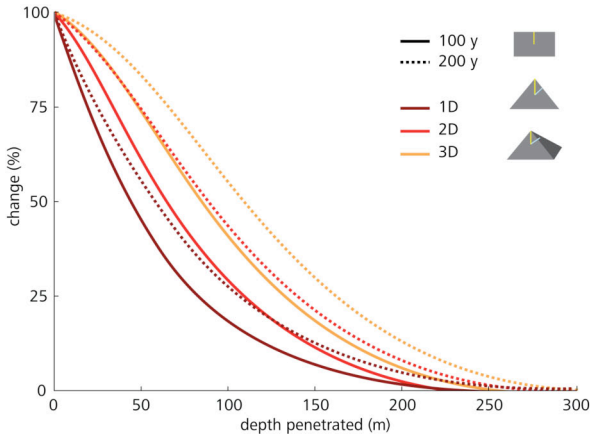

Figure 4.5. Percentage of a temperature signal at the surface that has penetrated to depth: This effect is shown for a one- (flat terrain), two- (ridge), and three-dimensional (pyramid) situation after 100 (solid lines) and 200 years (dotted lines). Values are plotted versus the shortest distance to the surface. From *Publication III* (Noetzli and Gruber in review).

Convex topography considerably accelerates the reaction of the subsurface thermal field to changing GST because of the effect of multi-lateral warming: The warming signal reaches the interior of a ridge or mountain from two and more sides, which results in a clear increase in the pace of subsurface warming compared to flat terrain. In Figure 4.5, the percentage of a surface temperature signal that has reached a certain depth is shown after 100 and 200 years for a flat plain (i.e., the one-dimensional example), a two-dimensional ridge, and a three-dimensional pyramid. The changes are considered along a vertical profile of 500 m in depth from the top of the geometry. The resulting temperature depressions for the two- and three-dimensional geometry, however, are not plotted versus the length of the profile, but versus the shortest distance of the profile to the surface (which is calculated as the depth along the profile times the cosine of the slope angle). In this way, multi-lateral warming causes the effect shown and not the fact that the distance to the surface is shorter than the depth of the profile. Figure 4.5 shows, for example, that 50% of the temperature signal has reached about 60 m after 200 years in flat situation. In the two-dimensional situation, it has already penetrated to about 90 m, and in the three-dimensional situation to about 115 m. The larger the surface of a convex geometry is compared to its horizontal projection, the larger is the increase in the pace of warming its interior. This effect is important for both, simulations over long time periods of several millennia and shorter periods in the order of decades or centuries, namely for the initialization process and for future scenarios.

4.3 Borehole Sites

4.3.1 Zugspitze: Planning of a Permafrost Borehole

As mentioned in the previous chapter, our modeling approach was applied for a preparatory study to select the location of a borehole for long-term permafrost monitoring on the Zugspitze (2,962 m a.s.l., Bavarian Alps, Germany) (Noetzli et al. 2006a). The project was initiated and financed by the Bavarian State Ministry of the Environment (Bayerisches Landesamt für Umwelt, LfU). The Zugspitze consists of an east-west oriented crest with a steep north-facing rock slope and a warmer and more gently sloped southern side. Based on results of the study, two boreholes were drilled from the southern slope of the summit area towards the northern part in August 2007 (Table 4.1, Figure 4.6), and first temperature measurements are now available. During drilling, ice was found as the northern part of the crest was reached in both boreholes, which confirms the occurrence of permafrost (pers. comm. A. v. Poschinger, LfU).

Table 4.1. Description of the eastern and western borehole on the Zugpitze Crest, Germany. #Therm. is the number of thermistors placed in the borehole.

	Angle/Length	Coordinates	# Therm.	Other
Borehole West Completed: 8.2007	20° / 44 m	RW: 4423582 HW:5254102 Z: 2922	25	Pierces the crest Extensometers
Borehole East Completed: 8.2007	25° / 58 m	RW: 4423583 HW:5254102 Z: 2922	3	Fibre-optic cable

Figure 4.6. Drilling on the Zugspitze in August 2007 (left) and the completed western borehole, which pierces the crest completely (right). Photos: www.stump.eu (accessed in March 2008).

Model simulations in the scope of the preparatory study were performed for equilibrium conditions, considering an isotropic and homogenous subsurface. MGST of the Zugspitze crest were computed for the period of 2000–2006 (based on climate data from the Zugspitze station; data source: Deutscher Wetterdienst). Results indicate permafrost existence only in roughly the top 500 m on the northern side of the crest, with a thickness of a few decameters (Figure 4.7). The permafrost limit is likely within the crest and steeply inclined. On the southern side, permafrost may be present in the top part and is probably discontinuous. Owing to the years from which climate data was taken, the temperatures of which clearly exceeded the average as compared to the previous decades, and the negligence of transient effects, the calculated permafrost extent is expected to be a minimal estimate and a second subsurface temperature field (*m2*) with 2 °C colder MGST was modeled to estimate a possible range of subsurface temperatures.

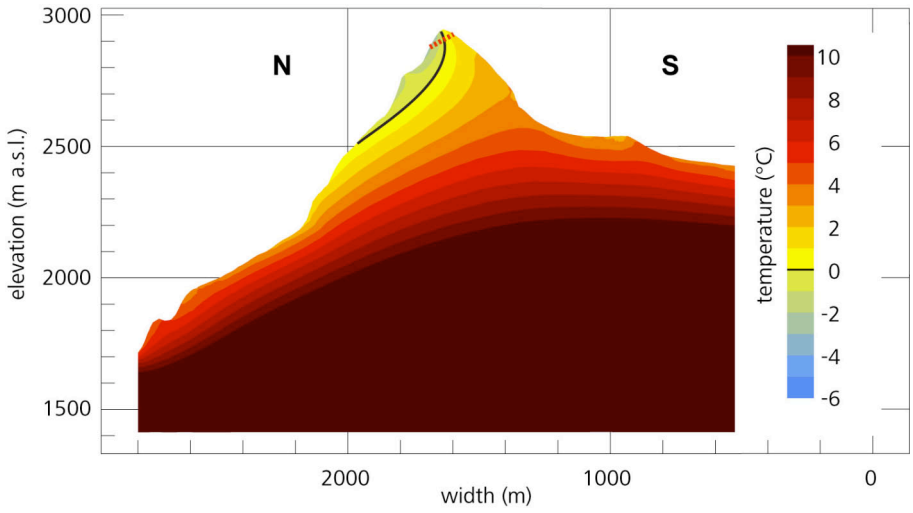

Figure 4.7. North-south cross section through the modeled temperature field of the Zugspitze crest at the borehole location. The 0 °C isotherm is shown by the black line and corresponds to the permafrost base. The red dashed line in the top of the ridge marks the position of the western borehole.

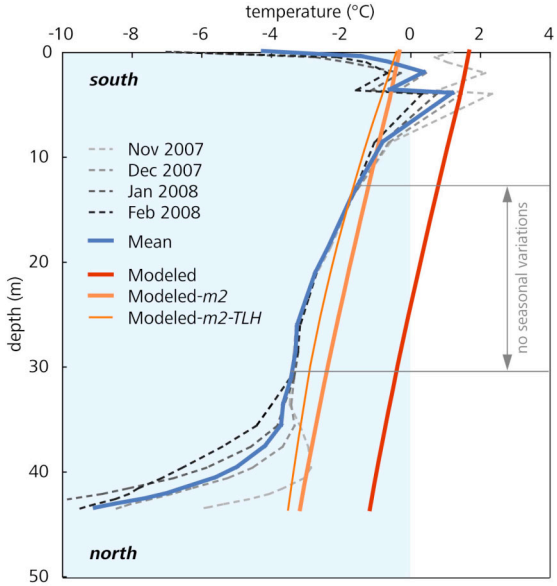

Figure 4.8. T(z) profiles measured in the western borehole in the Zugspitze crest compared with profiles extracted from modeled temperature fields. Borehole measurements are daily means for the first days of the months November 2007 to February 2008. In addition, the mean of the four profiles is displayed. *m2* is the corrected modeled temperature field, and *m2-TLH* is an additional run performed with initialization and latent heat effects considered.

Figure 4.8 depicts T(z) profiles for the modeled temperature field and first measured data in the western borehole for November 2007 to February 2008 (i.e., daily mean temperatures for each first day of the four months). As expected, the modeled temperature profile based on MGST 2000–2006 is too warm. The temperature profile of the corrected temperature field *m2* fits the measurements better, and is about 1 °C warmer than measured. To estimate the error produced by neglecting transient effects and latent heat in the preparatory study, we performed an additional model run *m2-TLH* using the initialization procedure developed in the scope of this work starting in 1850 (cf. *Publication III*, Noetzli and Gruber in review), and a porosity of 10%. Results from this simulation show still higher temperatures than measured, but differences are below 1 °C and in the range of 0.5 °C for the parts of the profile that are not subject to seasonal variations, namely between about 12 and 32 m of depth.

4.3.2 Schilthorn: Current and Future Subsurface Temperatures

A second comparison of modeling results with measured data was accomplished for the Schilthorn crest in the Bernese Alps, Switzerland, and is accounted in detail in *Publication IV* (Noetzli et al. 2008). Modeling was performed for a transient, homogeneous temperature field for a north-south cross crest profile and including the effects of latent heat. The modeled thermal regime of the Schilthorn crest can be characterized by a cold zone below the upper part of the northern slope, permafrost occurrence at shallow depth on the southern slope and in the lowest part of the northern slope, and rather homogeneous conditions below the lower part of the northern slope (Figure 4.9, left). These three zones can also be clearly distinguished in results from repeated geophysical measurements using ERT along the same profile (Hilbich et al. 2008, Noetzli et al. 2008). In contrast to ERT profiles, which mainly allow for a qualitative validation of the general pattern of temperature distribution, comparison with extracted T(z)-profiles at the borehole locations shows the accuracy of the modeled temperature values (see *Publication IV*, Noetzli et al. 2008). In general, the modeled profiles correspond to the measured data, i.e., modeled temperatures ranges are correct for the entire profiles (i.e., between 0 and –1.5 °C), temperature gradients with depth are small, and for both measured and modeled profiles the oblique borehole shows a slightly more curved profile. Temperatures of the modeled profile, however, are about 0.2 °C colder on average than the measured values and differences range up to 1 °C in the uppermost decameter.

We additionally modeled the scenario subsurface temperature field of the Schilthorn for the coming two centuries (Figure 4.9, right, not included in *Publication IV*). We used the same GST changes as in the transient simulations shown above, namely +3 °C/100y.

Results indicate no permafrost at the surface already in about 50 years, and a rapidly shrinking warm permafrost body inside the crest. In 200 years, no permafrost will remain in the Schilthorn crest according to modeling results. Even if surface temperature would only rise 2 °C, permafrost will most likely disappear in the Schilthorn crest in the next two centuries.

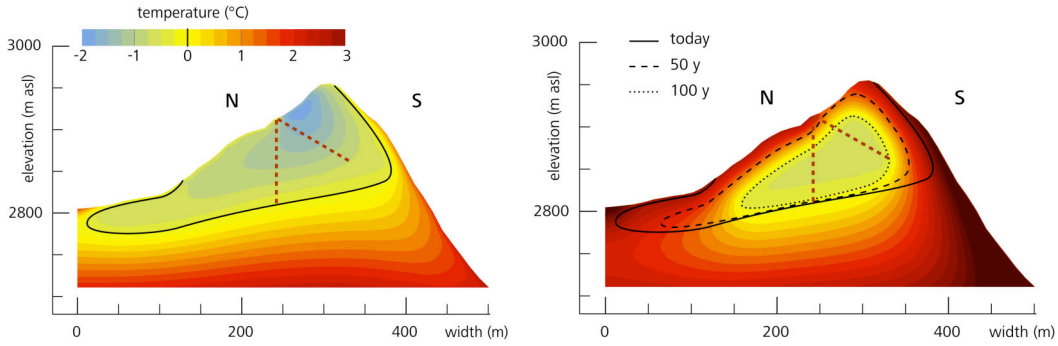

Figure 4.9. Modeled temperature distribution in the Schilthorn crest, Switzerland for today (left) and in 100 years (right). In addition, the 0 °C isotherms are displayed for today (black line), in 50 years (dashed line), and in 100 years (dotted line). Dashed red lines indicate the location of the two 100 m boreholes.

4.4 Case Study Matterhorn

The subsurface temperature field of the Matterhorn, where many rock falls have occured from its southern and eastern slopes in recent years, was simulated as a case study for real topography. With its distinctive three-dimensional geometry the Matterhorn constitutes a prime example for application of the modeling approach. Parts of the results presented in this section are included in *Publication III* (Noetzli and Gruber in review).

A north-south and a perpendicular east-west cross section through the resulting temperature field are shown in Figure 4.10. MGST were modeled based on climate time series from the high-alpine station Corvatsch (Data source Meteo Swiss), which is located in a similar inner alpine climate (Gruber et al. 2004b), and a 25 m DEM (DEM Level 2 by Swisstopo). For details on the modeling procedure see *Publication III* (Noetzli and Gruber in review). The extreme geometry of the Matterhorn leads to a three-dimensional subsurface temperature field with strong lateral heat fluxes from south towards north and smaller heat fluxes from east towards west. For present-day conditions the entire upper half of the mountain is modeled within permafrost, and warm permafrost zones are situated in the middle part of the south face and the lower part of the east face. In one century, permafrost is about to disappear on the south and east face and the warm permafrost zone will increase both in volume and vertical extent. In the scenario calculated for the coming 200 years,

nearly the entire near-surface layer of the Matterhorn will be in warm permafrost, in particular, the entire south and east face (down to nearly 100 m), the lower half of the north face, and the lower two thirds of the west face.

In recent years, a number of smaller rock falls have occurred on the Matterhorn. On July 15, 2003 around 1,000 m^3 detached from the Matterhorn East Ridge (Hörnligrat) at an elevation of about 3,500 m a.s.l. Similar events occurred near the south-west (Liongrat, at 3,800 m a.s.l.) and north-west (3,650 m a.s.l.) ridges in the same year, and again in 2006 (Liongrat, at 3,800 m a.s.l.). In at least two of the starting zones, massive ice was visible immediately after the event (Figure 2.5 and pers. comm. G. Mazzone, mountain guide, Zermatt). Surface temperatures of the starting zone on the Hörnligrat are in the range of about –1 to +1 °C and indicate warm permafrost conditions (Figure 4.11). The permafrost boundary runs vertical within the Hörnligrat. Similarly, the other starting zones are located within the areas where warm permafrost occurs today according to modeling results.

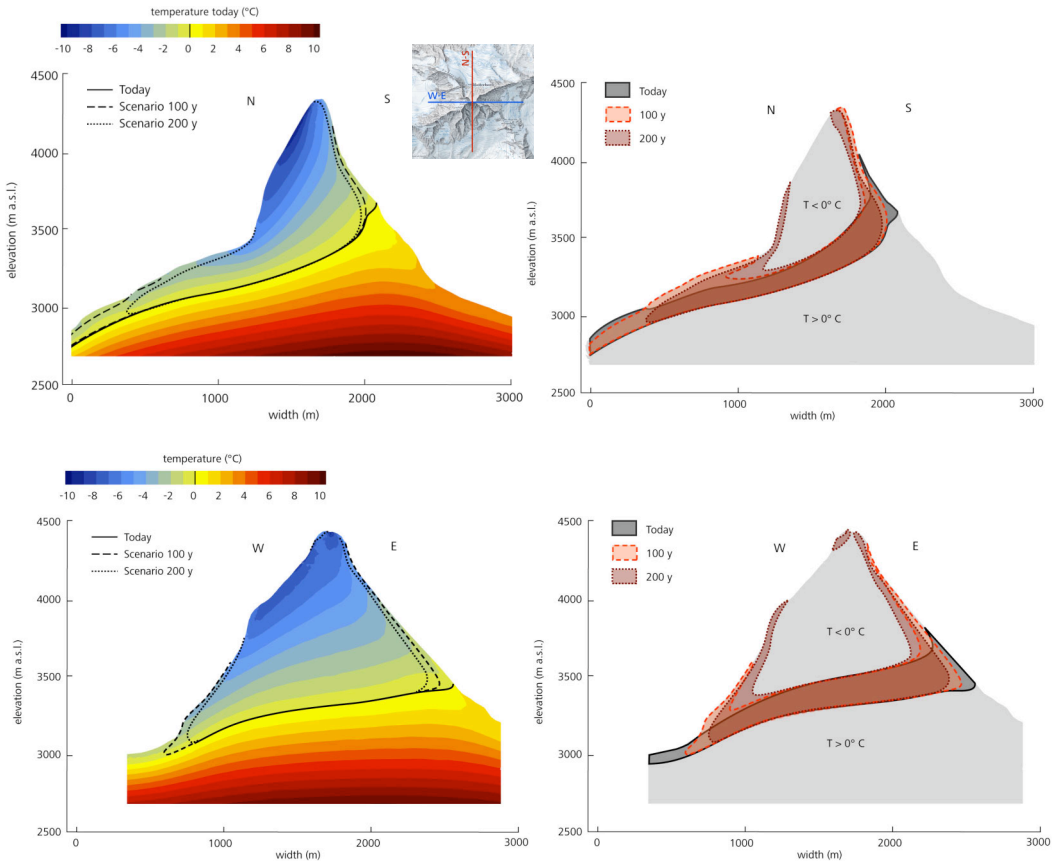

Figure 4.10. North-south (top) and east-west (below) cross section through the temperature field of the Matterhorn. On the left, the present-day temperature field is displayed, together with the permafrost boundary today, in 100 years, and in 200 years. On the right, the extent of the warm permafrost zone (i.e., temperatures between -2 and 0 °C) is depicted for the same time periods.

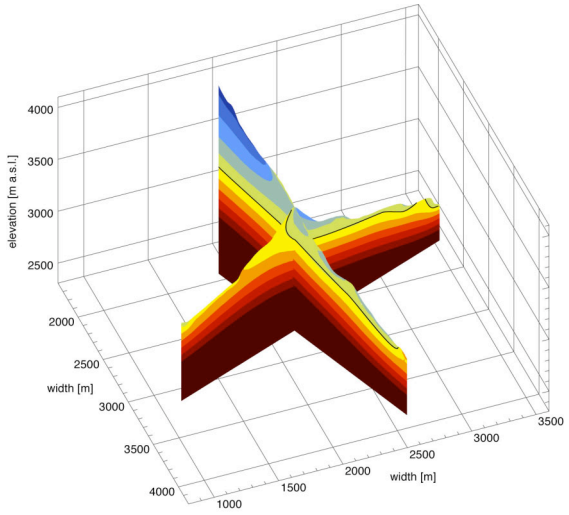

Figure 4.11. Slices through the temperature field of the Matterhorn at the rock fall starting zone on Hörnligrat, taken along and perpendicular to the ridge. The slices intersect at the rock fall starting zone.

In the scope of this thesis, we carried out simulations of the thermal conditions of a number of other rock fall starting zones, namely Jungfrau east ridge (CH, October 1937, 3,800 m a.s.l., south-east-exposed), Punta Thurwieser (I, September 2004, 3,600 m a.s.l., south-exposed), Les Drus (F, 1997, 2003, 2005, 3,200 m a.s.l., west-exposed), Dents Blanches (CH, October 2006, 2,600 m a.s.l., north-exposed). All starting zones were modeled within warm permafrost and/or close to the permafrost boundary. Interestingly, all events detached from ridges or ridge-like situations, where the subsurface thermal field is considerably modified by a warmer or colder mountain side nearby and strong lateral heat fluxes exist. Most events detached from the warmer side of the ridge or peak.

Chapter 5

General Discussion

In this chapter, we will summarize and link the discussions presented in the four research papers. The intention is to comprehensively discuss the modeling approach and the main findings of the thesis, and to point to their main implications in current mountain permafrost research. We will deal with the limitations of the modeling approach (e.g., due to processes that are not simulated) as well as the uncertainties associated with chosen values of ground properties, which is important for the interpretation of the results presented in the previous chapter. Finally, we reflect on the implications of the results in terms of permafrost mapping, interpretation of borehole temperature profiles, and slope stability.

5.1 Modeling Approach

The work conducted in this thesis is based on experimentation with a modeling procedure that combines results from RCMs, distributed surface energy balance in complex topography, and three-dimensional subsurface heat conduction. For the interpretation of the results, a number of uncertainties and limitations have to be kept in mind. These uncertainties relate to the representation of relevant processes in the model on the one hand and to assumptions of parameter values on the other hand, and are discussed below.

Since subsurface properties at depth in mountains are scarcely known, we approximated them by typical values found in literature. As shown in the sensitivity analysis, errors caused by uncertain values of thermal conductivity, heat capacity, and heat production increase with depth and length of the simulation, whereas errors caused by uncertainties in the content of subsurface ice and freezing characteristics of the material decrease.

Uncertainties in the ranges of GST changes are high for both, past and the future climate variations. Climate reconstructions generally agree well on the general pattern of climate fluctuations, whereas the absolute amplitude of the temperature variations varies signi-

ficantly (Esper et al. 2005). That is, uncertainties of absolute temperature values are larger than of patterns of initialized temperature fields. A temperature depression of –15 °C instead of –10 °C during the maximum of the last Ice Age, for example, leads to a difference of more than 1 °C at depth. As shown in *Publication II* (Salzmann et al. 2007a), the topographic setting influences the resulting GST change. Information that would allows us to simulate this effect for past climate variations, however, is not available and would require complete climate time series of the past millennium and more. For initialization runs we therefore assumed GST changes to follow changes in air temperatures. Uncertainties related to this simplification, however, are smaller than those related to the amplitudes of temperature fluctuations.

For future scenario calculations, we assumed the temperature to rise linearly instead of exponentially as typically proposed in climate change scenarios. This may slow down the warming compared to our model simulations. On the other hand, the temperature increase assumed here represents a mean change in GST of bedrock in Alpine terrain for different climate scenarios (Salzmann et al. 2007b) and is at the lower range of the scenarios presented for air temperature change by the IPCC (2007), where an increase twice as high is not considered unrealistic or extreme for the European Alps

Further, changes in surface cover (glacier extent, debris cover, snow pack, etc.) are not taken into account in our simulations, but can be essential for the evolution of surface and subsurface temperatures. Haeberli (1983) points to higher temperatures at the glacier base than on rock directly exposed to the atmosphere during past cold periods. That is, our approach overestimates paleoclimatic effects below previously glacier-covered areas. This is likely the case, for example, for the lower parts of the north and east side of the Matterhorn (cf. Section 4.4), which are still partly glacier-covered at present. Further, snow that remains in the roughness of steep bedrock may have a cooling effect on steep slopes even in summer (Gruber and Haeberli, 2007). Corresponding processes have been studied extensively (see Chapter 2.1.3), but the effect of snow on the subsurface thermal regime in steep rock has not yet been quantified.

Neglecting water circulation along the joint systems of bedrock is a serious limitation of our approach. For example, advective heat transfer along clefts can amplify subsurface heat transfer and lead to thaw corridors in permafrost, which substantially modify a purely conductive system. A number of observations in the hot summer of 2003 were attributed to heat transfer by moving water, since they cannot be explained by conduction alone. The active layer on the Schilthorn crest increased from about 4.5 m in the previous (and following) years to nearly 9 m (PERMOS 2007). Another example is the timing of several

rock falls that occurred in July and August, that is, before the maximum active layer thickness was reached around September. So far, however, these observations are limited to the uppermost layer and the summer season. Knowledge or observations of advective heat transfer at greater depth is hardly available.

The combination of the models is accomplished uni-directionally by using output from one model as input for the next. Full model coupling would allow for energy fluxes in the opposite direction and feedback mechanisms between atmosphere, surface, and subsurface. This may be important, for example, on the colder side in the topmost part of a steep ridge, where a considerable lateral heat flux from the warmer side may contribute to the surface energy balance. The feedback from a rock surface to the atmosphere is likely small since moisture content and correspondingly energy consumption due to evaporation are low.

Keeping in mind these uncertainties and simplifications, results from validation steps are encouraging and we consider the modeling approach suitable and promising for the simulation of transient subsurface temperature fields in alpine bedrock permafrost. As indicated by the results described in the previous chapter, such transient and three-dimensional modeling approaches are essential to the understanding and assessment of mountain permafrost distribution and, in particular, its evolution over time.

5.2 Interpretation of Results

Since a large part of the research conducted in this thesis is based on model experiments with idealized case studies, the question arises whether and how our findings can be transferred to natural and more complex situations. Based on the steps taken for model validation and despite the uncertainties listed above, we are confident that the main processes determining the subsurface temperature field in high mountains are represented in the modeling approach, and that value ranges (i.e., mean deviations in the range of 1–2 °C) as well as temperature distribution patterns (i.e., direction of heat fluxes, sign of temperature gradients) are calculated realistically. The results presented therefore demonstrate the three-dimensional character of mountain permafrost and its way to respond to changing climatic conditions. It has to be emphasized, however, that temperature fields in natural situations are more complex. Further, results presented in the case studies, although encouragingly consistent with field observations, may deviate from real situations depending on the uncertainties outlined above (e.g., glacier coverage, cf. previous section) as well as the quality of the input data.

We have demonstrated a significant acceleration of the reaction of subsurface temperatures to changing surface temperatures due to multi-lateral warming. Considering the virtual decoupling of mountains from the geothermal heat flux, the low ice content, and permafrost temperatures that are warm compared to those in high latitude permafrost, Alpine bedrock permafrost is particularly sensitive to changes in atmospheric conditions and prone to degradation. Expected changes for the next centuries result in hardly any remaining permafrost in steep slopes exposed to the south, large transient effects, and generally warmer mountains with temperature anomalies, which will eventually penetrate to great depth.

5.3 Implications for Permafrost Research

5.3.1 Mapping of Mountain Permafrost

Traditional two-dimensional maps, such as the one published by FOEN (2006), serve as indicators of potential permafrost occurrence based on the conditions at the surface, but do not provide sufficient information to comprehensively assess the distribution of mountain permafrost. It must be kept in mind that at locations outside permafrost but close to its boundary or adjacent to a colder slope, permafrost may be present at shallow depth. For a detailed permafrost assessment, e.g., for infrastructure planning or the re-analysis of rock fall starting zones, three-dimensional and transient modeling is required.

5.3.2 Interpretation of Borehole Profiles

Based on our modeling approach, we reproduced the current temperature profiles at both borehole sites investigated (Schilthorn and Zugspitze). Keeping in mind the uncertainties of the computation, namely the quality of the climate data, negligence of the snow cover, and the assumption of a homogeneous subsurface, results achieved are encouraging. Further, the modeling study has proven useful and appropriate for the planning of a borehole location in mountain permafrost.

The interpretation of borehole temperature profiles measured in mountain permafrost remains a delicate and very complex task, because topography not only complicates a stationary subsurface temperature field, but also modifies the size, pace, and direction of a surface temperature signal intruding into the ground. That is, based on the deviations from the stationary profile alone, the profile can only be interpreted in terms of the relative GST history, because equal deviations from the equilibrium profile at locations of the same depth but in different topographies are not necessarily the consequence of a GST variation of the

same amplitude. In addition, the surface and subsurface characteristics that vary both in space and time may also influence the transient behavior of the temperature field at depth.

Based on the experiences gained in the scope of this work, the reconstruction of past climates from borehole measurements in mountains is subject to a large number of uncertainties, which are typically larger than the climate variations during the time period that can be resolved in the upper 100 m (i.e., mainly the past century). Moreover, the accelerating influence of mountain topography results in a shorter memory of the subsurface thermal fields for past climate conditions than that in flat terrain. As a consequence, temperature monitoring in mountain permafrost boreholes is important for current and future thermal conditions and the provision of data to validate and enhance modeling approaches, rather than the detailed reconstruction of past climates.

The modeling tools presented in this thesis, however, are supportive for the interpretation of T(z) profiles measured in boreholes in mountain permafrost. Firstly, they enable the determination of the stationary temperature profile for a borehole location, which forms the basis for the understanding of a subsurface temperature field and its transient behavior. In a second step, using an initialization procedure the present-day temperature profile can be approached and results compared to measured data representing present-day conditions. In this way, confidence in the modeling and in the choice of parameters of GST changes and subsurface characteristics can be enhanced and a possible transient behavior can be modeled, which, however, does not necessarily have to be a correct representation of reality. For this purpose, long-term measurement time series over periods of a few decades are required and these must be compared to forward simulations over the same time period. This process would allow to reduce the system by one degree of freedom.

5.3.3 Slope Stability

Laboratory experiments, theoretical considerations, and observations of past rock fall events from permafrost slopes (cf. Chapters 2 and 4) indicate that permafrost degradation is an important transient stability factor for steep mountain rock walls, and that zones in warm permafrost are especially sensitive.

First results from three-dimensional analysis of the thermal conditions in rock fall starting zones also point to warm permafrost conditions and locations near the permafrost boundary and, hence, confirm these findings. All rock fall starting zones examined are located in ridge-like situations and failure occurred on the warmer side with no or warm permafrost at the surface. A thawing or migrating permafrost boundary, which runs more or less vertically in such a situation, may be especially sensitive and lead to rock failure. In order to make sound statements on the thermal conditions under which such instabilities develop,

however, systematic investigation of more rock fall starting zones and thorough temperature analysis in combination with other factors (geological, hydrological, etc.) is required (cf. Fischer and Huggel 2008).

The development of warm permafrost zones in the next two centuries was simulated for the example of the Matterhorn and results show a considerable increase in both volume and vertical extent. Warm permafrost zones are about to develop beyond historical precedence and new volumes of material will be subject to critical temperature ranges. Enlargement of these zones together with deeper degradation of permafrost increases the probability of large rock avalanches from permafrost slopes.

Chapter 6

Summary, Outlook, and Conclusion

On the basis of existing models for climate scenarios, surface energy balance in steep terrain, and subsurface heat conduction, this thesis developed a procedure for the transient three-dimensional modeling of mountain permafrost, focusing on model combination and handling of topography. Based on the modeling procedure, we conducted numerical experimentation and applied it to a number of idealized and real test cases. This chapter reviews steps taken and results gained in the scope of this thesis, discusses possible future research, and eventually presents the final conclusion.

6.1 Summary of Progress

The distribution and thermal conditions of mountain permafrost are governed by processes from global to local scale, which correspond to processes in the atmosphere, at the surface, and in the subsurface. In this study, we designed a modeling procedure that considers these three process domains: A distributed surface energy balance model specifically designed for extrapolation of energy fluxes to mountain terrain was combined with a three-dimensional subsurface heat conduction scheme via its upper boundary condition. The heat conduction scheme was successfully adapted to include mountain topography and latent heat effects. An initialization procedure was developed for transient model runs, since GST variations in the past have a significant influence on present-day subsurface temperatures in mountains. By comparison of initialized and stationary temperature fields we assessed and quantified the effect past climate variations have on current permafrost conditions in the Alps. For calculations of possible future subsurface temperature fields, we constructed and applied scenario climate time series from RCM results using a multi model approach and assessed possible GST changes in Alpine topography. Based on these GST changes, we estimated the resulting changes in the underground.

The modeling procedure was tested in three steps: 1) the surface energy balance model was validated based on measured near-surface rock temperatures, 2) modeled temperature fields were compared with borehole data and results from geophysical soundings, and 3) sensitivity studies were conducted to assess possible errors that arise from uncertainties in past and future GST changes and the lack of detailed knowledge of subsurface characteristics.

We defined the main topographic features of mountain topography and simplified them to geometric forms. Based on these geometric forms we performed numerical experimentation and systematically addressed the research questions stated in the first chapter. Numerical experiments included both, steady state and transient model runs. Eventually, the modeling procedure was applied to real topographies including a modeling study to designate the location of a new permafrost borehole, the characterization of current and possible future subsurface temperature fields at an existing borehole site, and first steps towards the re-analysis of rock fall starting zones located in permafrost.

6.2 Major Results

The results are described in detail in Chapter 4 and in *Publications I–IV*. The most important findings of this thesis are summarized in this section and organized according to the research questions stated in the first chapter.

How does steep topography influence the distribution of subsurface temperatures?

- A stationary temperature field in high mountains is for the most part controlled by spatially varying surface temperatures and geometric effects. Isotherms incline steeply and, in the uppermost parts of ridges or mountains, are nearly vertical. A strong lateral heat flux exists from the warmer to the colder sides of a mountain and, therefore, the thermal field in the upper part of mountains is virtually independent of the geothermal heat flux from the Earth's interior.
- Subsurface temperatures in steep mountains primarily change with the position between different mountain sides, rather than with the vertical distance from the surface as is typically the case in flat terrain.
- Permafrost may occur at locations where surface temperatures are positive even in equilibrium conditions. Irregularities at the surface, such as spurs, can induce local permafrost occurrence in an otherwise permafrost-free rock wall.

How big is the influence of past climate variations on present-day mountain permafrost conditions?

- Past GST variations that influence present-day permafrost temperatures in the Alps are the last glacial period and the major temperature fluctuations in the past millennium (i.e., the Medieval Warmth, the Little Ice Age, and recent warming).
- Transient effects exist in the interior of high-mountain peaks and amount to up to -3 °C at a distance of 500 m from the surface, i.e., for the innermost part of big mountains. For topographic features such as ridges or smaller mountains, however, the influence of past climate variations on the permafrost temperatures is small (i.e., below 1 °C).

How will permafrost in high mountains react to projected future changes in atmospheric conditions?

- An average rise in GST of 3.5 °C between the time periods 1982–2002 to 2071–2091 was calculated for steep Alpine rock walls. Variability in computed GST changes, however, is high and mainly caused by the variation of scenario climate time series used, rather than by topography.
- Subsurface temperature fields will considerably deviate from stationary conditions and can be characterized by long-term and deep reaching perturbations, generally rising temperatures, and an increase in both volume and vertical extent of warm permafrost zones. Heat fluxes near the surface will increase, and change their direction on northern slopes.
- In the next 200 years, roughly the top 250 m of the underground in steep rock slopes will be affected by changing atmospheric conditions. Except for northern expositions and the highest peaks of the European Alps, permafrost in the uppermost decameters will have disappeared or become warm in the next two centuries. At depth, however, substantial permafrost volumes will remain for centuries to millennia.
- Convex topography significantly accelerates the pace of a surface temperature signal entering into the subsurface, which, together with the fast reaction of the surface to changes in atmospheric conditions and the low ice content, makes bedrock permafrost in high mountains particularly sensitive to degradation

In addition, the following findings result from this thesis:

- In low porosity rock, the influence of latent heat on the temperature depressions caused by past GST variations can be neglected. In connection with future warming, however, latent heat effects delay the pace of permafrost degradation and influence the pattern of the subsurface temperature field.

- The distribution and extent of temperatures little below the melting point in warming permafrost is determined by the freezing characteristics of the subsurface material. A small freezing range leads to more homogenous temperature fields and T(z) profiles with small temperature gradients.
- Subsurface thermal regimes of the borehole locations on Schilthorn (Switzerland) and Zugspitze (Germany) are influenced by both topography and transient effects. Due to the cold northern slope and the recent 20th century warming permafrost exists on the southern side of both crests at shallow depth.
- Cross validation of subsurface temperature fields from modeling and ERT monitoring enables a sound and more reliable interpretation of the subsurface thermal field than based on only one of the two.

6.3 Future Research

The scientific work conducted in this context has left some questions and processes only partially answered or understood, and inspired several new ones. In the following section, we describe further research that might be conducted to address them. First, we concentrate on possible enhancements of the modeling procedure and secondly, on possible future applications of it.

Extension of the Modeling Procedure

Addressing the limitations of the modeling procedure listed in Section 5.1 may enhance our modeling procedure. This includes the coupling or integration of a snow heat transfer module, full model coupling, and the integration of surface cover types such as glaciers or ice faces. Full model coupling means that feedback mechanisms of energy fluxes are accounted for. This is hardly feasible for impact models and RCMs at present. For the coupling of TEBAL with the three-dimensional heat conduction scheme this could be accomplished, for example, by exchanging the ground temperature at a certain depth for each time step taken in the simulation. That is, for each time step, the energy balance is calculated, the resulting temperature is set in the three-dimensional heat conduction scheme at a certain depth (which is not significantly influenced by lateral heat fluxes), and re-extracted from there after the heat conduction equation has been solved. The benefit of such coupling, however, has not yet been assessed.

A snow module is required to compute reliable upper boundary conditions of the heat transfer model for less steep slopes (e.g., the Schilthorn), since a snow cover considerably alters GSTs, which has been studied extensively for flat terrain (e.g., Keller and

Gubler 1993, e.g., Zhang et al. 2001). Further, the thermal effect of a thin snow cover remaining in parts of steep rock walls, which is hardly known at present, could be assessed based on such a model. Corresponding measurements are integrated in the scope of the PERMOS network and provide data for validation.

In this study, the modeling approach has been applied and validated for use of long-term evolution of permafrost at greater depth than the ZAA. An application of the model using shorter time scales and higher mesh resolution in the uppermost meters could allow for the simulation of seasonal cycles, which may be important, for example, for the timing or triggering of smaller rock fall events as observed in summer 2003 or locations with considerable seasonal freeze/thaw cycles, which may lead to a thermal offset.

Mapping Alpine Permafrost

The results point to significant permafrost occurrence below locations where GST is positive, which is not considered in traditional two-dimensional maps. Signatures that point to probability or depth ranges of deeper permafrost occurrence could indicate this and supplement existing maps and mapping approaches. A possible way could be to establish rules for permafrost occurrence at shallow depth based on the distance to permafrost boundary and colder mountain slopes. In this way, results from complex three-dimensional modeling may be adapted for models of reduced complexity.

In general, the modeling approach and corresponding rules for two-dimensional mapping (cf. above) help to better assess distribution and extent of mountain permafrost occurrence, as well as its possible changes in the future, since topographic three-dimensional or transient effects cannot be estimated based on traditional permafrost mapping tools alone.

Influence of Surface and Subsurface Properties

Changing glacier cover or disappearing ice faces influence the subsurface temperature field because they substantially alter the ground surface temperature at their base (Ludwig 2003). Resulting thermal consequences on the subsurface temperature pattern and paleoclimatic effects have not yet been systematically investigated and quantified. Similarly, the thermal effects of debris or a thin snow cover on steeper rock walls has to be analyzed. Model experiments and corresponding measurements may provide insight into their sensitivity and relevance for the subsurface thermal regime.

A substantial lack of knowledge relates to the subsurface characteristics in steep rock and their temporal and spatial variability. This could be improved by field measurements and sensitivity studies, as well as by their combination. Here, the joint interpretation of model results with data from geophysical monitoring (Hilbich et al. 2008, Krautblatter and

Hauck 2007, Noetzli et al. 2008) is promising. This approach may also be valuable for the provision of quantitative input data for better representation in the model. For example, unfrozen water or ice-contents as determined by repeated geophysical soundings (Hauck et al. 2008), can provide valuable information, which is important for the transient modeling of borehole profiles. As shown in *Publication IV* (Noetzli et al. 2008), modeled temperature fields can also help to gain confidence in results from field measurements. The range of thermal effects from variable subsurface properties (e.g., variable lithologies with different thermal conductivities, variable ice content) and local inhomogeneities (e.g., ice-filled cracks, or cracks that are ice-filled in winter, but not in summer) can be addressed in case studies using the presented modeling procedure.

Periglacial Rock Fall Events

By re-analysis of rock fall starting zones, the thermal conditions before and at the time of the event may be estimated and improve knowledge of the temperature conditions under which instabilities developed. Based on results, topographic or thermal situations that are especially sensitive to slope instabilities related to permafrost degradation as well as their location, extent, and future development may be determined.

6.4 Conclusion

In this thesis, several steps were successfully taken towards the understanding of the transient and three-dimensional character of mountain permafrost below the near-surface layer on the one hand, and the integrative modeling of involved processes on the other hand. Mountain permafrost distribution at depth has a three-dimensional character with steeply inclined isotherms and lateral heat fluxes, which minimizes the influence of the geothermal heat flux from the Earth's interior. Due to multi-lateral warming in steep topography, subsurface temperatures react relatively fast to changes in surface thermal conditions. Effects from past climate variations exist, and significant transient effects evolve from recent and projected future warming. Modeling tools as presented in this study are a prerequisite for the comprehensive analysis of distribution and evolution of mountain permafrost and bear potential for further development and application. For the near future, important research topics are the influence of surface and subsurface characteristics that vary in time and space, the application of the modeling procedure for the interpretation of temperatures recorded in boreholes in complex topography, and the re-analysis of past rock falls events to learn about the thermal and topographic conditions under which they may have developed.

Bibliography

Akagawa, S., and Fukuda, M. 1991. Frost heave mechanism in welded tuff. *Permafrost and Periglacial Processes*, 2, 301–309.

Allen, S., Owens, I., and Huggel, C. 2008. A first estimate of mountain permafrost distribution in the mount cook region of New Zealand's Southern Alps. *Proceedings of the 9th International Conference on Permafrost*, Fairbanks, US.

Anderson, D.M., and Tice, A.R. 1972. Predicting unfrozen water contents in frozen soils from surface area measurements. *Highway Research Record*, 393, 12–18.

Bader, H.P., and Weilenmann, P. 1992. Modeling temperature distribution, energy and mass flow in a (phase changing) snowpack. I Model and case studies. *Cold Regions Science and Technology*, 20, 157–181.

Barsch, D. 1969. Permafrost in der oberen subnivalen Stufe der Alpen. *Geographica Helvetica*, 24, 10–12.

Barsch, D. 1971. Rockglacier and ice-cored moraines. *Geografiska Annaler*, 53, 203–206.

Barsch, D., and Caine, N. 1984. The nature of mountain geomorphology. *Mountain Research and Development*, 4, 287–298.

Beniston, M., Diaz, H.F., and Bradley, R.S. 1997. Climatic change at high elevation sites: An overview. *Climatic Change*, 36, 233–251.

Brown, R.J.E., and Péwé, T.L. 1973. Distribution of permafrost in North America and its relationship to the environment, a review 1963–1973. *Proceedings of the 2nd International Conference on Permafrost. Proceedings*, Yakutsk, USSR, 71–100.

Brun, E., Martin, E., Simon, V., Gendre, C., and Coleou, C. 1989. An energy and mass model of snow cover suitable for operational avalanche forecasting. *Journal of Glaciology*, 35, 333–342.

Carslaw, H.S., and Jaeger, J.C. 1959. *Conduction of heat in solids*, Clarendon Press, Oxford, 510 pp.

Cermák, V., and Rybach, L. 1982. Thermal conductivity and specific heat of minerals and rocks. In: *Landolt-Börnstein Zahlenwerte und Funktionen aus Naturwissenschaften und Technik, Neue Serie, Physikalische Eigenschaften der Gesteine (V/1a)*, Edited by G. Angeneister, Springer, Berlin, 305–343.

Chinn, T.J., McSaveney, M.J., and McSaveney, E.R. 1992. *The Mount Cook rock avalanche of 14 December 1991*, Institute of Geological and Nuclear Sciences.

Corripio, J.G. 2003. Vectorial algebra algorithms for calculating terrain parameters from DEMs and solar radiation modelling in mountainous terrain. *International Journal of Geographical Information Science*, 17, 1–23.

Davies, M.C.R., Hamza, O., and Harris, C. 2001. The effect of rise in mean annual temperature on the stability of rock slopes containing ice-filled discontinuities. *Permafrost and Periglacial Processes*, 12, 137–144.

Deline, P. 2001. Recent Brenva rock avalanches (Valley of Aosta): new chapter in an old story? *Geografia Fisica e Dinamica Quaternaria*, 55–63.

Dramis, F., Govi, M., Guglielmin, M., and Mortara, G. 1995. Mountain permafrost and slope instability in the Italian Alps: the Val Pola landslide. *Permafrost and Periglacial Processes*, 6, 73–82.

Erbs, D.G., Klein, S.A., and Duffie, J.A. 1982. Estimation of the diffuse radiation fraction for hourly, daily and monthly average global radiation. *Solar Energy*, 28, 293–304.

Esper, J., Wilson, R.J.S., Frank, D.C., Moberg, A., Wanner, H., and Luterbacher, J. 2005. Climate: past ranges and future changes. *Quarternary Science Reviews*, 24, 2164–2166.

Etzelmüller, B., Farbrot, H., Gudmundsson, A., Humlum, O., Tveito, O.E., and Björnsson, H. 2007. The regional distribution of mountain permafrost in Iceland. *Permafrost and Periglacial Processes*, 18, 185–199.

Etzelmüller, B., and Hoelzle, M. 2001. Mapping and distribution modelling of mountain permafrost. *Norwegian Journal of Geography*, 55, 185.

Etzelmüller, B., Hoelzle, M., Heggem, E.S.F., Isaksen, K., Mittaz, C., Vonder Mühll, D., Ødegård, R.S., Haeberli, W., and Sollid, J.L. 2001. Mapping and modelling the occurrence and distribution of mountain permafrost. *Norwegian Journal of Geography*, 55, 186–194.

Evans, S.G., and Clague, J.J. 1988. Catastrophic rock avalanches in glacial environment. *Proceedings of the Fifth International Symposium on Landslides*, Lausanne, Switzerland, July 10–15, 1153─1158.

Fischer, L., and Huggel, C. 2008. Methodical design for stability assessments of permafrost affected high-mountain rock walls. *Proceedings of the 9th International Conference on Permafrost*, Fairbanks, US, 439–444.

Fischer, L., Kaeaeb, A., Huggel, C., and Noetzli, J. 2006. Geology, glacier changes, permafrost and related slope instabilities in a high-mountain rock wall: Monte Rosa east face, Italian Alps. *Natural Hazards and Earth System Sciences*, 6, 761–772.

FOEN 2006, Hinweiskarte Permafrost Schweiz, Federal Office for the Environment, Bern.

Frauenfelder, R., Haeberli, W., Hoelzle, M., and Maisch, M. 2001. Using relict rockglaciers in GIS-based modelling to reconstruct Younger Dryas permafrost distribution patterns in the Err-Julier area, Swiss Alps. *Norwegian Journal of Geography*, 55, 195–202.

French, H.M. 2007. *The periglacial environment*. 3rd ed., John Wiley and Sons Ltd, Chichester, UK, 458 pp.

Frey, E.A. 2007. *Messung und Modellierung der Basistemperatur der alpinen Schneedecke*. MSc Thesis, University of Zurich, Zurich, 95 pp.

Gertseema, M., Clague, J.J., Schwab, J.W., and Evans, S.G. 2006. An overview of recent large catastrophic landslides in northern British Columbia, Canada. *Engineering Geology*, 83, 120–143.

Gold, L.W., and Lachenbruch, A.H. 1973. Thermal conditions in permafrost – a review of North American literature. *Proceedings of the 2nd International Conference on Permafrost. Proceedings*, Yakutsk, USSR, 3–25.

Goodrich, L.E. 1978. Some results of a numerical study of ground thermal regimes. *Proceedings of the 3rd International Conference on Permafrost. Proceedings*, Edmonton, Canada, 30–34.

Gruber, S. 2005. *Mountain permafrost: Transient spatial modelling, model verfication and the use of remote sensing*. PhD Thesis, University of Zurich, Zurich.

Gruber, S., and Haeberli, W. 2007. Permafrost in steep bedrock slopes and its temperature-related destabilization following climate change. *Journal of Geophysical Research*, 112, doi:10.1029/2006JF000547.

Gruber, S., and Hoelzle, M. 2001. Statistical modelling of mountain permafrost distribution: local calibration and incorporation of remotely sensed data. *Permafrost and Periglacial Processes*, 12, 69–77.

Gruber, S., and Hoelzle, M. 2008. The cooling effect of coarse blocks revisited. *Proceedings of the 9th International Conference on Permafrost*, Fairbanks, US, 557–562.

Gruber, S., Hoelzle, M., and Haeberli, W. 2004a. Permafrost thaw and destabilization of Alpine rock walls in the hot summer of 2003. *Geophysical Research Letters*, 31, doi:10.1029/2004GL0250051.

Gruber, S., Hoelzle, M., and Haeberli, W. 2004b. Rock wall temperatures in the Alps: Modelling their topographic distribution and regional differences. *Permafrost and Periglacial Processes*, 15, 299–307.

Gruber, S., King, L., Kohl, T., Herz, T., Haeberli, W., and Hoelzle, M. 2004c. Interpretation of geothermal profiles perturbed by topography: The Alpine permafrost boreholes at Stockhorn Plateau, Switzerland. *Permafrost and Periglacial Processes*, 15, 349–357.

Gruber, S., Peter, M., Hoelzle, M., Woodhatch, I., and Haeberli, W. 2003. Surface temperatures in steep alpine rock faces – A strategy for regional-scale measurement and modelling. *Proceedings of the 8th International Conference on Permafrost, Proceedings*, Zürich, 325–330.

Guymon, G.L., and Hromadka, T.V. 1977. *Finite element model of transient heat conduction with isothermal phase change (two and three dimensional).* CRREL Spec. Rep., Corps of Engineers, U.S. Army., Hanover, NH, USA., 163 pp.

Guymon, G.L., Hromadka, T.V., and Berg, R.L. 1984. Two-Dimensional Model of Coupled Heat and Moisture Transport in Frost-Heaving Soils. *Journal of Energy Resources Technology-Transactions of the Asme*, 106, 336–343.

Haeberli, W. 1973. Die Basis-Temperatur der winterlichen Schneedecke als möglicher Indikator für die Verbreitung von Permafrost in den Alpen. *Zeitschrift für Gletscherkunde und Glazialgeologie*, 9, 221–227.

Haeberli, W. 1975. *Untersuchungen zur Verbreitung von Permafrost zwischen Flüelapass und Piz Grialetsch (Graubünden)*. Mitteilungen der VAW-ETH Zürich ed., ETH Zürich, Zürich, 221 pp.

Haeberli, W. 1983. Permafrost-glacier relationships in the Swiss Alps - today and in the past. *Proceedings of the 4th International Conference on Permafrost. Proceedings*, Fairbanks, Alaska, 415–420.

Haeberli, W. 1992a. Construction, environmental problems and natural hazards in periglacial mountain belts. *Permafrost and Periglacial Processes*, 3, 111–124.

Haeberli, W. 1992b. Possible effects of climatic change on the evolution of Alpine permafrost. In: *Greenhouse-impact on cold-climate ecosystems and landscapes*, Edited by M. Boer and E. Koster, Catena Supplement, 23–35.

Haeberli, W., and Burn, C.R. 2002. Natural hazards in forests: glacier and permafrost effects as related to climate change. In: *Environmental Change and Geomorphic Hazards in Forests*, Edited by R. C. Sidle, CABI Publishing, Wallingford/New York, 167–202.

Haeberli, W., Cheng, G., Gorbunov, A.P., and Harris, S.A. 1993. Mountain permafrost and climatic change. *Permafrost and Periglacial Processes*, 4, 165–174.

Haeberli, W., Hallet, B., Arenson, L., Elocin, R., Humlum, O., Kääb, A., Kaufmann, V., Ladanyi, B., Matsuoka, N., Springman, S., and Vonder Muehll, D. 2006. Permafrost creep and rock glacier dynamics. *Permafrost and Periglacial Processes*, 17, 189–214.

Haeberli, W., Huggel, C., Kääb, A., Zgragggen-Oswald, S., Polkvoj, A., Galushkin, I., Zotikov, I., and Osokin, N. 2004. The Kolka-Karmadon rock/ice slide of 20 September 2002: an extraordinary event of historical dimensions in North Ossetia, Russian Caucasus. *Journal of Glaciology*, 50, 533–546.

Haeberli, W., Wegmann, M., and Vonder Mühll, D. 1997. Slope stability problems related to glacier shrinkage and permafrost degradation in the Alps. *Eclogae Geologicae Helvetiae*, 90, 407–414.

Haenel, R., Rybach, L., and L., S. 1988. Fundamentals of geothermics. In: *Handbook of terrestrial heat-flow density determination*, Edited by R. Haenel, et al., kluwer Academic Pub., 9–57.

Handschin, T. 2007. *Felsstuerze im Hitzesommer 2003 – Analyse und Modellierung thermischer Bedingungen*. MSc Thesis, University of Zurich, Zurich, 81 pp.

Hanson, S., and Hoelzle, M. 2004. The thermal regime of the active layer at the Murtèl rock glacier based on data from 2002. *Permafrost and Periglacial Processes*, 15, 273–282.

Harris, C., Davies, M.C.R., and Etzelmüller, B. 2001a. The assessment of potential geotechnical hazards associated with mountain permafrost in a warming global climate. *Permafrost and Periglacial Processes*, 12, 145–156.

Harris, C., Haeberli, W., Vonder Mühll, D., and King, L. 2001b. Permafrost monitoring in the high mountains of Europe: the PACE project in its global context. *Permafrost and Periglacial Processes*, 12, 3–11.

Harris, C., Rea, B., and Davies, M. 2001c. Scaled physical modelling of mass movement processes on thawing slopes. *Permafrost and Periglacial Processes*, 12, 125–135.

Harris, C., Vonder Mühll, D., Isaksen, K., Haeberli, W., Sollid, J.L., King, L., Holmlund, P., Dramis, F., Guglielmin, M., and Palacios, D. 2003. Warming permafrost in European mountains. *Global and Planetary Change*, 39, 215–225.

Harris, N.H., and Chapman, D.S. 1997. Borehole temperatures and a baseline for 20th Century global warming estimates. *Science*, 275, 1618–1621.

Harris, S.A., and Pedersen, D.E. 1998. Thermal regimes beneath coarse blocky material. *Permafrost and Periglacial Processes*, 9, 107–120.

Hauck, C. 2001. *Geophysical methods for detecting permafrost in high mountains*. PhD Thesis, ETH-Zürich, Zürich, 204 pp.

Hauck, C., Bach, M., and Hilbich, C. 2008. A 4-phase model to quantify subsurface ice and water content in permafrost regions based on geophysical datasets. *Proceedings of the 9th International Conference on Permafrost*, Fairbanks, US, 675–680.

Hilbich, C., Hauck, C., Hoelzle, M., Scherler, M., Schudel, L., Voelksch, I., Vonder Muehll, D., and Maeusbacher, R. 2008. Monitoring mountain permafrost evolution using electrical resistivity tomography: A 7-year study of seasonal, annual, and long-term variations at Schilthorn, Swiss Alps. *Journal of Geophysical Research*, 113, doi:10.1029/2007JF000799.

Hoelzle, M. 1994. *Permafrost und Gletscher im Oberengadin. Grundlagen und Anwendungsbeispiele für automatisierte Schätzverfahren*. PhD Thesis, ETH Zürich, Zürich, 119 pp.

Hoelzle, M., and Gruber, S. 2008. Borehole and Ground Surface Temperatures and their Relationship to Meteorological Conditions in the Swiss Alps. *Proceedings of the 9th International Conference on Permafrost*, Fairbanks, US, 723–728.

Hoelzle, M., and Haeberli, W. 1995. Simulating the effects of mean annual air temperature changes on permafrost distribution and glacier size. An example from the Upper Engadin, Swiss Alps. *Annals of Glaciology*, 21, 400–405.

Hoelzle, M., Haeberli, W., and Keller, F. 1993. Application of BTS-measurements for modelling permafrost distribution in the Swiss Alps. *Proceedings of the 6th International Conference on Permafrost. Proceedings*, Beijing, China, 272–277.

Hoelzle, M., Haeberli, W., and Stocker-Mittaz, C. 2003. Miniature ground temperature data logger measurements 2000-2002 in the Murtèl-Corvatsch area. *Proceedings of the 8th International Conference on Permafrost, Proceedings*, Zürich, 419–424.

Hoelzle, M., Mittaz, C., Etzelmüller, B., and Haeberli, W. 2001. Surface energy fluxes and distribution models of permafrost in European mountain areas: an overview of current developments. *Permafrost and Periglacial Processes*, 12, 53–68.

Huang, S., Pollak, H.N., and Shen, P.Y. 2000. Temperature trends over the last five centuries reconstructed from borehole temperatures. *Nature*, 403, 756-758.

Huggel, C., Kääb, A., Haeberli, W., and Krummenacher, B. 2004. Regional scale GIS-models for assessment of hazards from glacier lake outbursts: evaluation and application in the Swiss Alps. *Natural Hazards and Earth System Sciences*, 3, 647–662.

Huggel, C., Oswald, S., Haeberli, W., Kääb, A., Polkvoj, A., Galushkin, I., and Evans, S.G. 2005. The 2002 rock/ice avalanche at Kolka/Karmadon, Russian Caucasus: assessment of extraordinary avalanche formation and mobility, and application of QuickBird satellite imagery. *Natural Hazards and Earth System Sciences*, 5, 173–187.

Humlum, O. 1997. Active layer thermal regime at three rock glaciers in Greenland. *Permafrost and Periglacial Processes*, 8, 383–408.

IPCC 2001. *Climate change 2001: The scientific basis. Contribution of working group I to the third assessment report of the Intergovernmental Panle on Climate Change*, Cambridge University Press, Cambridge and New York, 881 pp.

IPCC 2007. *Climate Change 2007: The Physical Science Basis. Contribution of Working Group I to the Fourth Assessment Report of the Intergovernmental Panel on Climate Change*, Cambridge University Press, Cambridge, United Kingdom and New York, 996 pp.

Isaksen, K., Vonder Mühll, D., Gubler, H., Kohl, T., and Sollid, J.L. 2000. Ground surface temperature reconstruction based on data from a deep borehole in permafrost at Janssonhaugen, Svalbard. *Annals of Glaciology*, 31, 287–294.

Jordan, R. 1991. *A one-dimensional temperature model for a snow cover: Technical documentation for SNTHERM.89.*, US Army Cold Regions Research and Engineering Laboratory, Hanover, NH, USA.

Keller, F. 1992. Automated mapping of mountain permafrost using the program PERMAKART within the Geographical Information System ARC/INFO. *Permafrost and Periglacial Processes*, 3, 133–138.

Keller, F. 2003. *Kurzbericht über die Steinschlagereignisse im heissen Sommer 2003 im Bergell (Project report on rock fall 2003 to the canton Graubünden)*, Institut für Tourismus und Landschaft (ITL), Academia Engiadina, Samedan. Switzerland.

Keller, F., Frauenfelder, R., Gardaz, J.-M., Hoelzle, M., Kneisel, C., Lugon, R., Phillips, M., Reynard, E., and Wenker, L. 1998. Permafrost map of Switzerland. *Proceedings of the 7th International Conference on Permafrost. Proceedings*, Yellowknife, Canada, 557–562.

Keller, F., and Gubler, H.U. 1993. Interaction between snow cover and high mountain permafrost, Murtèl-Corvatsch, Swiss Alps. *Proceedings of the 6th International Conference on Permafrost. Proceedings*, Beijng, China, 332–337.

Keusen, H.R., and Haeberli, W. 1983. Site investigation and foundation design aspects of cable car construction in Alpine permafrost at the "Chli Matterhorn", Wallis, Swiss Alps. *Proceedings of the 4th International Conference on Permafrost. Proceedings*, Fairbanks, Alaska, 601–605.

King, L., and Kalisch, A. 1998. Permafrost distribution and implications for construction in the Zermatt area, Swiss Alps. *Proceedings of the 7th International Conference on Permafrost. Proceedings*, Yellowknife, Canada, 569–574.

Kohl, T. 1999. Transient thermal effects at complex topographies. *Tectonophysics*, 306, 311–324.

Kohl, T., and Hopkirk, R.J. 1995. ‚FRACTure' a simulation code for forced fluid flow and transport in fractured porous rock. *Geothermics*, 24, 345–359.

Kohl, T., Signorelli, S., and Rybach, L. 2001. Three-dimensional (3-D) thermal investigation below high Alpine topography. *Physics of the Earth and Planetary Interiors*, 126, 195–210.

Konzelmann, T., Van de Wal, R.S.W., Greuell, W., Binanja, R., Henneken, E.A.C., and Abe-Ouchi, A. 1994. Parameterization of global and longwave incoming radiation for the Greenland Ice Sheet. *Global and Planetary Change*, 9, 143–164.

Korup, O. 2005. Distribution of landslides in southwestern New Zealand. *Landslides*, 2, 43–51.

Krautblatter, M., and Hauck, C. 2007. Electrical resistivity tomography monitoring of permafrost in solid rock walls. *Journal of Geophysical Research*, 112, doi:10.1029/2006JF000546.

Kukkonen, I.T., and Safanda, J. 2001. Numerical modelling of permafrost in bedrock in northern Fennoscandia during the Holocene. *Global and Planetary Change*, 29, 259–273.

Lachenbruch, A.H., Cladouhos, T.T., and Saltus, R.W. 1988. Permafrost temperatures and the changing climate. *Proceedings of the 5th International Conference on Permafrost. Proceedings*, Trondheim, Norway, 9–17.

Lachenbruch, A.H., and Marshall, B.V. 1986. Changing climate: geothermal evidence from permafrost in the Alaskan Arctic. *Science*, 234, 689–696.

Lehning, M., Bartelt, P.B., Brown, R.L., Fierz, C., and Satyawali, P. 2002. A physical SNOWPACK model for the Swiss Avalanche warning services. Part III: Meteorological boundary conditions, thin layer formation and evaluation. *Cold Regions Science and Technology*, 35, 169─184.

Lewkowicz, A.G., and Bonnaventure, P.P. 2008. Interchangeability of mountain permafrost probability models, Northwest Canada. *Permafrost and Periglacial Processes*, 19, 49–62.

Lewkowicz, A.G., and Ednie, M. 2004. Probility mapping of mountain permafrost using the BTS method, wolf Creek, Yukon Territory, Canada. *Permafrost and Periglacial Processes*, 15, 67–80.

Ludwig, F. 2003. *Variable Oberflächenbedingungen als Ursache der Temperaturverteilung im Untergrund alpiner Permafrostgebiete - Limitationen der Klimarekonstruktion aus Bohrlochtemperaturprofilen im Permafrost*. MSc Thesis, Justus-Liebig University, Giessen, 62 pp.

Luethi, M., and Funk, M. 2001. Modelling heat flow in a cold, high-altitude glacier: interpretation of measurements from Colle Gnifetti, Swiss Alps. *Journal of Glaciology*, 47, 314–324.

Luetschg, M. 2004. *A model and field analysis of the interaction between snow cover and Alpine permafrost*. PhD Thesis, University of Zurich, Zurich, 258 pp.

Lunardini, V.J. 1991. *Heat transfer with freezing and thawing.* Developments in Geotechnical Engineering, CRREL, U.S. Army Corps of Engineers, Hanover, NH, USA.

Luterbacher, J., Dietrich, D., Xoplaxi, E., Grosjean, M., and Wanner, H. 2004. European seasonal and annual temperature variability, trends and extremes since 1500. *Science*, 303, 1499–1503.

Mittaz, C., Imhof, M., Hoelzle, M., and Haeberli, W. 2002. Snowmelt evolution mapping using an energy balance approach over an alpine terrain. *Arctic, Antarctic and Alpine Research*, 34, 264–281.

Mottaghy, D., and Rath, V. 2006. Latent heat effects in subsurface heat transport modeling and their impact on paleotemperature reconstructions. *Geophysical Journal International*, 164, 236–245.

Murton, J.B., Coutard, J.-P., Lautridou, J.P., Ozouf, J.C., Robinson, D.A., and Williams, R.B.G. 2001. Physical modelling of bedrock segregation in permafrost. *Permafrost and Periglacial Processes*, 12, 255–266.

Mustafa, O., Gude, M., and Hoelzle, M. 2003. Modeling permafrost distribution in the northern Alps using global radiation. *Proceedings of the 8th International Conference on Permafrost, Extended Abstracts*, Zürich, 111–112.

Nicolsky, D.J., Romanovsky, V.E., and Tipenko, G.S. 2007. Using in-situ temperature measurements to estimate saturated soil thermal properties by solving a sequence of optimization problems. *The Cryophere*, 1, 41–58.

Noetzli, J., and Gruber, S. in review. Transient thermal effects in Alpine permafrost. *The Cryophere*.

Noetzli, J., Gruber, S., and Friedel, S. 2007a. Modeling transient permafrost temperatures below steep alpine topography. *Proceedings of the COMSOL User Conference*, Grenoble, 139─143.

Noetzli, J., Gruber, S., and Haeberli, W. 2006a. *3D-Modellierung der thermischen Bedingungen im Bereich des Gipfelgrated der Zugspitze*. Unpublished Report, Institute of Geography, University of Zurich, Zurich, 19 pp.

Noetzli, J., Gruber, S., Kohl, T., Salzmann, N., and Haeberli, W. 2007b. Three-dimensional distribution and evolution of permafrost temperatures in idealized high-mountain topography. *Journal of Geophysical Research*, 112, doi:10.1029/2006JF000545.

Noetzli, J., Hilbich, C., Hauck, C., Hoelzle, M., and Gruber, S. 2008. Comparison of simulated 2D temperature profiles with time-lapse electrical resistivity data at the Schilthorn crest, Switzerland. *Proceedings of the 9th International Conference on Permafrost*, Fairbanks, US, 1293–1298.

Noetzli, J., Hoelzle, M., and Haeberli, W. 2003. Mountain permafrost and recent Alpine rock-fall events: a GIS-based approach to determine critical factors. *Proceedings of the 8th International Conference on Permafrost*, Zürich, 827–832.

Noetzli, J., Huggel, C., Hoelzle, M., and Haeberli, W. 2006b. GIS-based modeling of rock/ice-avalanches from permafrost areas. *Computational Geosciences*, 10, 161–178.

Oke, T.R. 1987. *Boundary layer climates*, Cambridge University Press, 435 pp.

Paul, F. 2003. *The new Swiss Glacier Inventory 2000. Application of remote sensing and GIS*. PhD Thesis, University of Zürich, Zürich, 192 pp.

PERMOS 2007. *Permafrost in Switzerland 2002/2003 and 2003/2004, Glaciological Report (Permafrost) No. 4/5*, Cryospheric Commission of the Swiss Academy of Sciences (SCNAT) and Department of Geography, University of Zurich, 104 pp.

Phillips, M. 2000. *Influences of snow supporting structures on the thermal regime of the ground in alpine permafrost*, Eidgenössische Forschungsanstalt WSL, Davos, 146 pp.

Plafker, G., and Ericksen, F.E. 1978. Nevados Huascaran avalanches, Peru. In: *Rockslides and Avalanches, Natural Phenomena*, Edited by B. Voight, Elsevier, Amsterdam, 277–314.

Plüss, C. 1997. *The energy balance over an alpine snow cover, point measurements and areal distribution*, Department of Geography, University of Zürich, Zürich, 115 pp.

Plüss, C., and Ohmura, A. 1997. Longwave radiation on snow-covered mountainous surfaces. *Journal of Applied Meteorology*, 36, 818–824.

Pollak, H.N., and Huang, J. 2000. Climate reconstruction from subsurface temperatures. *Annual Review of Earth and Planetary Sciences*, 28, 339–365.

Ravanel, L. 2006. *Contribution à l'étude des écroulements dans les parois à permarost de la haute montagne alpine – L'example du Petit Dru (massif du Mont Blanc) depuis la fin du Petit Age Glaciaire*. MSc Thesis, University of Savoie, 116 pp.

Roer, I. 2007. *Rockglacier konematics in a high-mountain geoecosystem*. PhD Thesis, University of Bonn, Bonn, 217 pp.

Romanovsky, V.E., Gruber, S., Instanes, A., Jin, H., Marchenko, S.S., Smith, S.L., Trombotto, D., and Walter, K.M. 2007. Frozen Ground. In: *Global outlook for ice and snow*, Edited by UNEP, UNEP/GRID-Arendal, Norway, 182–200.

Romanovsky, V.E., and Osterkamp, T.E. 2000. Effects of unfrozen water on heat and mass transport processes in the active layer and permafrost. *Permafrost and Periglacial Processes*, 11, 219–239.

Romanovsky, V.E., T.E., O., and Duxbury, N.S. 1997. An evaluation of three numerical models used in simulations of the active layer and permafrost temperature regimes. *Cold Regions Science and Technology*, 26, 195–203.

Rozman, J., Rozic, A., Budkovic, A., and Budkovic, T. 2004. Rock fall in the southern wall of Punta Thurwieser (Italy) on September 18, 2004 (in Slovenian). *Geologija*, 47, 221–232.

Rykiel, E.J.J. 1996. Testing ecological models: the meaning of validation. *Ecological Modelling*, 90, 229–244.

Salzmann, N. 2006. *The use of results from Regional Climate Models for local-scale permafrost modeling in complex high-mountain topography – possibilities, limitations and challenges for the future*. PhD Thesis, University of Zurich, Zurich, 70 pp.

Salzmann, N., Frei, C., Vidale, P.L., and Hoelzle, M. 2007a. The application of Regional Climate Model output for the simulation of high-mountain permafrost scenarios. *Global and Planetary Change*, 56, 188–202.

Salzmann, N., Noetzli, J., Gruber, S., Hauck, C., Hoelzle, M., and Haeberli, W. 2007b. RCM-based ground temperature scenarios in high-mountain topography and their uncertainty ranges. *Journal of Geophysical Research*, 112, doi:10.1029/2006JF000527.

Schaer, C., Vidale, P.L., Lüthi, D., Frei, C., Häberli, C., Liniger, M.A., and Appenzeller, C. 2004. The role of increasing temperature variability in European summer heatwaves. *Nature*, 427, 332–336.

Seregina, N.V. 1989. Some of the mathematical models used in Geocryology and methods of their numerical solution (in Russian). Edited, Moscow State University, Moscow, 243–246.

Smith, M.W., and Riseborogh, D.W. 2002. Climate and the limits of permafrost: a zonal analysis. *Permafrost and Periglacial Processes*, 13, 1–15.

Sosio, R., Crosta, G.B., and Hungr, O. 2008. Complete dynamic modeling calibration for the Thurwieser rock avalanche (Italian Central Alps). *Engineering Geology*, doi: 10.1016/j.enggeo.2008.1002.1012.

Stocker-Mittaz, C. 2002. *Permafrost distribution modeling based on energy balance data*. PhD Thesis, University of Zurich, Zurich, 122 pp.

Stocker-Mittaz, C., Hoelzle, M., and Haeberli, W. 2002. Permafrost distribution modeling based on energy-balance data: a first step. *Permafrost and Periglacial Processes*, 13, 271–282.

Vonder Muehll, D., Noetzli, J., and Roer, I. 2008. PERMOS – a comprehensive monitoring network of mountain permafrost in the Swiss Alps. *Proceedings of the 9th International Conference on Permafrost*, Fairbanks, US, 1869–1874.

Vonder Mühll, D. (Ed.) 2001, *Thermal variations of mountain permafrost: an example of measurements since 1987 in the Swiss Alps*, Kluwer Academic Publishing, Dordrecht, 83–95 pp.

Wang, K. 1992. Estimation of ground surface temperatures from borehole temperature data. *Journal of Geophysical Research*, 97, 2095–2106.

Washburn, A.L. 1979. *Geocryology – A survey of periglacial processes and environments*, Edward Arnold Ltd., London, 406 pp.

Wegmann, M. 1998. *Frostdynamik in hochalpinen Felswänden am Beispiel der Region Jungfraujoch-Aletsch*. PhD Thesis, ETH Zürich, Zürich, 143 pp.

Wegmann, M., Gudmundsson, G.H., and Haeberli, W. 1998. Permafrost changes in rock walls and the retreat of Alpine glaciers: a thermal modelling approach. *Permafrost and Periglacial Processes*, 9, 23–33.

Williams, P.J., and Smith, M.W. 1989. *The Frozen Earth*. 1 ed., Cambridge University Press, Cambridge, 306 pp.

WMO 1997. *GCOS/GTOS plan for terrestrial climate-related observation*. GCOS32, World Meteorological Organization.

Zhang, T., Barry, R.G., and Haeberli, W. 2001. Numerical simulations of the influence of the seasonal snow cover on the occurrence of permafrost at high latitudes. *Norwegian Journal of Geography*, 55, 261–266.

Part II – Publications

Publication I

Three-dimensional Distribution and Evolution of Permafrost Temperatures in Idealized High-mountain Topography

The question addressed in this paper is how complex topography and spatially variable surface temperatures influence the pattern of the subsurface thermal field. We conducted numerical experimentation with typical idealized features of alpine topography, such as ridges, peaks, and spurs. The approach combines a distributed surface energy-balance model with a three-dimensional ground heat conduction scheme. In addition, time-dependent simulations for a future scenario were performed using downscaled data from Regional Climate Models (RCMs).

Main Findings

- Mountain topography and spatially variable surface temperatures influence the subsurface thermal field even in equilibrium conditions. Isotherms incline steeply and strong lateral heat fluxes exist from the warmer to the colder side of a mountain. The thermal field in the upper part is virtually independent of the geothermal heat flux from the Earth's interior.
- Mountain permafrost occurs at locations were surface conditions do not indicate it. Irregularities at the surface (e.g., spurs) can induce local permafrost occurrence. Traditional two-dimensional maps, hence, only provide limited information to assess permafrost distribution at depth in high-mountain topography.
- Scenario calculations for the next 200 years point to strong transient perturbations in the upper about 250 m of the subsurface temperature field, and permafrost that remains inside the mountains for long time periods.
- Strongest heat fluxes exist in the upper part of a mountain. With rising temperatures they significantly increase near the surface.

Citation

Noetzli, J., Gruber, S., Kohl, T., Salzmann, N., and Haeberli, W. 2007. Three-dimensional distribution and evolution of permafrost temperatures in idealized high-mountain topography. *Journal of Geophysical Research*, 112, F02S13, doi:10.1029/2006JF000545.

Three-Dimensional Distribution and Evolution of Permafrost Temperatures in Idealized High-Mountain Topography

Jeannette Noetzli[1], Stephan Gruber[1,2], Thomas Kohl[3], Nadine Salzmann[1] and Wilfried Haeberli[1]

[1]Glaciology and Geomorphodynamics Group, Department of Geography, University of Zurich, Switzerland

[2]EDYTEM Lab, UMR 5204 CNRS – Université de Savoie, France

[3]GEOWATT AG, Dohlenweg 28, 8050 Zurich, Switzerland

Correspondence to:

Jeannette Noetzli, Glaciology and Geomorphodynamics Group, Department of Geography, University of Zurich, Winterthurerstrasse 190, CH–8057 Zurich, Email: jnoetzli@geo.unizh.ch, Phone +41 44 635 51 19.

Abstract

Permafrost degradation is regarded as a crucial factor influencing the stability of steep rockwalls in alpine areas. Discernment of zones of fast temperature changes requires knowledge about the temperature distribution and evolution at and below the surface of steep rock. In complex high-mountain topography, strong lateral heat fluxes result from topography and variable surface temperatures and profoundly influence the subsurface thermal field. To investigate such three-dimensional effects, numerical experimentation was conducted using typical idealized geometries of high mountain topography, such as ridges, peaks or spurs. The approach combines a surface energy-balance model with a three-dimensional ground heat conduction scheme to investigate below ground temperature distribution and permafrost occurrence in high mountain topography. Time-dependent simulations are based on scenario data gained from Regional Climate Models. Results indicate complex three-dimensional patterns of temperature distribution and heat flow density below mountainous topography for equilibrium conditions, which are additionally perturbed by transient effects. Permafrost occurs at many locations where temperatures at the surface do not indicate it, e.g., on the south face of ridges or below the edges of a peak. The modeling tools applied bear potential for a number of studies in high-mountains addressing questions related to permafrost distribution and evolution at depth in real topographies, as for instance the re-analysis of temperature-related instabilities.

Published in Noetzli, J., Gruber, S., Kohl T., Salzmann, N., and Haeberli, W. 2007. Three-dimensional distribution and evolution of permafrost temperatures in idealized high-mountain topography. Journal of Geophysical Research, 112, F02S13, doi: 10.1029/2006JF000545.

1 Introduction

Permafrost in European mountains has warmed by 0.5 to 0.8 °C in the upper tens of meters during the past century [*Harris et al.*, 2003]. This effect is connected to changes in atmospheric conditions and, in view of projected climatic change [*Intergovernmental Panel on Climate Change*, 2001; *Knutti et al.*, 2002; *Stott and Kettleborough*, 2002; *Zwiers*, 2002], is likely to intensify in the future. Permafrost degradation is regarded as one of the crucial factors influencing the stability of steep rock faces in high mountains and a temperature-dependent reduction in rockwall stability has recently been demonstrated both in theory and laboratory experiments [*Davies et al.*, 2001; *Haeberli et al.*, 1997; *Harris et al.*, 2001a]. The exceptional rockfall activity during the hot summer of 2003 in the European Alps [e.g., *Keller*, 2003] provided additional strong evidence for a relation between rockfall and climate change via permafrost degradation and pointed to the serious and fast response of perennially frozen steep rock to increasing air temperatures [*Gruber et al.*, 2004a; *Schiermeier*, 2003]. Frozen rock-joints were shown to reach minimal stability little below 0 °C, i.e., a jointed rock slope may become unstable as the ice warms [*Davies et al.*, 2001]. Thus, instabilities are expected to originate mainly in warm permafrost areas [*Deline*, 2001; *Dramis et al.*, 1995; *Haeberli et al.*, 1997], where the detachment zones of many rockfalls that occurred in the Alpine periglacial areas during the past century are located [*Noetzli et al.*, 2003]. We therefore consider both warming and thawing of permafrost as degradation.

To discern zones of fast permafrost degradation detailed knowledge about the ground temperature distribution and evolution is required, both at and below the surface. In alpine environments most topographic features such as mountain peaks or steep ridges are three-dimensional in nature and three-dimensional thermal effects exist in the underground: Variable topography influences the distribution of the heat flow density [*Kohl*, 1999; *Sergueev et al.*, 2003] and two-dimensional variations in surface temperatures lead to three-dimensional effects in the underground, such as strong lateral heat fluxes [*Gruber et al.*, 2004b]. These effects profoundly affect the temperature distribution at depth, violating the common assumption of predominantly one-dimensional vertical heat transport. Little is known, however, about how these effects influence permafrost occurrence in high mountains. Widely established permafrost distribution models are typically based on proxy variables of selected factors of the surface energy balance without considering the thermal conditions at depth [*Etzelmüller et al.*, 2001; *Gruber and Hoelzle*, 2001; *Haeberli*, 1975; *Hoelzle and Haeberli*, 1995; *Hoelzle et al.*, 2001; *Keller*, 1992]. Also newly developed physics-based approaches to determine near-surface temperatures, such as TEBAL [*Gruber*, 2005; *Stocker-Mittaz et al.*, 2002], the CoupModel [*Jansen and Karlberg*, 2004] or SNOWPACK [*Bartelt and Lehning*, 2002; *Lehning et al.*, 2002; *Luetschg* 2004], do not take into account a three-dimensional character of the subsurface heat flow.

This study explores the influence of three-dimensional high-mountain topography on the subsurface thermal field in steady state, and its evolution over time given changing surface temperatures. We investigate whether there are typical locations exposed to significantly faster permafrost degradation related to topography effects. For this purpose, we developed a modeling chain that considers the processes in the atmosphere (climate), at the surface (energy balance) and in the deeper subsurface (heat conduction): We combined a surface energy balance model with a three-dimensional heat conduction scheme and for time-dependent calculations we obtained scenario climate time series from Regional Climate Models (RCMs). Owing to the complex and highly variable conditions found in nature, our study is based on numerical experimentation with idealized test cases of typical topographic features in high-mountains. The results obtained are thus more easy to interpret and a step towards assessing natural and more complex situations.

2 Background

A wealth of studies exists about the influence of inhomogeneous surface conditions (e.g., lakes, buildings) on ground temperatures [for a review see *Gold and Lachenbruch* [1973]) and about the perturbation of a vertical steady state heat flow field induced by topography leading to increased heat fluxes below valleys and lower values below mountain ridges (for a review see *Kohl* [1999]). A few recent studies report on the subsurface thermal regime below complex mountain topography involving transient effects [e.g., *Kohl*, 1999; *Kohl et al.*, 2001; *Sergueev*, 2003]. In most studies surface temperatures were held constant or related to air temperatures and their changes alone. Yet in rugged topography the aspect-dependent variation of the radiation balance is a major factor influencing the distribution of surface temperatures [*Mittaz et al.*, 2000]. *Blackwell et al.* [1980] and *Safanda* [1999] calculated surface temperatures subject to variable slope orientation and found that it perturbs the subsurface temperature field and heat flow density significantly. This effect was also discussed by *Kukkonen and Safanda* [2001], but only one-dimensional vertical heat transfer was considered. First approaches taking into account aspect-dependent surface temperatures as well as two-dimensional heat fluxes that originate from mountain sides having different temperatures were presented in case studies in the Swiss Alps [*Gruber et al.*, 2004b; *Wegmann et al.*, 1998] and substantial influence of lateral heat fluxes on the ground temperatures was demonstrated. So far, however, the two- and three-dimensional influence of both topography and variable surface temperatures on the ground thermal regime in high mountains has not been systematically investigated, and little is known about subsurface permafrost below complex alpine topography.

3 Numerical Modeling of Ground Temperatures in Idealized Geometries

3.1 Modeling Approach

We perform model simulations for idealized test-cases in order to assess natural and more complex situations. We identified ridges and mountain peaks as the main forms typically comprising alpine topography and simplified them to triangular prisms and pyramid geometries (Figure 1). In addition, in many rockwalls spurs can be found that modify the surface. To model thermal surface and subsurface conditions of these geometries we generated corresponding artificial digital elevation models (DEMs) of triangular prisms, pyramids and surfaces with spurs and varied their topographic attributes: elevations were set between 2,000 and 4,500 m a.s.l., representing the common elevation range of permafrost in the Alps, slope values were set between 50° and 70°, corresponding to the typical slope range for steep rockwalls in high mountains, and the four main slope orientations were considered. The spatial resolution of the DEMs was set to 20 m, a resolution often used in regional-scale permafrost modeling [Salzmann et al., 2006a]. However, for the regular geometric forms considered here the spatial resolution is not significant.

Ground temperatures for geometries were modeled by coupling an energy balance model and a heat-conduction scheme (Figure 2). The energy balance model TEBAL [*Gruber*, 2005; *Stocker-Mittaz et al.*, 2002] is driven by climate time series and calculates mean annual ground surface temperatures (MAGST). These are imposed as upper boundary condition in the numerical heat conduction scheme FRACTure [*Kohl and Hopkirk*, 1995], which computes a three-dimensional subsurface temperature field. In the first step, model simulations were performed for equilibrium conditions to describe the thermal regime of the subsurface under the influence of topography and spatial variability of the surface temperatures alone. In a second step, time-dependent experiments were conducted, allowing for changing surface temperatures induced by climate change. Time-dependent calculations were based on model runs of the energy balance model, driven by scenario climate time series generated based on output from RCMs. RCM output was downscaled to local mountain situations using different application procedures [*Salzmann et al.*, 2007b]. Transient calculations were performed with pure heat conduction and, additionally, taking into account the effect of pore ice and latent heat.

3.2 Modeling of Rock Surface Temperatures

The surface temperature distribution has been identified to be one of the most sensitive parameters when estimating below ground temperatures [e.g., *Rybach and Pfister*, 1994]. Surface temperatures are controlled by the energy balance at the surface and mainly depend on climatologic variables, on topographic factors and on surface characteristics [*Hoelzle et al.*, 2001; *Mittaz et al.*, 2000]. In complex high mountain topography a realistic calculation of surface temperatures is particularly im-

portant as they are highly variable in space and time and are the main cause for lateral ground heat fluxes. As thick snow cover and coarse blocky active layers [*Harris and Pederson*, 1998] are largely absent in steep rock, the surface temperatures of a rockwall change primarily with aspect (shortwave radiation), altitude (sensible heat and longwave incoming radiation) and lithology [*Gruber et al.*, 2004c; *Lewkowicz*, 2001; *Wegmann*, 1998].

3.2.1 TEBAL Model

The energy-balance model TEBAL simulates time series of surface energy fluxes and near-surface temperatures in complex topography, based on input of observed climate time series and topographic information (i.e., a single point with known values of elevation, slope and aspect or an input surface grid such as a DEM). Climate time series are usually taken from operational climate stations and include air temperature, air pressure, relative humidity, wind speed and direction, precipitation as well as global radiation in daily or hourly resolution. Surface (albedo, emissivity and surface roughness) and subsurface characteristics (thermal conductivity, heat capacity and pore volume) have to be supplied for each point.

The surface energy balance and resulting temperatures are calculated based on the following steps: Clear-sky short-wave incident radiation is modeled taking into account sun-terrain geometry based on *Corripio* [2003], as well as atmospheric attenuation based on a standard atmosphere. Measured global radiation is partitioned into direct and diffuse components [*Erbs et al.*, 1982]. Diffuse radiation from the sky and surrounding terrain is calculated in a lumped approach, using sky and terrain view factors and ground albedo [*Stocker-Mittaz et al.*, 2002]. Long-wave radiation from the sky [*Konzelmann et al.*, 1994] and surface temperatures are used to calculate long-wave irradiance in complex topography using terrain and sky view factors [*Plüss and Ohmura*, 1997]. For steep rockwalls, the turbulent latent heat flux was reduced by a factor of 100 due to the assumed lack of snow cover and surface water. Vapor pressure is parameterized according methods described by *Flatau et al.* [1992] and *Plüss* [1997]. Both latent and sensible turbulent fluxes are calculated using the bulk method [*Oke*,1987, cf. *Suter et al,*. 2004]. The residuals of the surface energy balance are assigned to the ground heat flux and used as boundary condition for a one-dimensional Crank-Nicholson heat-conduction scheme. The resulting temperature for the surface node is converged with the initial guess of surface temperature using a secant iteration procedure. Effects of latent heat during freeze or thaw of water in the rock is included as apparent heat capacity based on saturated conditions and an exponential representation of unfrozen water content.

In the context of this paper, we used the version of the TEBAL model with hourly time steps which allows for the investigation of effects caused by diurnal fluctuations (e.g., convective clouding) that result in differing surface temperatures of east- and west-facing slopes. For daily time steps the TEBAL model has been validated earlier by *Gruber et al.* [2004c]. We re-validated the model for hourly time steps in an analogous manner using the same data and parameters: 14 logger-measured

rockwall temperature time series in the Swiss Alps for the hydrological year 2001/2002 were simulated and only topographic factors (slope, elevation and aspect) were adjusted to each logger site (Figure 3). Locations of the data loggers are distributed over the elevation range 2,000 to 4,500 m a.s.l. and all aspects [*Gruber et al.*, 2004c]. The driving time series were taken from the climate stations Corvatsch (3,315 m a.s.l.) and Jungfraujoch (3,580 m a.s.l., Data source: MeteoSwiss). Surface characteristics were set to albedo=0.2, emissivity=0.96 and roughness length=0.0001 m and an atmospheric lapse of 0.006 K m^{-1} is assumed. Volumetric heat capacity was set to 2.0 x 10^6 J m^{-3} K^{-1} and thermal conductivity to 2.5 W K^{-1} m^{-1} based on published values [*Cermák and Rybach*, 1982; *Safanda*, 1999; *Wegmann et al.*, 1998]. The lower boundary of the heat-conduction scheme is set at a depth of 15 m. Due to transient and three-dimensional effects it is not known whether the heat flux here is positive or negative and it is therefore assumed to be zero.

The overall simulation of daily mean rock temperatures resulted in a mean coefficient of determination (r^2) of 0.78 and in a mean absolute difference in MAGST of 1.7 °C which lies within the accuracy range of the previous validation with daily time steps and is considered encouraging. It should be kept in mind that calculated surface temperatures accumulate all errors in the input data, extrapolations (over large horizontal and vertical distances in extreme terrain geometries) and parameterizations of all other variables and fluxes. Convective clouds, for instance, reduce surface temperatures through shading of direct radiation and are spatially and temporally highly variable. The difficulties to model such phenomena may also be the main reason for a small seasonal bias in the differences between modeled and measured temperatures (Figure 3) as cloud effects are mainly important during summer. Furthermore, visibility horizons (e.g., for local shadow effects) or any site specific information other than topographic were not included in the validation runs.

In mountainous topography surface temperatures at a given elevation vary strongly between aspects due to the different amount of direct short-wave solar radiation received. This is the primary factor leading to lateral heat fluxes in the subsurface. It is therefore important for this study to correctly model differences in surface temperature as related to slope exposition. For a check, we compared the temperature offset for modeled and measured data: Modeled temperature differences for a location at an elevation of 3,000 m a.s.l. and with a 60° slope are approximately 7 °C between north and south exposition and 2.5 °C between east and west, respectively. These values correspond well to the measured data of rock temperatures [*Gruber et al.*, 2003, 2004c].

3.2.2 Model TEBAL Runs

MAGST was calculated for a ten-year period (1990–1999) using hourly time series from the high elevation site at Corvatsch (3,315 m a.s.l.), Upper Engadine (Data source: MeteoSwiss) for the DEMs described above. Surface and subsurface characteristics as well as the lower boundary condition were set according to the validation runs and a spin-up of one year was added before the start of the actual model run to initialize the temperature profile. As only the surface temperatures were

used for coupling with the heat conduction scheme a spin-up time of one year is considered sufficient. The resulting MAGST grid was used for coupling with the heat conduction scheme.

3.3 Modeling of Subsurface Temperatures in Bedrock

3.3.1 Thermal Processes in Bedrock Solved by the Numerical Tool FRACTure

Below ground temperatures in bedrock are generally controlled by the spatial and temporal variations of surface temperatures and the upward flow of heat from the interior of the earth. They are further modified by topography as well as by material properties and advection processes. The effects of fluid flow can be neglected in bedrock permafrost as a first approximation [*Kukkonen and Safanda*, 2001]. Further processes such as radiogenetic heat production are not considered as they only become important at great depth (i.e., >1,000 m). In our approach, a conductive transient thermal field under highly variable topography is considered in an isotropic and homogeneous medium [*Carslaw and Jaeger*, 1959]:

$$\frac{\delta T}{\delta t} = \kappa \nabla^2 T \quad (1)$$

where T[K] is the temperature at times t [s] and κ [$m^2 s^{-1}$] is thermal diffusivity, defined as the ratio of thermal conductivity λ [$W\ m^{-1}\ K^{-1}$] to volumetric heat capacity ρc_p [$J\ m^{-3}\ K^{-1}$]. This parameter describes the pace at which the signal propagates into the subsurface. Water contained in the pore space and crevices of rock delays the response to surface warming by the uptake of latent heat and can influence the time and depth scales of permafrost degradation by an order of magnitude [*Kukkonen and Safanda*, 2001; *Romanovsky and Osterkamp*, 2000; *Wegmann*, 1998]. The latent heat effect can be handled by substituting an apparent heat capacity ρc_a for the volumetric heat capacity ρc_p of unfrozen soil in the heat transfer equation [e.g. *Mottaghy and Rath*, 2006], based on an approximately exponential representation of unfrozen water content [*Dash et al.*, 1995; *Williams and Smith*, 1989]:

$$\rho c_a = \rho c_p + \rho_i L_f \frac{d\theta_u}{dT} \quad (2)$$

where ρ_i is the density of ice, L_f is the specific latent heat of fusion for ice and θ_u is the volumetric unfrozen water content.

The finite element code FRACTure (Flow, Rock And Coupled Temperature effects) [*Kohl and Hopkirk*, 1995] was broadly applied in the past for temperature calculations below complex topography [*Kohl*, 1998]. Herein the simulator was used for the calculation of the above-described processes of subsurface temperatures in a forward modeling scheme. FRACTure allows for the calculation of heat transfer processes in a full three-dimensional formulation. Recent developments enable an easy integration of topography and locally varying surface conditions into a robust and well-tested calculation scheme.

For the definition of the boundary conditions and transient effects the following assumptions were taken: Temporal variations of the near-surface temperatures have diurnal to millennial timescales and lead to thermal disturbances with variable penetration depths and amplitudes [*Lunardini*, 1996; *Kohl*, 1998]. In this study, we ignore annual temperature variations that may penetrate up to about 12 m in bedrock (*Gruber et al.*, 2004b) and only consider long-term variations as related to climate change (time scales of decades to centuries). However, long-term surface temperature variability still occurs on much shorter timescales than the geological processes that determine the geothermal heat flow. Therefore, the climatologic perturbations are treated as transient effects defined for the upper boundaries. The transient thermal field is then superimposed on a steady state temperature regime defined from the lower basal heat flow boundary condition. This corresponds to the approach used by *Pollak and Huang* [2000]. For time-dependent calculations so-called load-time functions were defined that describe the evolution of the upper boundary condition (see below).

3.3.2 Model Runs

Structural data such as topography and subsurface material properties were assigned to a discretization scheme with the generation of the finite element (FE) mesh. The FE-mesh was created for different geometries. Vertical refinement was increased from 250 m at depth to 10 m for elements closest to the surface. Laterally, the element size was set to 20 m corresponding to the DEM resolution. Below the geometry, a roughly discretisized rectangle box with a height of 1,000 m and no heat transfer across its sides was added. In total, the mesh consisted of around 35,000 nodes. A uniform lower boundary condition heat flux of 70 m W m^{-2} (*Medici and Rybach*, 1995) was set and as upper boundary condition the modeled MAGST (see above) was imposed.

In the purely diffusive and stationary state, the thermal conductivity is the only petrophysical parameter of importance. It was set to 2.5 W K^{-1} m^{-1} based on published values [*Cermák and Rybach*, 1982; *Safanda*, 1999; *Wegmann et al.*, 1998]. In transient simulations, the temperature change experienced additionally depends upon the volumetric heat capacity, set to 2.0 x 10^6 J m^{-3} K^{-1} [*Cermák and Rybach*, 1982], and on the ice/water content. The porosity for rock was set to 3% [*Cermák and Rybach*, 1982]. For sensitivity studies thermal conductivity, geothermal heat flux and porosity were varied in the simulations. Transient calculations were conducted with yearly time-steps. Time steps were increased from 10 s to 1 y within roughly 100 steps during spin-up. Sensitivity runs with higher refinement of the FE-mesh or changing to smaller time-steps did not significantly change any of the results and a maximum difference in modeled temperatures was assessed to be <0.1 °C.

3.3.3 Time-dependent Calculations

The transient calculations were started from the steady-state conditions of the above-described runs. In FRACTure so called load-time functions are used to calculate time-dependent boundary conditions:

$$T_{n+1} = T_n + \Delta t(1-\gamma)\frac{dT}{dt} \qquad (3)$$

where T_n is the initial boundary condition, T_{n+1} is the boundary condition at time t_n, Δt is the length of the time step, dT/dt is the time derivative of the local temperature and γ is a time integration parameter (i.e., γ=0.5 corresponds to the often used Crank-Nicholson scheme).

To define a boundary condition T_n and corresponding load time functions, we calculate future surface temperatures based on TEBAL-runs with scenario climate time series driving the model. The scenario climate time series were generated from output of RCM simulations in the scope of a study by *Salzmann et al.* [2007]. In their study a matrix of different emission scenarios, RCMs and application procedures was used to assess possible changes in surface temperatures in steep high-mountain rockwalls: A set of 12 RCM-based daily climate time series was created from the results of five RCM simulations that were performed within the European project PRUDENCE [see *Christensen et al.*, 2002]. Three RCMs (CHRM from the ETH-Z in Switzerland [see *Lüthi et al.*, 1996], RegCM from the ICTP in Italy [see *Giorgi et al.*, 1999], and HIRHAM from the DMI in Denmark [see *Christensen et al.*, 1996]) were driven by the HadAM3H GCM from the Hadley Center (UK) as forced by the SRES emission scenarios A2 and B2 (CHRM only by A2). The results of the RCM control (1961–1990) and scenario runs (2071–2100) were adapted for high-mountain situations using the so-called delta and bias approaches that are discussed in detail by *Salzmann et al.* [2007]. The constructed scenario climate time series were applied to TEBAL and the average change in surface temperature was calculated for 36 specific topographical situations. Results showed an approximately 1 °C stronger warming on north-facing rockwalls compared to south-facing rockwalls within the next 100 years and the climate conditions at Corvatsch (3,315 m a.s.l.), Upper Engadine, that can mainly be attributed to differing amounts of direct solar radiation received. As the RCM results used do not provide diurnal fluctuations, no difference between the warming in east- and west-facing slopes could be modeled. The exact modeling procedure and detailed results of this study are described by Salzmann et al. [2007].

Based on the results from these scenario runs, three types of linear load-time functions were defined to distinguish warming on north-, south- and east/west-oriented slopes. Possible changes in MAGST between the time periods 1982–2002 and 2071–2091 were simulated for a 60° slope at an elevation of 3,500 m a.s.l. Because all scenarios are equally valid, the median of all runs was calculated to derive a best guess of the possible temperature change: for north-oriented slopes we assumed a linear temperature change over the next 100 years of +3.5 °C, for south- and east/west-oriented slopes the change was set to 2.5 °C and 3 °C, respectively.

4 Subsurface Temperatures in Mountainous Topography

4.1 Steady State Conditions

Due to the difficulties in illustrating three-dimensional situations in two-dimensional graphics the main results are visualized for cross-sections of ridges. In Figure 4 the ground temperature fields of six idealized ridges with altitudes between 2,000 and 4,000 m a.s.l., north-south and east-west aspects and a slope of 60° are shown. The permafrost base corresponds to the 0 °C-isotherm and is highlighted by a black line. The temperature distribution is governed by the difference in surface temperatures between the two flanks of the ridges, which leads to near-vertical isotherms in the top part of the ridge. Isotherms are curved as a result of the geometry. The main heat flux is directed horizontally from the warmer to the colder side in the top part and diagonally upwards in the middle part of the ridge. Vertical heat fluxes only exist at the base of the geometry (Figure 5, left). The heat flux density is largest at the top due to the largest temperature difference on the shortest distance. In addition, a zone of increased temperature gradients and heat flux can be found at the foot of the colder side. A corresponding zone of lower heat flux density is located in the middle of the warmer side.

A larger difference in MAGST between the two sides of a mountain, i.e. north-south vs. east-west ridges (cf. Figure 4a–c vs. d–f), leads to larger horizontal temperature gradients, to more vertical isotherms and, hence, to a stronger horizontal heat flux. This effect also increases with the steepness of the topography. Changes in elevation have no major effect on the relative temperature distribution pattern. However, as the isotherms are inclined, the shape of the permafrost body changes significantly with elevation (Figure 4). At elevations up to 4,000 m a.s.l. thick permafrost exists on both sides. Permafrost thickness (which we consider here in the direction of heat conduction into the subsurface, i.e., vertical to the surface) decreases with increasing height mainly on the warmer side. At elevations lower than ca. 3,500 m a.s.l. surface temperatures are above 0 °C on the southern side of our model. But at these heights permafrost may exist right below the surface, induced by the opposite colder mountain flank (e.g., Figure 4b, c, f).

To demonstrate the influence of the geothermal heat flux on the temperature distribution in steep topography, we re-calculated the thermal field of a ridge with a zero heat flux lower boundary condition. The result was then subtracted from the thermal field modeled with the constant lower boundary condition used in the model runs (Figure 6). The influence of the geothermal heat flux decreases exponentially towards the top and becomes negligible in the upper half of the geometry (Figure 6a): the top part of the ridge is virtually decoupled from the half-space below the geometry under consideration. A lower thermal conductivity slightly increases the influence of the geothermal heat flux (Figure 6b), whereas steeper and more extreme topography decreases it.

In a pyramid geometry similar effects can be observed but with four sides having different surface temperatures. With slices taken along the x, y, and z axis the three-dimensional nature of the permafrost body in alpine topography becomes visible (Figure 7) and effects not present in two-dimensional ridge situations can be shown. For instance, permafrost can be found only meters to decameters below the surface of the edges of the pyramid: In Figure 8 this is visualized in cross sections along the edges. Additionally, irregularities on rockwall surfaces such as spurs with sides exposed to different aspects may modify the subsurface temperature field. In Figure 9 an example of a spur on a south-facing rockwall is shown. Due to the lower temperatures on the western side of the spur, lower subsurface temperatures are induced inside and even below the spur. This leads, for instance, to local permafrost occurrence in a south-facing rockwall that generally does not contain permafrost.

4.2 Transient Ground Temperatures

In a simple experiment, time and depth scales of the influence of a climatic signal on ground temperatures can be demonstrated with a one-dimensinal solution for the vertical temperature distribution and a step-like increase in surface temperature [*Carslaw and Jaeger*, 1959]:

$$T = T_0 \times erfc\left(\frac{z}{2\sqrt{\kappa \times t_i}}\right) \qquad (4)$$

where T_0 [K] is the change in MAGST, z [m] is the depth, κ [$m^2 s^{-1}$] is the thermal diffusivity and t_i [s] is the duration after the change. Thus, taking κ=1.25 x 10^{-6} $m^2 s^{-1}$, 50% of the amplitude of the temperature step has reached a depth of approximately 60 m after a time period of 100 years and 25% has reached around 100 m. Considering a time period of 200 years the respective values amount to 80 m for 50% and 150 m for 25% of the signal. This means that within only one or two centuries of after a temperature increase permafrost occurrence several hundred meters below the surface is not substantially affected. This corresponds to the results obtained in our simulations: In the three-dimensional situations modeled, a change in MAGST propagates into the ground perpendicularly to the surface from two or more sides (Figure 10), leading to an increase in the pace at which permafrost degrades. For more exposed three-dimensional situations such as a pyramid, the warming even takes place from 4 different sides (Figure 11). With raising surface temperatures the permafrost base changes until it is situated parallel to the surface. In the examples shown in Figure 11, it can be seen that the permafrost base mainly changes on the warmer side because of the curved form of the isotherms. After a period of 100 or 200 years the parts deeper than ca. 200 m are still not reached by the climate signal (Figures 10 and 11). A permafrost body can remain unaffected by changes at the surface over centuries to millennia where temperatures little below the surface have changed significantly and many parts of the surface have become free of permafrost.

The main heat flux is directed horizontally from the warmer to the colder side (Figure 5, middle, and 5, right) as shown for equilibrium conditions, but strongest heat fluxes exist in the upper part on the warmer side. Temperature gradients and heat fluxes near the surface increase strongly due to the larger temperature difference between the warming surface and the temperatures at depth that still remain unchanged. On the colder side a reversal of the direction of heat fluxes takes place and, hence, at the depth reached by the temperature signal a zone exists where heat flows towards it from both sides.

Where the temperature raises towards 0 °C, energy is needed to melt ice contained in pore spaces. This effect leads to a delay in the propagation of the temperature signal into the subsurface and increases the time lag between changes in surface conditions and temperatures at depth. The difference between model runs with and without latent heat is illustrated in Figure 12. Locations where a difference can be observed show the areas where temperature changes take place just below 0 °C and, hence, where permafrost is actually degrading. The influence, as calculated with a porosity of 3% and homogeneous material properties, amounts to a maximum of about 0.5 °C within 100 years. Considering the low porosity of rock this difference can be referred to as substantial, and latent heat effects additionally modify the distribution of the underground thermal field at the degrading permafrost boundaries.

5 Discussion

With the experiments conducted in this study we demonstrated the strong three-dimensional effects on the subsurface thermal field and the occurrence of permafrost in high mountain topography. In the upper parts of the geometries under consideration the influence of the geothermal heat flux is negligible and ground temperatures and heat fluxes are governed almost solely by variable temperatures at the surface of the mountain sides: temperatures change with position between the mountain sides and heat fluxes are mainly horizontal. Due to the three-dimensional effect of mountainous topography, permafrost occurs inside mountains only a few meters to decameters below the surface where MAGST is clearly above 0 °C. These effects were shown for simplified geometries even in steady state conditions. In terms of temperature-related instabilities, a thawing and migrating permafrost base in such a situation may, for instance, lead to rockfall occurring on the warm or 'permafrost-free' side of a ridge or peak. In fact, several detachment zones exist, where slope failure occurred in similar situations as, for instance, the event at Punta Thurwieser on 18 September 2004 in the Italian Val Zebrù [*Cola*, 2005]. The rockfall detached at an elevation of approximately 3600 m a.s.l. from a 70° steep and south-exposed rockwall that is part of a mainly east-west-trending ridge. This situation is comparable to the one shown in Figure 4b. The starting zone of the rockfall event on 15 July 2003 at the Hörnligrat, the NE-ridge of the Matterhorn, Switzerland, is located in a situation where

permafrost occurs only below the surface (cf. Figure 8b). Consequently, it is important to consider the effects of complex topography and variable surface temperatures when assessing below ground temperatures and permafrost occurrence in high-mountains. Traditional two-dimensional permafrost maps can serve as indicators of potential permafrost occurrence in an area, but they do not provide sufficient information on the conditions at depth. However, it has to be emphasized that the steady state conditions shown do not describe a situation as found today in nature and that transient perturbations to the steady state temperature field exist as described below. Nevertheless, they are a step towards understanding the temperature distribution at depth in high-mountain terrain.

Three-dimensional mountain topography also plays a decisive role for temperature changes entering into the ground. In the time-dependent simulations it can be seen that the warming signal that intrudes into the underground perpendicularly to the surface reaches the permafrost body from more than one side, i.e. from 2 sides in the case of a ridge, from even 4 sides in a pyramid-like situation. Together with the above described decoupling from the geothermal heat flux this describes a basic difference to permafrost degradation in high latitudes or in more gentle terrain and increases the pace of deeper permafrost degradation.

The transient effects caused by changing surface temperatures additionally complicate the temperature distribution below the surface. Changes at the surface and the upper hundred meters are substantial as modeled for the next 100 years and the conditions assumed in test-cases. For instance, in Figure 9 the lower limit of permafrost distribution at the surface rises to nearly 4,000 m a.s.l. on south-facing rockwalls, which is higher than most peaks in the European Alps. However, a substantial permafrost body remains in the underground but surface conditions no longer indicate it. For a realistic assessment of today's thermal state and permafrost distribution at grater depth in high mountains it is therefore necessary to consider transient effects in addition to three-dimensional effects. For example, an assumed 10 °C cooler surface temperature during the last Pleistocene Ice Age 70,000–10,000 years B.P. still causes a temperature difference of more than –4 °C at a depth of 1,000 m compared to steady state conditions [*Kohl et al.*, 2001; cf. also *Safanda and Rajver*, 2001]. The recent much smaller 20th century warming [*Beniston et al.*, 1997; *Diaz and Bradley*, 1997; *Haeberli and Beniston*, 1998] has not yet penetrated to greater depth but affects temperatures in the upper decameters. When additionally considering the retarding influence of pore ice on temperature evolution, even in low-porosity rockwalls, temperatures may be much colder than in the example above and substantial permafrost may remain today inside high mountains.

The direction of heat fluxes is important, for instance, for the direction of unfrozen water migrating in pore spaces. As seen in Figure 5, with rising temperatures at the surface, a zone develops on the colder side of a mountain where heat flows towards it from two sides. This can influence the movement of unfrozen water in the pore space and the distribution of ice content in the subsurface [cf. also *Gruber and Haeberli*, 2007].

In the highly variable topography found in natural environments the subsurface temperature field is a complex result of many interrelated influences and may differ substantially from the simplified test cases presented. The calculation of surface temperatures using TEBAL is validated for near-vertical situations of bare rock and we assumed average values for and a homogeneous distribution of surface and subsurface characteristics. Modifications are likely to be caused by various factors, such as snow remaining in less steep parts, heavy fracturing of the rock due to weathering or geological discontinuities [*Gruber and Haeberli*, 2007]. Knowledge about the water and ice content of rockwalls, its freezing characteristics and its spatial and temporal variability is absent or rare. Massive ice in jointed rock (as found in many rockfall scarps in 2003, e.g., the Matterhorn south face) can lead to a highly complex thermal field and strongly retard degradation at depth. The hydrology of rockwalls and water possibly percolating therein, which may lead to non-conductive heat transfer within the subsurface, are poorly understood so far. Such effects may counter the retarding effect caused by the uptake of latent heat. First results from the application of geophysical monitoring in the Turtmann Valley, Swiss Alps, point to their importance in connection with permafrost occurrence in solid rockwalls [M. Krautblatter et al., Electrical resistivity tomography monitoring of permafrost in solid rock walls, submitted to *Journal of Geophysical Research*, 2007].

We accomplished the combination of RCMs, energy balance and heat conduction models by passing output from one model as input to the next. The model chain represents processes initiated by changes in atmospheric conditions that lead to changes in the surface energy balance and below-ground temperatures. However, the models are not yet fully coupled and output from a first model serves as input to the next without accounting for possible feedback. This first approach using such a model chain bears potential for a number of studies and may provide a basis for numerical experimentation in order to investigate thermal processes in frozen rockwalls and for case studies of real topography. It may also be beneficial for the re-analysis of rockfall events that occurred in periglacial areas, for support of engineering studies (e.g. cable cars) or interpretation of geothermal profiles. The perturbation of the ground thermal field also constitutes a major obstacle for the interpretation of transient signals contained in T(z)-profiles measured in boreholes located in high mountains [*Gruber et al.*, 2004b; *Kohl and Gruber*, 2003]. Its separation from topographic effects is crucial for the quantification of the warming signal. Only then, conclusions on the temperature history at the surface may be drawn correctly from the inversion of these profiles, e.g. for monitoring programs such as PACE [*Harris et al.*, 2001b] or PERMOS [*Vonder Mühll et al.*, 2004].

6 Conclusions and Perspectives

The experiments conducted in this study and the results described above lead to the following conclusions:

- The steady state temperature field below high mountain topography is mainly controlled by spatially varying surface temperatures between different mountain sides and is little influenced by the geothermal heat flux in the higher parts. Isotherms are nearly vertical and a strong heat flux is directed from the warmer to the colder side of the mountain.
- Permafrost may occur underground at locations where surface temperatures do not indicate it, even in steady state conditions. Traditional 2-D maps do not provide sufficient information to assess permafrost distribution at depth in complex high-mountain topography.
- Irregularities on the surface, such as spurs, may modify ground temperatures and induce local permafrost occurrence.
- Permafrost degradation in steep topography takes places from different sides, affecting both the permafrost table and the permafrost base. This leads to an increase in the pace of deeper permafrost degradation as compared to permafrost in flat terrain, where warming typically penetrates vertically into the ground.
- Owing to the long time needed for a temperature signal to penetrate to greater depth, permafrost can remain inside mountains over centuries. At some locations where surface temperatures rise above 0 °C substantial permafrost occurrence can be found. Time scales involved in deep permafrost degradation are on the order of millennia, even without the retarding effect of latent heat. The influence from past cold periods such as the last ice age is likely to still be found in the interior of mountain peaks.
- With rising surface temperatures, heat fluxes strongly increase near the surface.
- For the assessment of permafrost occurrence in complex topography, the three-dimensional situation as well as transient effects should be taken into account. Preferably, physically based three-dimensional models are used.
- An energy balance model has been successfully combined with a numerical 3-D heat conduction scheme to model ground temperatures and permafrost distribution at depth in complex topography. In addition, output from RCMs was downscaled to local climate conditions and used for time-dependent model runs.

Permafrost in steep bedrock slopes is still a very young field of research and many factors influencing the ground thermal regime in steep rock are poorly understood today. Examples include the influence of snow cover, ice contained in pore spaces, percolating water or local inhomogeneities [*Gruber and Haeberli*, 2007]. The focus of future activities is on realistic process understanding and quantitative and numeric modeling of the processes involved in permafrost degradation in steep high mountain rock walls. For the understanding and quantification of present-day or future temperature conditions the time scales needed in model spin up to account for transient effects of past cold

periods are investigated. The model chain applied in this study may be established for future studies on the subsurface distribution and evolution of mountain permafrost, such as the re-analysis of recent periglacial rockfall events or the study of the present transient state of thermal fields in real topographies. A validation study combining the models presented with measured temperature data and geophysical soundings for a test site in Switzerland is planned for the near future.

Acknowledgements. This study was supported by the Swiss National Science Foundation, as part of the NF 20-10796./1 project 'Frozen rock walls and climate change: transient three-dimensional investigation of permafrost degradation'. The authors appreciate their financial support. Careful comments by two anonymous reviewers and the editors are greatly acknowledged.

References

Bartelt, P. B., and M. Lehning (2002), A physical SNOWPACK model for avalanche warning services, Climatic Change, 36, 233–251.

Beniston, M., H. F. Diaz, and R. S. Bradley (1997), Climatic change at high elevation sites: An overview, Climatic Change, 36, 233–251.

Blackwell, D.D., J.L Steele, Ch.A. Brott, (1980), The terrain effect on terrestrial heat flow, J. Geophys. Res., 9 (B85), 4757–4772.

Carslaw, H. S., and J. C. Jaeger (1959), Conduction of heat in solids, 510 pp., Clarendon Press, Oxford.

Cermák, V., and L. Rybach (1982), Thermal conductivity and specific heat of minerals and rocks, in Landolt-Börnstein Zahlenwerte und Funktionen aus Naturwissenschaften und Technik, Physikalische Eigenschaften der Gesteine (V/1a), edited by G. Angeneister, Springer, Berlin.

Christensen, J. H., O. B. Christensen, P. Lopez, E. Van Meijgaard and M. Botzet (1996), The HIRHAM4 Regional Atmospheric Climate Model, Scientific Report 96–4, 51 pp., DMI, Copenhagen.

Christensen, J. H., T. R. Carter and F. Giorgi (2002), PRUDENCE employs new methods to assess European climate change, EoS Trans., 83, 147.

Cola, G. (2005), La grande frana della cresta Sud-Est della Punta Thurwieser (Thurwieser-spitze) 3658 m, (Alta Valtellina, Italia), Terra Glacialis, 8, 38-45.

Corripio, J. G. (2003), Vectorial algebra algorithms for calculating terrain parameters from DEMs and solar radiation modelling in mountainous terrain, Int J. Geogr. Inf. Sc., 17, 1–23.

Dash, J. G., H. Fu, and J. S. Wettlaufer (1995), The premelting of ice and its environmental consequences, Rep. Prog. Phys., 58.

Davies, M. C. R., O. Hamza, and C. Harris (2001), The effect of rise in mean annual temperature on the stability of rock slopes containing ice-filled discontinuities, Permafrost Periglac., 12, 137–144.

Deline, P. (2001), Recent Brenva rock avalanches (Valley of Aosta): new chapter in an old story? Geogr. Fis. Din. Quarter., 55–63.

Diaz, H. F., and R. S. Bradley (1997), Temperature variations during the last century at high elevation sites, Climatic Change, 36, 253–279.

Dramis, F., M. Govi, M. Guglielmin, and G. Mortara (1995), Mountain permafrost and slope instability in the Italian Alps: the Val Pola landslide, Permafrost Periglac., 6, 73–82.

Erbs, D. G., S. A. Klein, and J. A. Duffie (1982), Estimation of the diffuse radiation fraction for hourly, daily and monthly average global radiation, Sol. Energy, 28, 293–304.

Etzelmüller, B., M. Hoelzle, E. S. F. Heggem, K. Isaksen, C. Mittaz, D. Vonder Mühll, R. S. Ødegård, W. Haeberli, and J. L. Sollid (2001), Mapping and modelling the occurrence and distribution of mountain permafrost, Norsk. Geol. Tidsskr., 55, 186 –194.

Flatau, P. J., R. L. Walko and W.R. Cotton (1992), Polynomial fits to saturation vapor-pressure, J. Appl. Meteorol., 31, 1507–1513.

Giorgi, F., Y. Huang, K. Nishizawa and C. Fu (1999), A seasonal cycle simulation over eastern Asia and its sensitivity to radiative transfer and surface processes, J. Geophys. Res., 104, 6403_6423.

Gold, L. W., and A. H. Lachenbruch (1973), Thermal conditions in permafrost – a review of North American literature, 2nd International Conference on Permafrost. Proceedings, National Academy of Sciences, Washington D.C., 3–25.

Gruber, S. (2005), Mountain permafrost: Transient spatial modelling, model verfication and the use of remote sensing, Ph.D. thesis, 121pp. Univ. of Zurich, Zurich, Switzerland.

Gruber, S., and M. Hoelzle (2001), Statistical modelling of mountain permafrost distribution: local calibration and incorporation of remotely sensed data, Permafrost Periglac., 12, 69–77.

Gruber, S. and W. Haeberli (2007), Permafrost in steep bedrock slopes and its temperature-related destabilization following climate change, J. Geophys. Res., 112, doi:10.1029/2006JF000547.

Gruber, S., M. Peter, M. Hoelzle, I. Woodhatch, and W. Haeberli (2003), Surface temperatures in steep alpine rock faces – A strategy for regional-scale measurement and modelling, 8th International Conference on Permafrost, Proceedings, Zurich, Switzerland, 325–330.

Gruber, S., M. Hoelzle, and W. Haeberli (2004a), Permafrost thaw and destabilization of Alpine rock walls in the hot summer of 2003, Geophys. Res. Let., 31, doi:10.1029/2004GL0250051.

Gruber, S., L. King, T. Kohl, T. Herz, W. Haeberli, and M. Hoelzle (2004b), Interpretation of geothermal profiles perturbed by topography: The Alpine permafrost boreholes at Stockhorn Plateau, Switzerland, Permafrost Periglac., 15, 349–357.

Gruber, S., M. Hoelzle, and W. Haeberli (2004c), Rock wall temperatures in the Alps: Modelling their topographic distribution and regional differences, Permafrost Periglac., 15, 299–307.

Haeberli, W. (1975), Untersuchungen zur Verbreitung von Permafrost zwischen Flüelapass und Piz Grialetsch (Graubünden), Mitteilungen der VAW-ETH Zürich, 221 pp., ETH Zürich, Zürich.

Haeberli, W., and M. Beniston (1998), Climate change and its impacts on glaciers and permafrost in the Alps, in AMBIO – A Journal of the Human Environment, edited by A. Rapp and E. Kessler, pp. 258–265, The Royal Swedish Academy of Sciences.

Haeberli, W., M. Wegmann, and D. Vonder Mühll (1997), Slope stability problems related to glacier shrinkage and permafrost degradation in the Alps, Eclogae Geol. Helv., 90, 407–414.

Harris, C., M. C. R. Davies, and B. Etzelmüller (2001a), The assessment of potential geotechnical hazards associated with mountain permafrost in a warming global climate, Permafrost Periglac., 12, 145–156.

Harris, C., W. Haeberli, D. Vonder Mühll, and L. King (2001b), Permafrost monitoring in the high mountains of Europe: the PACE project in its global context, Permafrost Periglac., 12, 3–11.

Harris, C., D. Vonder Mühll, K. Isaksen, W. Haeberli, J. L. Sollid, L. King, P. Holmlund, F. Dramis, M. Guglielmin, and D. Palacios (2003), Warming permafrost in European mountains, Global Planet. Change, 39, 215–225.

Harris, S.A., and D.E. Pedersen (1998), Thermal regimes beneath coarse blocky material, Permafrost Periglac., 9, 107–120.

Hoelzle, M., and W. Haeberli (1995), Simulating the effects of mean annual air temperature changes on permafrost distribution and glacier size. An example from the Upper Engadin, Swiss Alps, Ann. Glaciol., 21, 400–405.

Hoelzle, M., C. Mittaz, B. Etzelmüller, and W. Haeberli (2001), Surface energy fluxes and distribution models of permafrost in European mountain areas: an overview of current developments, Permafrost Periglac., 12, 53–68.

IPCC (2001), Third assessment report, Working Group 1, Cambridge University Press, Cambridge.

Jansson, P.E., and L. Karlberg, 2004, Coupled heat and mass transfer model for soil-plant-atmosphere systems, Royal Institute of Technology, Dept of Civil and Environmental Engineering, Stockholm, 435 pp.

Keller, F. (1992), Automated mapping of mountain permafrost using the program PERMAKART within the Geographical Information System ARC/INFO, Permafrost Periglac., 3, 133–138.

Keller, F. (2003), Kurzbericht über die Steinschlagereignisse im heissen Sommer 2003 im Bergell(Project report on rockfall 2003 to the Kanton Graubuenden), report, Institut für Turismus und Landschaft Academia Engiadina, Samedan, Switzerland.

Knutti, R., T. F. Stocker, F. Joos, and G. K. Plattner (2002), Constraints on radiative forcing and future climate change from observations and climate model ensembles, Nature, 416, 719–723.

Kohl, T. (1998), Paleclimatic signals – can they be washed out?, Tectonophysics, 291, 225–234.

Kohl, T. (1999), Transient thermal effects at complex topographies, Tectonophysics, 306, 311–324.

Kohl, T., and R. J. Hopkirk (1995), ‚FRACTure' a simulation code for forced fluid flow and transport in fractured porous rock, Geothermics, 24, 345–359.

Kohl, T., and S. Gruber (2003), Evidence of paleaotemperature signals in mountain permafrost areas, 8th International Conference on Permafrost, Extended Abstracts, University of Zurich, Zurich.

Kohl, T., S. Signorelli, and L. Rybach (2001), Three-dimensional (3-D) thermal investigation below high Alpine topography, Phys. Earth Planet. In., 126, 195-210.

Konzelmann, T., R. S. W. Van de Wal, W. Greuell, R. Binanja, E. A. C. Henneken, and A. Abe-Ouchi (1994), Parameterization of global and longwave incoming radiation for the Greenland Ice Sheet, Global Planet. Change, 9, 143–164.

Krautblatter, M., C. Hauck, and R. Dickau (submitted), First DC resitivity monitoring of permafrost in solid rockwalls, J. Geophys. Res.

Kukkonen, I. T., and J. Safanda (2001), Numerical modelling of permafrost in bedrock in northern Fennoscandia during the Holocene, Global Planet. Change, 29, 259–273.

Lehning, M., P. B. Bartelt, R. L. Brown, C. Fierz, and P. Satyawali (2002), A physical SNOWPACK model for the Swiss Avalanche warning services. Part III: Meteorological boundary conditions, thin layer formation and evaluation, Cold Reg. Sci. Technol., 35, 169–184.

Lewkowicz, A. G. (2001), Temperature regime of a small sandstone tor, latitude 80°N, Ellesmere Island, Nunavut, Canada, Permafrost Periglac., 12, 351–366.

Luetschg, M. (2004), A model and field analysis of the interaction between snow cover and Alpine permafrost, Ph.D. thesis, 258 pp., University of Zurich, Zurich.

Lunardini, V.J. (1996), Climatic warming and the degradation of warm permafrost, Permafrost Periglac., 7, 311–320.

Lüthi, D., A. Cress, C. Frei and C. Schär (1996), Interannual variability and regional simulations, Theor. Appl. Climatolo. 53, 185–209.

Medici, F., and L. Rybach, (1995), Geothermal Map of Switzerland 1995 (Heat Flow Density), Matériaux pour la Géologie de la Suisse, Géophysique 30. Schweizerische Geophysikalische Kommission.

Mittaz, C., M. Hoelzle, and W. Haeberli (2000), First results and interpretation of energy-flux measurements of Alpine permafrost, Ann Glaciol., 31, 275–280.

Mottaghy, D. and V. Rath (2006), Latent heat effects in subsurface heat transport modeling and their impact on paleotemperature reconstructions, Geophys. J. Int., 164, 236–245.

Noetzli, J., M. Hoelzle, and W. Haeberli (2003), Mountain permafrost and recent Alpine rock-fall events: a GIS-based approach to determine critical factors, 8th International Conference on Permafrost, Zürich, Switzerland, 827–832.

Oke, T. R. (1987), Boundary Layer Climates, 2nd ed., Routledge.

Plüss, C. (1997), The Energy Balance Over an Alpine Snowcover, Point Measurements and Areal Distribution, Ph.D. thesis, 115 pp., Univ. of Zurich, Zurichm Switzerland.

Plüss, C., and A. Ohmura (1997), Longwave radiation on snow-covered mountainous surfaces, J. Appl. Meteorol., 36, 818–824.

Pollak, H. N., and J. Huang (2000), Climate reconstruction from subsurface temperatures, Ann Rev. Earth Pl. Sc., 28, 339–365.

Romanovsky, V. E., and T. E. Osterkamp (2000), Effects of unfrozen water on heat and mass transport processes in the active layer and permafrost, Permafrost Periglac., 11, 219–239.

Rybach, L., and M. Pfister (1994), How to predict rock temperatures for deep Alpine tunnels, J. Appl. Geophys., 31, 261–270.

Safanda, J. (1999), Ground surface temperature as a function of slope angle and slope orientation and its effect on the subsurface temperature field, Tectonophysics, 306, 367–375.

Safanda, J., and D. Rajver (2001), Signature of the last ice age in the present subsurface temperatures in the Czech Republic and Slovenia, Global Planet. Change, 29, 241–257.

Salzmann, N., S. Gruber, M. Hugentobler, and M. Hoelzle, 2007a, The influence of different Digital Terrain Models (DTMs) on alpine permafrost modeling, Environ Model Assess, doi 10.1007/s10666-006-9065-3.

Salzmann, N., C. Frei, P. L. Vidale, and M. Hoelzle (2007b), The Application of Regional Climate Model output for the simulation of high-mountain permafrost scenarios, Global Planet. Change, 56, 188–202.

Salzmann, N., J. Noetzli, C. Hauck, S. Gruber, and W. Haeberli (2007), RCM-based ground temperature scenarios in high-mountain topography and their uncertainty ranges, J. Geophys. Res., 112, doi:10.1029/2006JF000527.

Schiermeier, Q., (2003), Alpine thaw breaks ice over permafrost's role, Nature, 424, 712.

Sergueev, D., G. Tipenko, V. Romanovsky, and N. Romanovskii (2003), Mountain permafrost thickness evolution under influence of long-term climate fluctuations (results of numerical simulation), 8th International Conference on Permafrost, Zurich, Switzerland, 1017–1021.

Stocker-Mittaz, C., M. Hoelzle, and W. Haeberli (2002), Permafrost distribution modeling based on energy-balance data: a first step, Permafrost Periglac., 13, 271–282.

Stott, P. A., and J. A. Kettleborough (2002), Origins and estimates of uncertainty in predictions of twenty-first century temperature rise, Nature, 416, 723–726.

Suter S., M. Hoelzle and A. Ohmura (2004), Energy balance at a cold, alpine firn saddle, Seserjoch, Monte Rosa. International Journal of Climatology, 24, 1423–1442.

Vonder Mühll, D., J. Noetzli, K. Makowski, and R. Delaloye (2004), Permafrost in Switzerland 2000/2001 and 2001/2002. Glaciological Rep. (Permafrost) No. 4/5, 80 pp., Glaciol. Comm., Swiss Acad. of Sci. Zurich, Switzerland.

Wegmann, M. (1998), Frost dynamics in high-alpine rock walls at the example of the Jungfraujoch-Aletsch Region, CH (Frostdynamik in hochalpinen Felswänden am Beispiel der Region Jungfraujoch-Aletsch), Ph.D. thesis, 143 pp., ETH Zurich, Zurich, Switzerland.

Wegmann, M., G. H. Gudmundsson, and W. Haeberli (1998), Permafrost changes in rock walls and the retreat of Alpine glaciers: a thermal modelling approach, Permafrost Periglac., 9, 23–33.

Williams, P. J., and M. W. Smith (1989), The Frozen Earth, 306 pp., Cambridge University Press, New York.

Zwiers, F. W. (2002), The 20-year forecast, Nature, 416, 690–691.

Figures

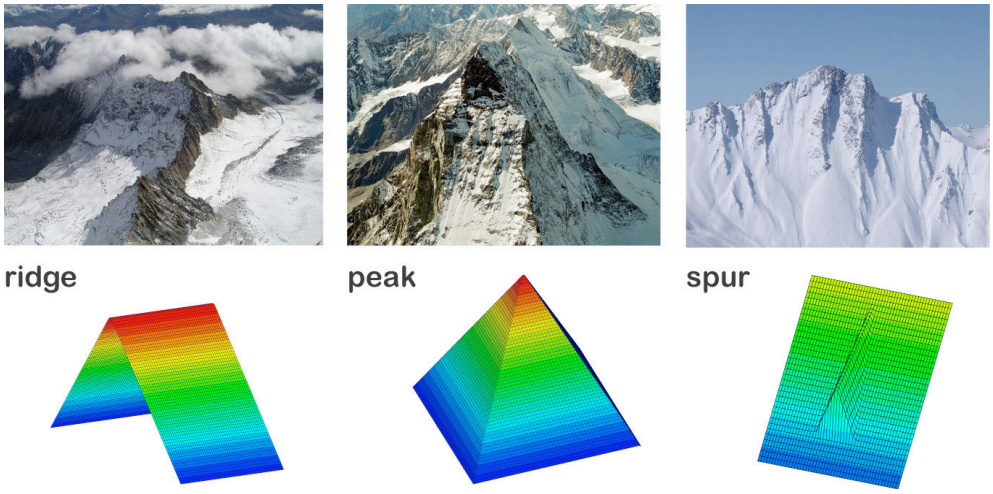

Figure 1. Examples of the most prevalent topographical forms of high mountain topography: ridges (left, Dammastock, CH) and peaks (middle, Matterhorn, CH) are simplified as triangle and pyramid geometries. Additionally, rockwalls are often modified by spurs (right, Piz Terri, CH). Photos left and middle taken by Ch. Rothenbühler.

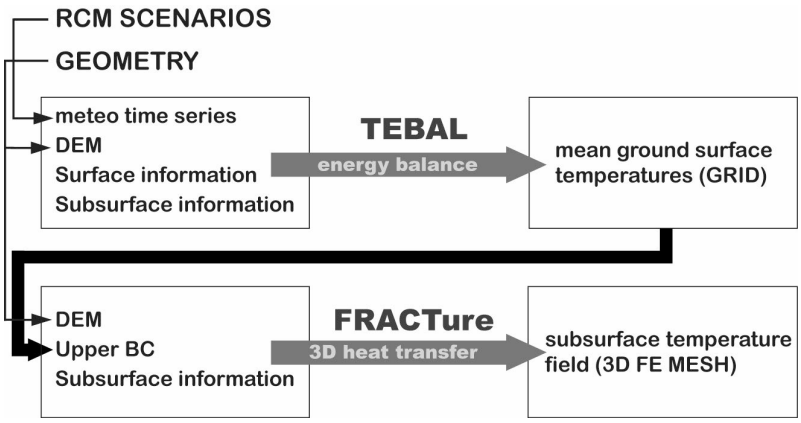

Figure 2. Ground surface temperatures are calculated by the energy balance model TEBAL [*Gruber*, 2005; *Stocker-Mittaz et al.*, 2002] and used as upper boundary condition in the FE heat conduction code FRACTure [*Kohl and Hopkirk*, 1995] that determines a three-dimensional subsurface temperature field. For time-dependent calculations, the energy-balance model was driven by climate time series generated based on output from Regional Climate Models (RCMs).

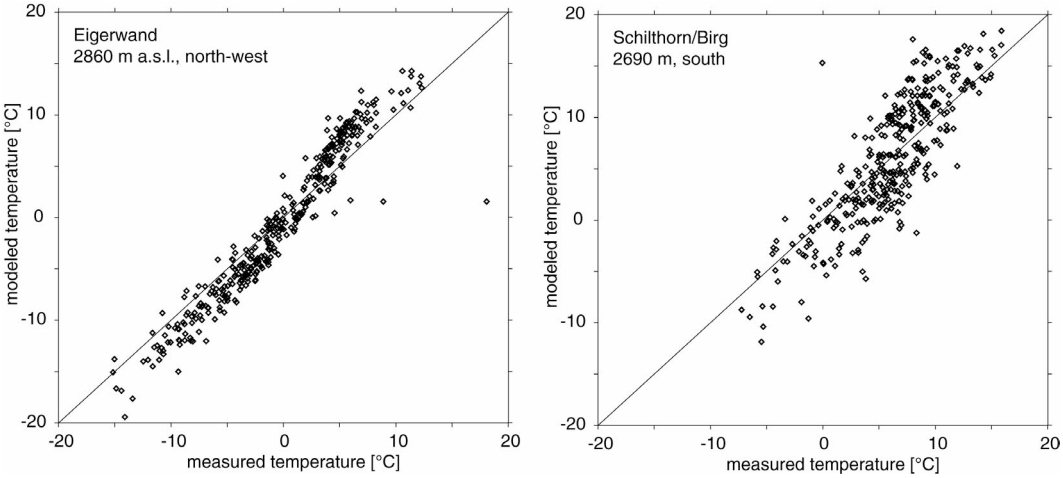

Figure 3. Measured versus modeled daily means of near-surface temperatures [°C] at two logger sites for the hydrological year 2001/2002. Modeled temperatures were calculated with the energy balance model TEBAL and hourly time steps.

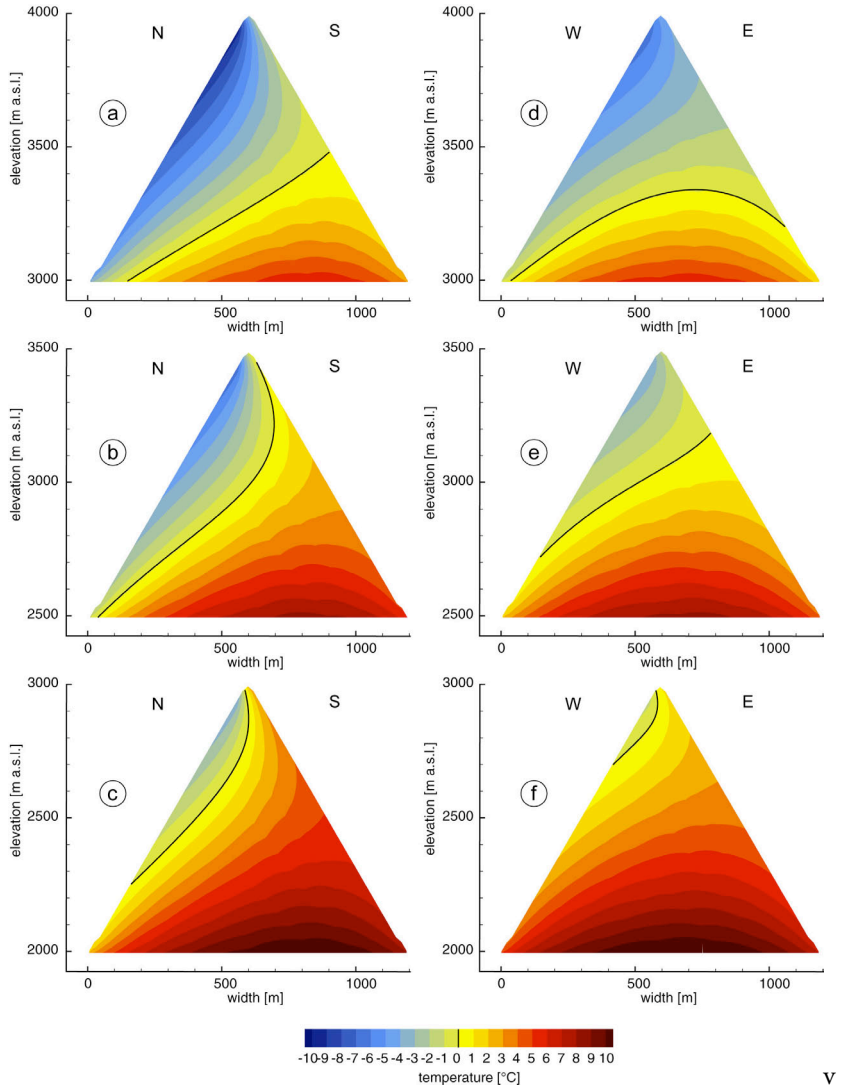

Figure 4. Steady-state subsurface temperature fields in six idealized ridges with a 60° slope. The black line corresponds to the 0 °C-isotherm and represents the permafrost boundary. Ridges a)-c) have north and south-facing slopes, ridges d)-f) west- and east-facing slopes, respectively. Three different elevation ranges are shown.

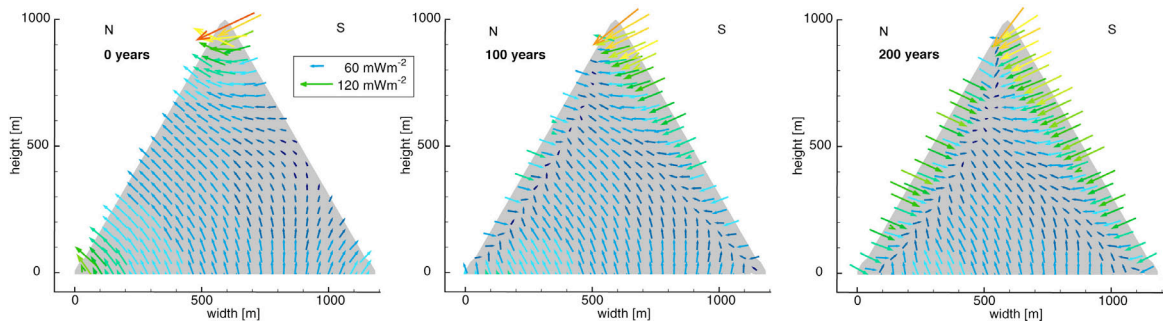

Figure 5. Distribution of heat fluxes in an idealized ridge with south- and north-facing slopes for steady state conditions (0 y), the situation after 100 y and after 200 y, considering a rise in ground surface temperatures of 3.5 °C on the northern and 2.5 °C in the southern flank, respectively.

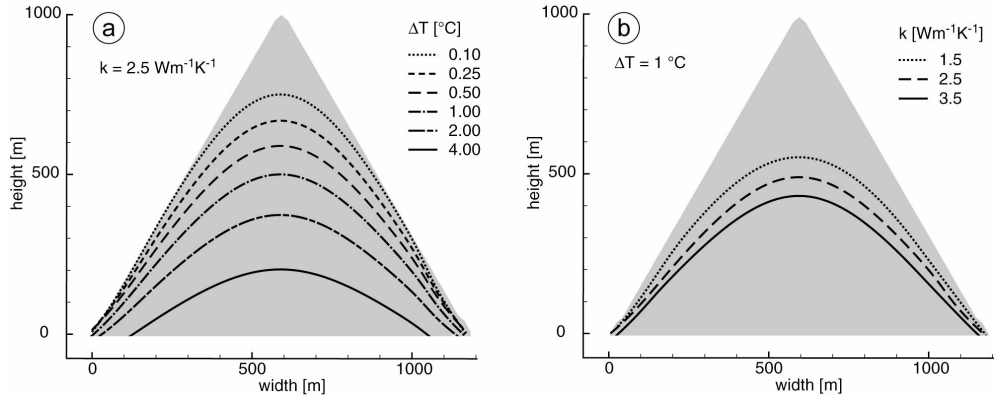

Figure 6. The influence of the geothermal heat flux exponentially decreases towards the top of the geometry. On the left (a), the temperature difference between model runs with a constant geothermal heat flux and one with a zero heat flux lower boundary condition is shown. On the right (b), the line above this difference amounts to less than 1 °C is drawn for different thermal conductivities.

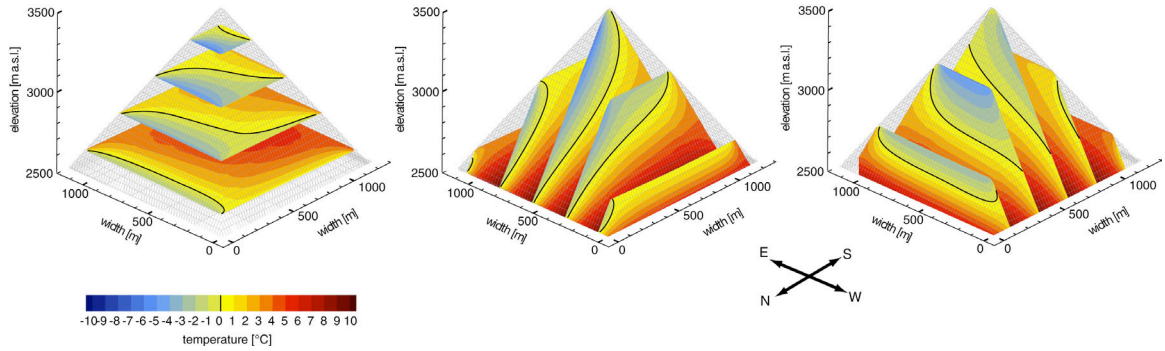

Figure 7. The temperature distribution in a pyramid that represents a simplified peak is visualized with x-, y- and z-slices. The black line corresponds to the 0 °C-isotherm and represents the permafrost boundary. The three-dimensional character of the permafrost body becomes evident.

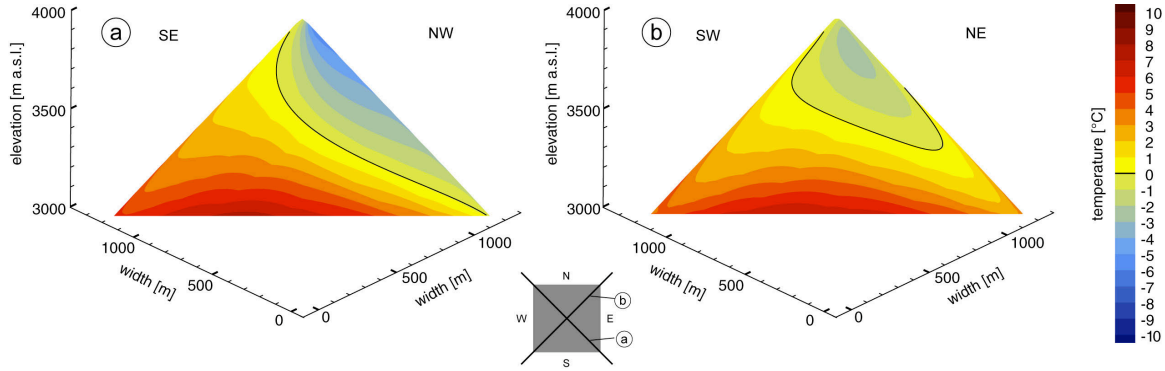

685

Figure 8. Steady state temperature distribution shown in two slices taken along the edges of a pyramid geometry. The temperatures a few decameters below the edges strongly differ from the thermal conditions at the surface as a result of three-dimensional effects.

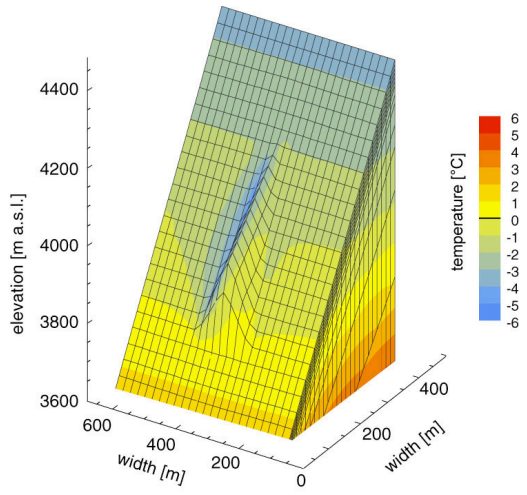

690 **Figure 9.** Situation of a spur on a south-facing rockwall. The spur modifies the surface temperatures and therewith the temperatures in the underground. This may lead to local permafrost occurrence in a rockwall that generally does not contain permafrost.

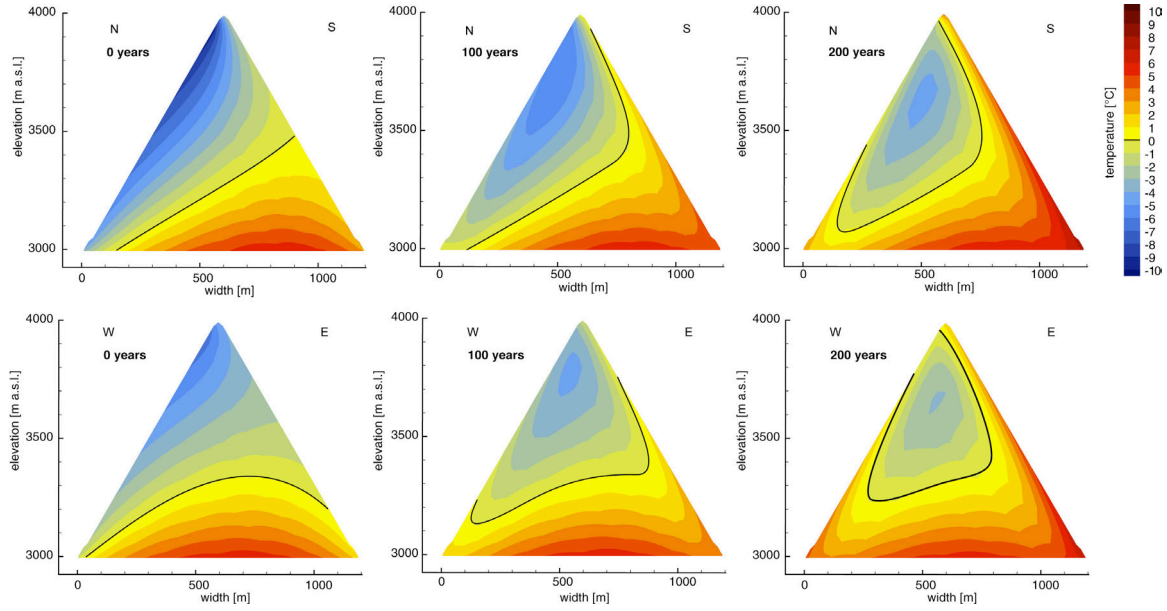

Figure 10. Evolution of subsurface temperatures in a ridge with a south and a north slope (top) and
695 an east and a west slope (bottom), respectively, for steady state and after a time period of 100 and 200 years. The warming at the surface was set to +3.5 °C for north slopes, +2.5 °C for south slopes and +3 °C for east and west slopes over a time period of 100 years The black line corresponds to the 0 °C-isotherm and represents the permafrost boundary.

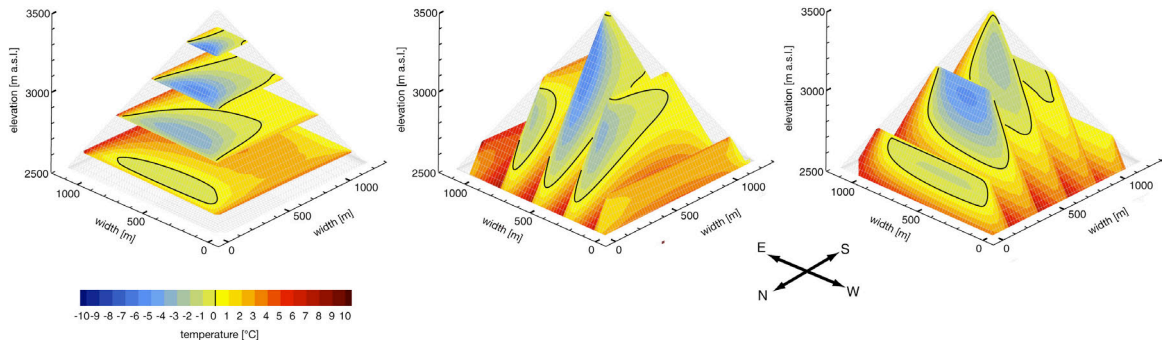

Figure 11. Temperature evolution of the pyramid situation shown in Figure 6, considering a warming at the surface of +3.5 °C for north slopes, +2.5 °C for south slopes and +3 °C for east and west slopes over a time period of 100 years. The black line corresponds to the 0 °C-isotherm and represents the permafrost boundary.

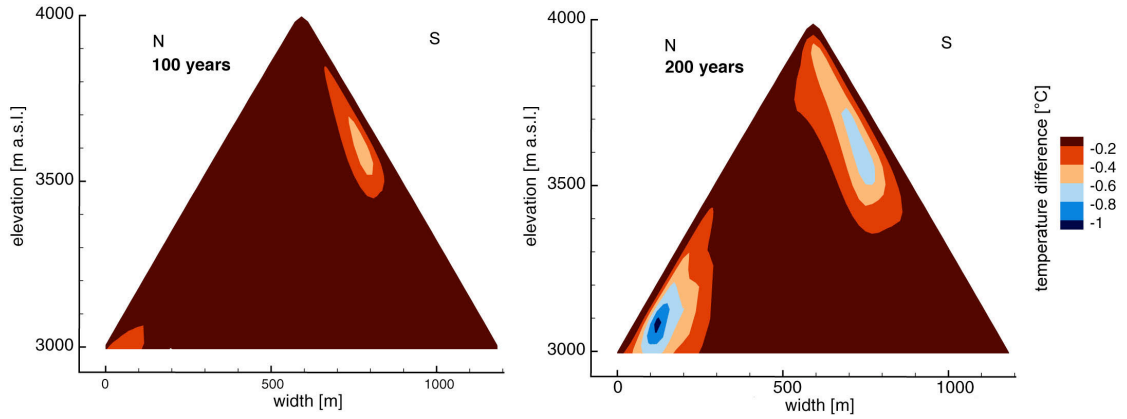

Figure 12. Difference between model runs with no heat source and such taking into account latent heat effects as modeled for a porosity of 3% and a time period of 100 (left) and 200 years (right). At locations that show differences between the model runs phase changes take place and, hence, these locations designate areas where permafrost is actually degrading.

Publication II

Ground Surface Temperature Scenarios for Complex High-Mountain Topographies Based on Regional Climate Model Results

This study focuses on changes in local scale ground surface temperatures (GST) for varying topographical situations (i.e., slope, aspect, and elevation) and the uncertainty ranges associated with the assessment of GST changes based on RCM output. We compiled 12 scenario climate time series using different RCMs, emission scenarios, and downscaling approaches. These time series were used to drive a one-dimensional energy balance model and calculate possible GST changes for 36 locations having different topographic settings.

Main Findings

- An average GST rise of 3.5 °C from 1982–2002 to 2071–2091 was calculated for steep Alpine rock walls. Variability in resulting GST changes is high and mainly caused by different scenario climate time series used, rather than by topography.
- For the topographic factors, a significant influence on the GST change was shown only for aspect. North faces are more sensitive to changes in atmospheric conditions, whereas variability of the results between different RCMs and scenarios is higher for south faces.
- The use of RCM-based climate scenarios is preferable to incremental scenarios for the calculation of GST changes in complex topography. Multi-model approaches allow for an assessment of possible ranges of change and of model uncertainties.

Citation

Salzmann, N., Noetzli, J., Hauck, C., Gruber, S., Hoelzle, M., and Haeberli, W. 2007. Ground surface temperature scenarios for complex high-mountain topographies based on Regional Climate Model results. *Journal of Geophysical Research*, 112, F02S12, doi:10.1029/2006JF000527.

Ground Surface Temperature Scenarios in Complex High-mountain Topography Based on Regional Climate Model Results

Nadine Salzmann[1], Jeannette Noetzli[1], Christian Hauck[2], Stephan Gruber[1,3], Martin Hoelzle[1] and Wilfried Haeberli[1]

[1]Glaciology and Geomorphodynamics Group, Department of Geography, University of Zurich, Switzerland

[2]Institute for Meteorology and Climate Research, University of Karlsruhe, Germany.

[3]EDYTEM Lab, UMR 5204 CNRS – Université de Savoie, France

Abstract

Climate change can have severe impacts on the high-mountain cryosphere, such as instabilities in rock walls induced by thawing permafrost. Relating climate change scenarios produced from global climate models (GCMs) and regional climate models (RCMs) to complex high-mountain environments is a challenging task. The qualitative and quantitative impact of changes in climatic conditions on local to micro scale ground surface temperature (GST) and the ground thermal regime is not readily apparent. This study assesses a possible range of changes in the GST (ΔGST) in complex mountain topography. To account for uncertainties associated with RCM output, a set of 12 different scenario climate time series (including 10 RCM-based and 2 incremental scenarios) was applied to the topography and energy balance (TEBAL) model to simulate average ΔGST for 36 different topographic situations. Variability of the simulated ΔGST is related primarily to the emission scenarios, the RCM, and the approach used to apply RCM results to the impact model. In terms of topography, significant influence on GST simulation was shown by aspect because it modifies the received amount of solar radiation at the surface. North faces showed higher sensitivity to the applied climate scenarios, while uncertainties are higher for south faces. On the basis of the results of this study, use of RCM-based scenarios is recommended for mountain permafrost impact studies, as opposed to incremental scenarios.

Published in Salzmann, N., J. Noetzli, C. Hauck, S. Gruber, M. Hoelzle, and W. Haeberli 2007. Ground surface temperature scenarios in complex high-mountain topography based on regional climate model results, Journal of Geophysical Research, 112, F02S12, doi:10.1029/2006JF000527.

1 Introduction

The ground thermal regime in high-mountain areas is primarily determined by regional atmospheric processes, the local surface and subsurface characteristics, topography, and heat flux from Earth's interior. Climatic changes cause changes in the ground surface temperature (ΔGST), which are determined by the energy balance at the surface. ΔGST is propagated in the subsurface primarily by heat conduction. In mountain areas with widespread permafrost occurrence such changes can have severe impacts, for example, on the stability of rock walls, debris slopes, and infrastructure [*Haeberli et al.*, 1997; *Diaz et al.*, 2003; *Schiermeier*, 2003; *Kääb et al.*, 2005]. *Davies et al.* [2001] demonstrated that rising temperature influences the stability of frozen rock joints, with minimal stability reached slightly below 0 °C.

Assessment of climate impacts on mountain permafrost is challenging. Simulation of climate scenarios at regional to local scales, as required for regional climate impact studies, is generally difficult, and is associated with many uncertainties [e.g., *Noguer et al.*, 1998; *Visser et al.*, 2000; *IPCC*, 2001a]. Mountain regions are therefore among the most ambitious areas for simulating future climate conditions [*Denis et al.*, 2002; *Frei et al.*, 2003], mainly because of their spatially heterogeneous environment and the regional to local climatic subsystems affected by topography. In terms of climate impacts on mountain regions, the high- mountain cryosphere constitutes a particularly sensitive system because of its proximity to melting conditions [*Haeberli and Beniston*, 1998]. It is not clear in detail, however, how climatic changes will affect GST in complex mountain topography.

Currently, the only physically plausible tools for simulating regional climate change scenarios are regional climate models (RCMs) [e.g., *Giorgi and Mearns*, 1999; *IPCC*, 2001b]. The possibilities of applying RCM results to an energy-balance model for simulation of GST in complex high-mountain topography was illustrated by *Salzmann et al.* [2007a]. Use of a single RCM scenario, however, is not sufficient for assessing the possible range of changes in GST, because of the uncertainties associated with modeling scenario climate conditions. These uncertainties arise from those in the forcing emission scenarios [*IPCC*, 2000] and the global climate models (GCMs) / RCMs [e.g., *Noguer et al.*, 1998; *Visser et al.*, 2000; *Pan et al.*, 2001; *Vidale et al.*, 2003; *Frei et al.*, 2006], and from possible future changes in climate variability [*Schär et al.*, 2004]. When applying RCM results to an impact model, the impact model itself is another source of uncertainty for the final outcome. As a consequence, assessment of a possible range of changes in GST requires application of a multimodel approach that includes various emission scenarios, RCMs, and application procedures.

The present study is concerned with assessing the possible range of changes in GST in complex high-mountain topography. For that purpose, changes in GST are simulated with the

Topography and Energy BALance (TEBAL) model for 36 different topographic situations, based on 12 different scenario climate time series (including 10 RCM-based and 2 incremental-scenario time series). As a first step, the study focuses on steep rock walls (>50°) because factors such as variable seasonal snow cover [e.g., *Zhang et al.*, 2001; *Ishikawa*, 2003; *Zhang*, 2005] and strongly heterogeneous surface layers [e.g., *Gorbunov et al.*, 2004; *Hanson and Hoelzle*, 2004], both of which significantly modify GST, can be neglected. Hence ΔGST on steep rock walls is a direct and unfiltered impact of changed atmospheric conditions. The influence of changed thermal surface conditions at greater depths is not treated in this study.

2 Data, Models, and Methods

2.1 Local Observed Climate Time Series

Observational data (OBS) were obtained for the climate station at Corvatsch (3,315 m a.s.l.) [46.25/9.49], Upper Engadine, Switzerland) from MeteoSwiss (Swiss Federal Office of Meteorology and Climatology). The Corvatsch area is among the most intensely investigated permafrost sites in the European Alps [*Hoelzle et al.*, 2002]. The climate station at Corvatsch began operation in 1981. To generate an observational time series covering the same period as the time slices of RCM control runs (CTRL; 1961–1990), the Corvatsch time series was extended with linear regression using neighboring high-elevation climate stations that (1) extend back to 1961, and (2) show high correlation with the Corvatsch climate time series (for details see *Salzmann et al.* [2007a]).

2.2 Scenario Climate Time Series

A set of 12 daily scenario climate time series was constructed (Figure 1) to be used with the TEBAL model, described below, which simulates local GST for given topographic situations. The set includes 10 RCM-based and 2 incremental scenario time series.

The RCM-based daily scenario climate time series were created from the results of five RCM simulations performed within the European project *Prediction of Regional scenarios and Uncertainties for Defining EuropeaN Climate change risks and Effects* (PRUDENCE) [*Christensen et al.*, 2002]. Results from the control (CTRL 1961–1990) and scenario (SCEN 2071–2100) simulations of the following three RCMs were used:

(1) Climate High Resolution Model (CHRM) [see *Lüthi et al.*, 1996; *Vidale et al.*, 2003] from the ETH-Z (Switzerland),

(2) Regional Climate Model (RegCM) [see *Giorgi et al.*, 1999; *Pal et al.*, 2000] from the ICTP (Italy), and

(3) regional atmospheric climate model (HIRHAM) [see *Christensen et al.*, 1996] from the DMI (Denmark).

Each of these RCMs was driven by the HadAM3H GCM from the Hadley Centre (UK), forced by the SRES emission scenarios A2 and B2 (CHRM only by A2). Model organization is represented schematically in Figure 1. The A2 and B2 emission scenarios [*IPCC*, 2000] assume different developments of the amount of greenhouse gas (GHG) emissions for the future. The A2 scenario projects high GHG emissions by assuming high population and energy growth combined with medium gross domestic production. For the B2 scenario, the driving forces are assumed to be more moderate compared to the A2 scenario and a lower level of GHG emission is therefore projected. A GCM forced with the A2 emission scenario simulates higher air temperatures than the same GCM forced with the B2 emission scenario. However, different GCMs simulate a range of possible air temperatures due to internal model limitations [e.g., *Visser et al.*, 2000; *Räisänen et al.*, 2004]. As a consequence, the lower and upper bounds of the uncertainty ranges of the air temperatures simulated by different GCMs and the two emission scenarios produce slight overlap [*IPCC*, 2001b].

Outputs from the RCMs was adapted for the high- mountain impact analysis using the so-called 'delta' and 'bias' approaches, discussed in detail by *Salzmann et al.* [2007a]. Both approaches use output from the single RCM grid box out of the four that are closest to the location of interest (Corvatsch) and whose monthly CTRL run data statistically fit best with the Corvatsch monthly observational time series. The local daily scenario climate time series (d-SCEN, b-SCEN) are calculated from the single RCM grid box results as follows:

$$\text{Delta: } d\text{-SCEN}_d = \text{OBS}_d + (\text{SCEN } 30_{y,m} - \text{CTRL } 30_{y,m}) \quad (1)$$

$$\text{Bias: } b\text{-SCEN}_d = \text{SCEN}_d + (\text{CTRL } 30_{y,m} - \text{OBS } 30_{y,m}) \quad (2)$$

where the subscripts d, 30 y, and m stands for 'daily', '30-year mean', and 'monthly', respectively. For solar radiation and precipitation, ratios are used rather than differences.

The main distinction between the two approaches is that the bias approach considers, whereas the delta approach ignores, a possible change in variability.

Variables from the RCM results in this study included 2 m temperature, precipitation, global radiation, and air pressure. Because we neglected snow cover (because of rock wall steepness) the most important variables for calculating GST are air temperature and global radiation [cf. *Lewkowicz*, 2001; *Gruber et al.*, 2004a]. Monthly 30-year averages for these variables are shown in Figures 2a and 2b, for OBS and for the constructed and adapted SCENs for Corvatsch. The 2 m temperature (Figure 2a) shows the largest changes during summer months for all RCMs and

emission scenarios. For global radiation (Figure 2b), the largest simulated changes occur in the (early) summer months.

In addition to the RCM-based scenario climate time series, two incremental scenario time series were created (cf. Figure 1). For these, observed air temperature was increased constantly by arbitrary amounts of 2 °C and 3 °C, throughout the 20-year time period. Other climate variables were not modified for these scenarios. Incremental scenario approaches are physically implausible and do not present a credible future scenario [*IPCC,* 1994]. However, because such climate scenarios require little effort and are easy to apply, they are commonly used in climate (cryosphere) impact studies [e.g., *Hoelzle and Haeberli*, 1995; *Stocker-Mittaz et al.*, 2002; *Zemp et al.*, 2006], albeit, in fact, more to explore system sensitivities than scenarios in an intrinsic manner.

2.3 Modeling Energy Balance in Complex Topography

The TEBAL energy balance model (Figure 3) simulates time series of surface energy fluxes and subsurface temperatures in complex topography, based on observed climate time series (usually taken from a climate station), topographic, and surface and subsurface information [*Gruber et al.*, 2004a, 2004b]. TEBAL was developed on the basis of an earlier model, PERMEBAL [*Stocker-Mittaz*, 2002; *Stocker-Mittaz et al.*, 2002]. Clear-sky short-wave incident radiation is modeled on the basis of sun-terrain geometry, following *Corripio* [2003], and atmospheric attenuation is based on a standard atmosphere. Measured global radiation is partitioned into direct and diffuse components [*Erbs et al.*, 1982]. Diffuse radiation from the sky and surrounding terrain is calculated in a lumped approach, using sky and terrain view factors and ground albedo [*Stocker-Mittaz et al.*, 2002]. Long-wave radiation from the sky [*Konzelmann et al.*, 1994] and surface temperatures are used to calculate long-wave irradiance in complex topography using terrain and sky-view factors [*Plüss and Ohmura*, 1997]. For steep rock walls, turbulent latent heat flux was reduced by a factor of 100 because of the assumed lack of snow cover and surface water. Vapor pressure is parameterized using methods described by *Flatau et al.* [1992] and *Plüss* [1997]. Latent and sensible turbulent fluxes were calculated using the bulk method [*Oke*, 1987; cf. *Suter et al.*, 2004]. Residuals of the surface energy balance are assigned to the ground heat flux and used as a boundary condition for the one-dimensional Crank-Nicholson subsurface heat-conduction scheme. The resulting temperature for the surface node is converged with an initial guess of surface temperature using a secant iteration procedure. Effects of latent heat during freeze or thaw of water in the rock is included in apparent heat capacity, based on an exponential representation of unfrozen water content.

We validated the version of TEBAL used in this study by simulating 14 logger-measured rock wall temperature time series in the Swiss Alps during the hydrological year 2001/2002 by adjusting slope, elevation, and aspect to each logger site, as described by *Gruber et al.* [2004a]. The daily time series used to drive the model were taken from the Corvatsch (3,315 m a.s.l.) and

Jungfraujoch (3,580 m a.s.l.) climate stations. The atmospheric lapse rate was taken as 0.006 K km^{-1}, volumetric heat capacity was set to 1.8 x 10^6 J m^{-3} K^{-1} and thermal conductivity to 2.2 W K^{-1} m^{-1}, based on *Cermak and Rybach* [1982] and *Wegmann et al.* [1998]. Horizons (e.g., local shadow effects) of the logger sites were not included in the validation runs. The overall simulation of the rock wall daily mean temperatures resulted in a mean coefficient of determination of r^2=0.85, an RMS of 3.31, and a mean absolute difference in MAGST (mean annual ground-surface temperature) of 1.05 °C.

2.4 Applied Approach Design

The 20-year observed daily climate time series (OBS: 1982–2002) from Corvatsch and the 12 constructed scenario climate time series (2071–2091) were applied to TEBAL to calculate the 20-year mean daily GST for 36 specific topographic situations, including three elevation levels (2,500, 3,500, 4,500 m a.s.l.), four slope angles (50°, 60°, 70°, 80°) and three aspects (north, east/west, south). To initialize the temperature profile in TEBAL, a 2-year spin-up in each run was included. Equal surface characteristics were used for each run. For an 'idealized' high-mountain rock wall, values of 0.0001 m, 0.96 and, 0.2 were used for roughness length, emissivity, and albedo.

The change in GST (ΔGST) for each of the 36 topographic situations was calculated by subtracting the 20-year GST average on the basis of the OBS climate time series from each 20-year GST average, based on the constructed scenario climate time series.

3 Discussion

An overview of simulated changes in average GST and its complex distribution is given in Figure 4, and supplemented by Figures 5, 6, and 7. Several findings are apparent.

Subset a The range of simulated ΔGST is high, averaging 3.5 °C. This was caused by the use of different emission scenarios, of different RCMs, and of the two approaches (delta and bias) applied. The relative distribution of the individually calculated ΔGST points within the calculated ranges is relatively constant throughout all topographic situations.

Subset b Of the three topographic parameters, only aspect has significant influence on ΔGST.

Subset c RCM-based scenarios (except rea2d) lead to significantly higher ΔGST for north facing slopes than for south facing slopes; the incremental scenarios are not sensitive to aspect.

Subset d The largest ΔGSTs were achieved by applying the A2 emission scenario.

Subset e If variability is allowed to change between OBS and SCEN (bias approach), the increase in ΔGST is reduced.

Subset f The approach applied can reverse the result that A2-forced scenario simulations generally yield higher ΔGST than B2-forced scenarios, also when the same RCM is used.

3.1 Higher Sensitivity of North Faces

A summary based on the median of all RCM simulation runs is given in Figure 5. The median is assumed to represent the 'best guess' of all modeled ΔGST. Prominent in Figure 5 is the difference between RCM-based and incremental scenarios. Although RCM-based scenarios show a 1 °C difference in ΔGST between north faces and south faces, sensitivity to aspect is not evident in the incremental scenarios. This is attributed to differences in solar radiation received at the surface. For incremental scenarios, air temperature was modified but global radiation was not, in contrast to RCM-based scenarios, where both variables were modified. The higher sensitivity of north faces is probably caused by the differences in solar radiation received at the surface of north and south faces. While the average GST of south faces is mainly a function of air temperature and incoming solar radiation throughout the entire year, the average on north faces in winter is to a large extent dependent on air temperature, because no direct solar radiation is received at the surface during that time of the year. Because the projected change of global radiation is highest during summer months (see Figure 2b), the relative change of global radiation is higher for north faces than for south faces. As a consequence, north faces are more sensitive to the climate scenarios applied in this study.

Another prominent result from Figure 5 is that aspect is the only topographic parameter with significant influence on ΔGST. The effects of elevation and slope are very small and probably within the internal noise level of the models. This result reflects the relatively high sensitivity of GST to solar radiation received at the surface, which is, in turn, a function of aspect.

3.2 Higher Variability on South Faces

Figure 6 shows the 'range of ΔGST' (RΔGST). In contrast to ΔGST, which decreases from north to south (see Figure 5), RΔGST increases from north to south by about 1 °C. The variability and thus the uncertainty about ΔGST are higher for south faces than north faces. Again, this is caused by the higher influence of solar radiation on south faces, which receive solar radiation during the entire year, while north faces only receive it during summer months.

A similar, but less pronounced effect is theoretically possible through the effect of slope on receipts of solar radiation, since steeper slopes potentially receive less solar radiation during the annual cycle [e.g., *Oke*, 1987]. However, the value of this effect depends on the related latitude and aspect. In this study, the effects of slope (and also of elevation) were weak.

3.3 Changes in N-S Differences

Under current climate conditions in the Swiss Alps, there is a measured difference in mean annual GST of about 6–8 °C between north and south exposed rock walls [*Gruber et al.*, 2004a]. Assuming that the results from Section 3.1, about a higher sensitivity of north faces are valid for the entire Swiss Alps, observed differences in rock wall GST would decrease under future scenario climate conditions as the GST on north faces would increase more than on south faces. Aspect-dependent warming of the surface will also affect qualitative changes of the ground thermal regime [*Noetzli et al.*, 2007] and can lead to enhanced rock fall activities on northern slopes, as observed in the European Alps during the hot and dry summer of 2003.

Large decreases (up to 2 °C) in N-S temperature differences result for HIRHAM and RegCM applied with the bias approach, independent of the forced emission scenario (Figure 7). Small decreases result with the delta approach, independent of the RCM type and emission scenario. The change in climate variability is therefore a dominant factor for the differential warming of north and south faces in the applied scenarios.

3.4 Combined Influences of Emission Scenario, RCM, Changed Variability, and Topography

Generally, the largest ΔGST is achieved by applying the A2 and the lowest by applying the B2 emission scenario, independent of RCM type. This tendency can, however, be reversed by the type of RCM used (Figure 4), consistent with the known uncertainties of GCMs / RCMs due to model internal limitations (Section 2.2). A change in climate variability (in our case forced by use of the bias approach), together with potentially higher solar radiation (e.g., due to south slope), can result in higher ΔGST with the B2 than with the A2 emission scenario, for the same RCM. This can be seen in Figure 4 (Subset f), where HIRHAM simulates higher ΔGST with the B2 emission scenario when the delta approach is applied than with the A2 emission scenario and the bias approach. This HIRHAM-specific behavior is likely to be caused by the higher global radiation of HIRHAM B2 compared to HIRHAM A2 during summer (Figure 2b) and/or by the change in variability associated with the bias approach.

The lowest values of RΔGST on south faces are modeled by HIRHAM B2 used with the bias approach (Figures 4 and 6). On north faces, the RegCM B2 used with the delta approach yields the lowest values of the range of GST change. The highest values are obtained by the HIRHAM A2 scenario used with the delta approach for almost all topographic situations (Figure 4). This is very likely caused by highest simulated annual air temperature of HIRHAM A2, during almost the entire year (see Figure 2a). However, a detailed explanation of the model behavior requires an extended analysis of the daily time series rather than analysis of averages, as presented here.

3.5 Significance of the Results

The results of this study are valid only for the specific and theoretical high-mountain situation assumed here. For other regions of the Alps, results must be adjusted according to the Alpine climatic subregion in which they are located, e.g., on the basis of the Alpine climate classification after *Schüpp* [1954]. For rock walls less steep than those assumed in this study, and larger areas, the important influence of a seasonal snow cover and changes in its timing and duration must be taken into account. Furthermore, different results would be obtained if different surface properties were used. Only three RCMs and two emission scenarios, forced by a single GCM, were used in this study. Use of different GCMs would increase the uncertainty range. Simulating ΔGST over a larger area requiring the use of a digital terrain model (DTM), introduces additional uncertainty [*Salzmann et al.*, 2007b].

In this study, the importance of global radiation was emphasized. Global radiation in high-mountain areas is influenced significantly by cloud convection during summer. RCMs with horizontal resolution of 50 km (as has been used here), cannot resolve such sub-grid processes. RCM results for global radiation are therefore associated with high uncertainty, particularly in mountainous areas and during summer. This problem is minimized in this study by adjusting the direct output from RCMs to a specific location, using the delta and bias approach.

4 Conclusion and Perspectives

In this study, we calculated and analyzed ΔGST and the RΔGST for 36 high-mountain topographic situations derived from an input matrix of 10 RCM-based scenario time series (including 3 RCMs, 2 SRES emission scenarios, 2 approaches) and 2 incremental scenario climate time series. We conclude the following.

- Use of RCM-based scenarios is preferable to incremental scenarios in impact studies in complex mountain topography. This preference may not hold for sensitivity analyses.
- Use of multimodel approaches, such as inclusion of different emission scenarios and GCMs / RCMs, is required to assess possible ranges of future ground surface temperature changes and to cover the range of uncertainty associated with the models.
- Aspect is more important than slope and elevation for the GST.
- The influence of topography on ΔGST is generally weaker than the influence of the different emission scenarios, RCMs, and application-approaches (delta/bias).
- Changes in the duration and thickness of seasonal snow cover will probably be the most important factor for changes in the ground thermal regime. Nevertheless, we show in this

study that relatively simple systems like steep rock walls also require detailed investigations about potential changes in GST.

On the basis of the strong variability of RCM output, there appear to be many uncertainties associated with possible impacts of climate change on GST in the complex topography of high-mountain environments. The range of uncertainties can only be assessed using physically plausible RCM-based scenarios, which take into consideration qualitative (e.g., increase of variability) and quantitative (e.g., increase of air temperature) changes of different atmospheric variables (e.g., global radiation).

If we assume that the general trend of our results is valid for the entire Alpine region, changes in GST and subsequent changes in the ground thermal regime can lead to serious rock falls and landslides that exceed the frequency and magnitude of known events.

The next steps for assessing scenarios of ground thermal regime in complex high-mountain topography include links to the subsurface [e.g., *Noetzli et al.*, 2007]. Furthermore, thorough analysis of the climate input time series from the RCMs, the time series of the GST, and the fluxes of the surface energy balance as opposed to averages is required. The input data set used to drive the local energy balance model TEBAL should be enlarged by including RCMs driven by different GCMs. Finally, use of probabilistic scenarios could further enhance the significance of the model results [e.g., *Wigley and Raper*, 2001; *Tebaldi et al.*, 2005].

Acknowledgments. This study was made possible thanks to the European Cooperation in the field of Scientific and Technical Research (COST-Action 719) and the Swiss National Science Foundation (NF-20- 10796./1). The RCM data were provided through the PRUDENCE data archive, funded by the EU through contract EVK2-CT2001-00132. We acknowledge the comments and suggestions of the editor and of the two anonymous reviewers and especially F. E. Nelson (Associate Editor) for his reviews and suggestions.

References

Cermak, V., and L. Rybach (1982), Thermal conductivity and specific heat of minerals and rocks, in Landolt-Bo¨rnstein Zahlenwerte und Funktionen aus Naturwissenschaften und Technik, Neue Ser. Phys. Eigensch. Gesteine, vol. 1a, edited by G. Angeneister, pp. 305–343, Springer, Berlin.

Christensen, J. H., O. B. Christensen, P. Lopez, E. Van Meijgaard, and M. Botzet (1996), The HIRHAM4 regional atmospheric climate model, Sci. Rep. 96-4, 51 pp., Dan. Meteorol. Inst., Copenhagen.

Christensen, J. H., T. R. Carter, and F. Giorgi (2002), PRUDENCE employs new methods to assess European climate change, Eos Trans. AGU, 83, 147.

Corripio, J. G. (2003), Vectorial algebra algorithms for calculating terrain parameters from DEMs and solar radiation modelling in mountainous terrain, Int. J. Geogr. Inf. Sci., 17, 1–23.

Davies, M. C. R., O. Hamza, and C. Harris (2001), The effect of rise in mean annual temperature on the stability of rock slopes containing icefilled discontinuities, Permafrost Periglacial Processes, 12, 137–144.

Denis, B., R. Laprise, D. Caya, and J. Co^te´ (2002), Downscaling ability of one-way nested regional climate models: The Big-Brother experiment, Clim. Dyn., 18, 627–646.

Diaz, H. F., M. Grosjean, and L. Graumlich (2003), Climate variability and change in high elevation regions: Past, present and future, Clim. Change, 59, 1–4.

Erbs, D. G., S. A. Klein, and J. A. Duffie (1982), Estimation of the diffuse radiation fraction for hourly, daily and monthly average global radiation, Sol. Energy, 28, 293–304.

Flatau, P. J., R. L. Walko, and W. R. Cotton (1992), Polynomial fits to saturation vapor-pressure, J. Appl. Meteorol., 31, 1507–513.

Frei, C., J. H. Christensen, M. De´que´, D. Jacob, R. G. Jones, and P. L. Vidale (2003), Daily precipitation statistics in regional climate models: Evaluation and intercomparison for the European Alps, J. Geophys. Res., 108(D3), 4124, doi:10.1029/2002JD002287.

Frei, C., R. Scho¨ ll, S. Fukutome, J. Schmidli, and P. L. Vidale (2006), Future change of precipitation extremes in Europe: Intercomparison of scenarios from regional climate models, J. Geophys. Res., 111, D06105, doi:10.1029/2005JD005965.

Giorgi, F., and L. O. Mearns (1999), Introduction to special section: Regional climate modeling revisited, J. Geophys. Res., 104, 6335–6352.

Giorgi, F., Y. Huang, K. Nishizawa, and C. Fu (1999), A seasonal cycle simulation over eastern Asia and its sensitivity to radiative transfer and surface processes, J. Geophys. Res., 104, 6403–6423.

Gorbunov, A. P., S. S. Marchenko, and E. Seversky (2004), The thermal environment of blocky materials in the mountains of central Asia, Permafrost Periglacial Processes, 15, 95–98.

Gruber, S., M. Hoelzle, and W. Haeberli (2004a), Rock-wall temperatures in the Alps: Modelling their topographic distribution and regional differences, Permafrost Periglacial Processes, 15, 299–307.

Gruber, S., M. Hoelzle, and W. Haeberli (2004b), Permafrost thaw and destabilization of Alpine rock walls in the hot summer of 2003, Geophys. Res. Lett., 31, L13504, doi:10.1029/2004GL020051.

Haeberli, W., and M. Beniston (1998), Climate change and its impact on glaciers and permafrost in the Alps, Ambio, 27(4), 258–265.

Haeberli, W., M. Wegmann, and D. Vonder Muehll (1997), Slope stability problems related to glacier shrinkage and permafrost degradation in the Alps, Eclogae Geol. Helv., 90, 407–414.

Hanson, S., and M. Hoelzle (2004), The thermal regime of the active layer at the Murtel rock glacier based on data from 2002, Permafrost Periglacial Processes, 15, 273–282.

Hoelzle, M., and W. Haeberli (1995), Simulating the effects of mean annual air temperature changes on permafrost distribution and glacier size. An example from the Upper Engadin, Swiss Alps, Ann. Glaciol., 21, 400–405.

Hoelzle, M., D. Vonder Muehll, and W. Haeberli (2002), Thirty years of permafrost research in the Corvatsch-Furtschellas area, eastern Swiss Alps: A review, Norw. J. Geogr., 56, 137–145.

Intergovernmental Panel on Climate Change (IPCC) (1994), Climate Change 1994: Radiative Forcing of Climate Change and Evaluation of the IPCC IS92 Emission Scenarios, edited by J. T. Houghton et al., Cambridge Univ. Press, Cambridge, U. K.

Intergovernmental Panel on Climate Change (IPCC) (2000), Emissions Scenarios 2000. Special Report of the Intergovernmental Panel on Climate Change, edited by N. Nakicenovic et al., 570 pp., Cambridge Univ. Press, U. K.

Intergovernmental Panel on Climate Change (IPCC) (2001a), Regional climate information—Evaluation and projections, in Climate Change –Third Assessment Report of the Intergovernmental Panel on Climate Change (IPCC), edited by F. Giorgi et al., chap. 10, pp. 583–638, Cambridge Univ. Press, New York.

Intergovernmental Panel on Climate Change (IPCC) (2001b), Climate Change 2001: The Scientific Basis: Report of the Intergovernmental Panel on Climate Change, edited by J. T. Houghton et al., Cambridge Univ. Press, Cambridge, U.K.

Ishikawa, M. (2003), Thermal regimes at the snow-ground interface and their implications for permafrost investigation, Geomorphology, 52(1–2), 105–20.

Kääb, A., J. M. Reynolds, and W. Haeberli (2005), Glacier and permafrost hazards in high mountains, in Global Change and Mountain Regions (A State of Knowledge Overview), edited by U. M. Huber, H. K. M. Bugmann, and M. A. Reasoner, pp. 225–234, Springer, Dordrecht, Netherlands.

Konzelmann, T., R. S. W. Van de Wal, W. Greuell, R. Binanja, E. A. C. Henneken, and A. Abe-Ouchi (1994), Parameterization of global and longwave incoming radiation for the Greenland Ice Sheet, Global Planet. Change, 9, 143–164.

Lewkowicz, A. G. (2001), Temperature regime of a small sandstone tor, latitude 80 degrees N, Ellesmere Island, Nunavut, Canada, Permafrost Periglacial Processes, 12, 351–366.

Lüthi, D., A. Cress, C. Frei, and C. Schär (1996), Interannual variability and regional simulations, Theor. Appl. Climatol., 53, 185–209.

Noetzli, J., S. Gruber, T. Kohl, N. Salzmann, and W. Haeberli (2007), Three-dimensional distribution and evolution of permafrost temperatures in idealized high-mountain topography, J. Geophys. Res., 112, F02S13, doi:10.1029/2006JF000545.

Noguer, M., R. G. Jones, and J. M. Murphy (1998), Sources of systematic errors in the climatology of a regional climate model over Europe, Clim. Dyn., 14, 691–712.

Oke, T. R. (1987), Boundary Layer Climates, 2nd ed., 435 pp. Routledge, London.

Pal, J. S., E. E. Small, and E. A. B. Eltahir (2000), Simulation of regionalscale water and energy budgets: Representation of subgrid cloud and precipitation processes within RegCM, J. Geophys. Res., 105, 29, 579–29, 594.

Pan, Z., J. H. Christensen, R. W. Arritt, W. J. Gutowski Jr., E. S. Takle, and F. Otieno (2001), Evaluation of uncertainties in regional climate change simulations, J. Geophys. Res., 106, 17, 735–17, 752.

Plüss, C. (1997), The energy balance over an alpine snowcover—Point measurements and areal distribution, Ph.D. dissertation, 115 pp., Geogr. Inst., Eidg. Tech. Hochsch., Zurich, Switzerland.

Plüss, C., and A. Ohmura (1997), Longwave radiation on snow-covered mountainous surfaces, J. Appl. Meteorol., 36, 818–824.

Räisänen, J., U. Hansson, A. Ullersteig, R. Döscher, L. P. Graham, C. Jones, H. E. M. Meier, P. Samuelson, and U. Willen (2004), European climate in the late twenty-first century: Regional simulations with two driving global models and two forcing scenarios, Clim. Dyn., 22, 13–31.

Salzmann, N., C. Frei, P.-L. Vidale, and M. Hoelzle (2007a), The application of regional climate model output for the simulation of high-mountain permafrost scenarios, Global Planet. Change, 56, 188–202, doi:10.1016/ j.gloplcha.2006.07.006.

Salzmann, N., S. Gruber, M. Hugentobler, and M. Hoelzle (2007b), The influence of different digital terrain models (DTMs) on alpine permafrost modeling, J. Environ. Modeling Assess, 12, 303–313.

Schär, C., P. L. Vidale, D. Lüthi, C. Frei, M. Häberli, M. A. Liniger, and C. Appenzeller (2004), The role of increasing temperature variability for European summer heat waves, Nature, 427, 332–336.

Schiermeier, Q. (2003), Alpine thaw breaks ice over permafrost's role, Nature, 424, 712.

Schüpp, M. (1954), Witterungsklimatologie der Schweiz, in Witterung und Klimatologie in Mitteleuropa, vol. 78, 2nd ed., edited by H. Flohn, pp. 159–167, Forsch. zur Dtsch. Landeskunde, Flensburg, Germany.

Stocker-Mittaz, C. (2002), Permafrost distribution modeling based on energy balance data, Ph.D. thesis, Univ. of Zurich, Zurich, Switzerland.

Stocker-Mittaz, C., M. Hoelzle, and W. Haeberli (2002), Modelling alpine permafrost distribution based on energy-balance data: A first step, Permafrost Periglacial Processes, 13, 271–82.

Suter, S., M. Hoelzle, and A. Ohmura (2004), Energy balance at a cold, alpine firn saddle, Seserjoch, Monte Rosa, Int. J. Climatol., 24, 1423–1442.

Tebaldi, C., R. Smith, D. Nychka, and L. O. Mearns (2005), Quantifying uncertainty in projections of regional climate change: A Bayesian approach to the analysis of multimodel ensembles, J. Clim., 18(10), 1524–1540.

Vidale, P. L., D. Lüthi, C. Frei, S. I. Seneviratne, and C. Schär (2003), Predictability and uncertainty in a regional climate model, J. Geophys. Res., 108(D18), 4586, doi:10.1029/2002JD002810.

Visser, H., R. J. M. Folkert, J. Hoekstra, and J. J. de Wolff (2000), Identifying key sources of uncertainty in climate change projections, Clim. Dyn., 45, 421–457.

Wegmann, M., G. H. Gudmundsson, and W. Haeberli (1998), Permafrost changes in rock walls and the retreat of Alpine glaciers: A thermal modelling approach, Permafrost Periglacial Processes, 9, 23–33.

Wigley, T. M. L., and S. C. B. Raper (2001), Interpretation of high projections for global-mean warming, Science, 293, 451–454.

Zemp, M., W. Haeberli, M. Hoelzle, and F. Paul (2006), Alpine glaciers to disappear within decades?, Geophys. Res. Lett., 33, L13504, doi:10.1029/ 2006GL026319.

Zhang, T. (2005), Influence of the seasonal snow cover on the ground thermal regime: An overview, Rev. Geophys., 43, RG4002, doi:10.1029/ 2004RG000157.

Zhang, T., R. G. Barry, and W. Haeberli (2001), Numerical simulation of the influence of the seasonal snow cover on the occurrence of permafrost at high altitudes, Norw. J. Geogr., 55, 261–266.

Figures

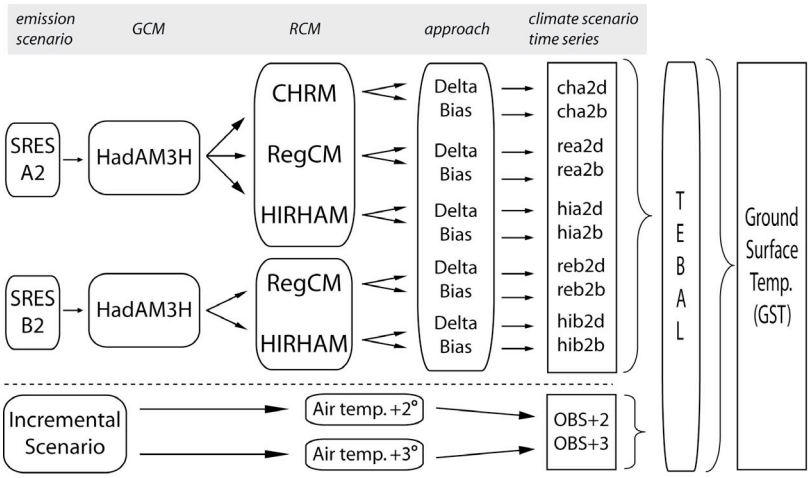

Figure 1. Matrix of the 12 constructed scenario climate time series, applied to the TEBAL energy balance model for simulation of GST.

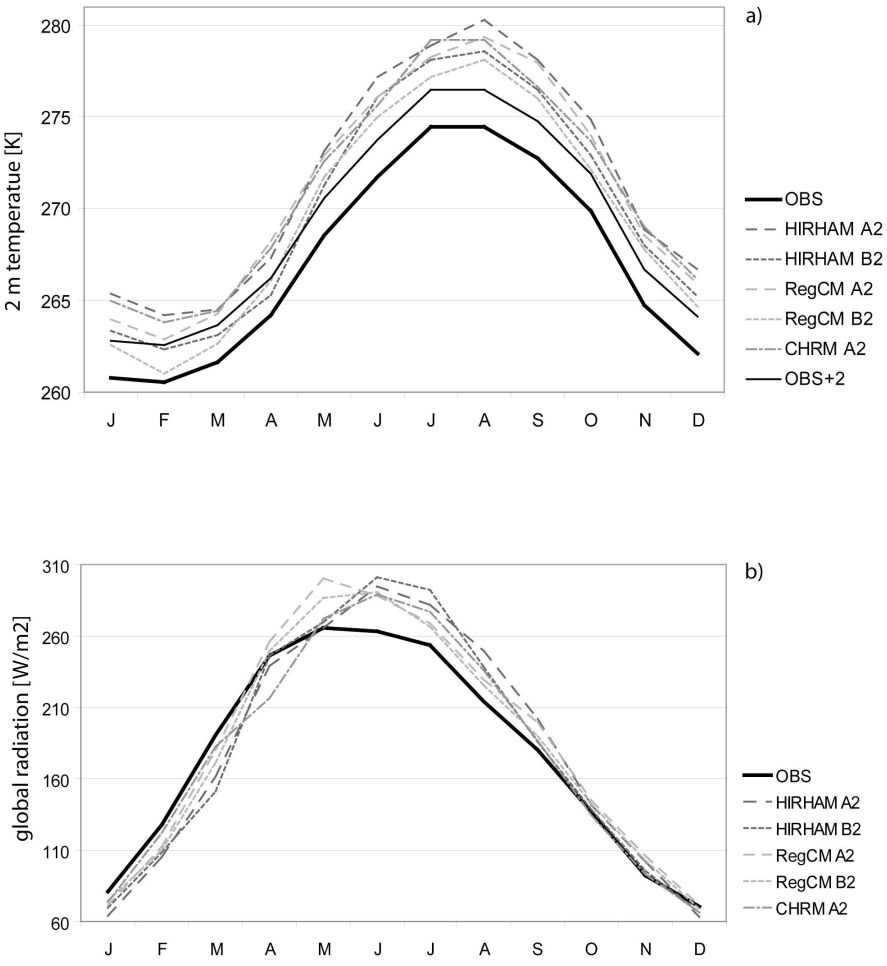

Figure 2. Monthly 30-year averages for (a) 2 m temperature and (b) global radiation of the OBS (Corvatsch) climate time series and constructed RCM-based scenario climate time series (adapted for Corvatsch).

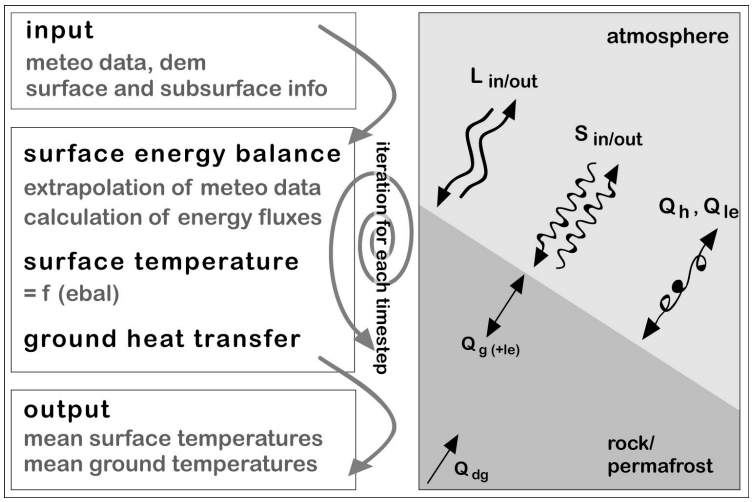

Figure 3. Structure of the TEBAL energy balance model.

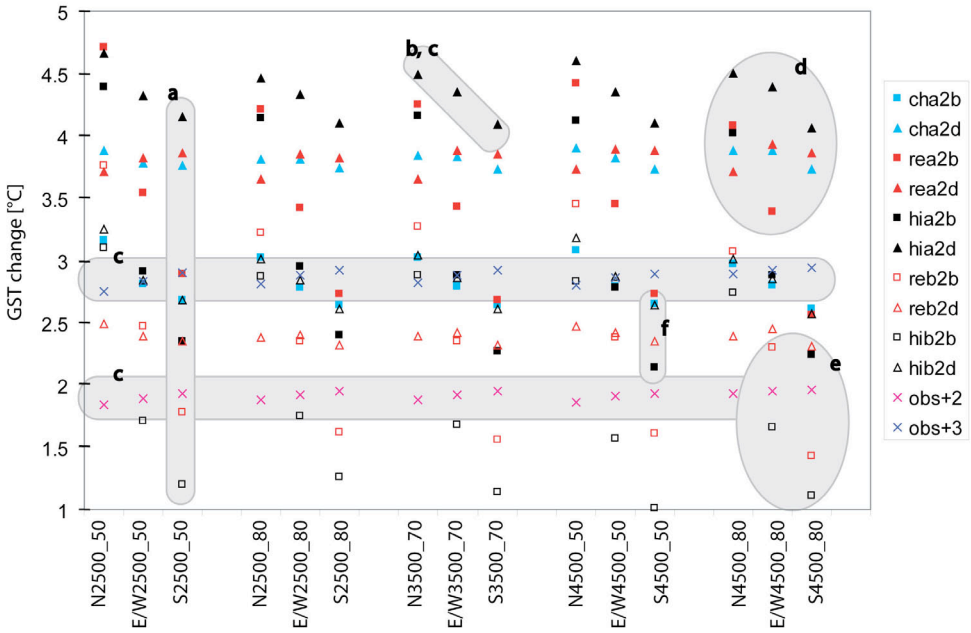

Figure 4. Plot of the 12 simulated GST changes (ΔGST=SCEN–OBS) for selected topographic situations. Each of the triplets on the x axis represents an elevation level with a specific slope allocated to the three different aspects (north, east/west, south); N2500_50 stands for north exposition, 2,500 m a.s.l., 50° slope. Owing to use of daily climate values (i.e., no afternoon convection), east and west are equal. Each RCM is represented by a different marker color. Simulations with the delta approach are represented by a triangle, and simulations with the bias approach are represented by a square. Solid markers represent ΔGST based on A2 emission

scenarios; open markers represent ΔGST based on B2 emission scenarios. Crosses represent results for the incremental scenarios. The highlighted subsets of GST results are marked with letters and are related to the summary at the beginning of this section.

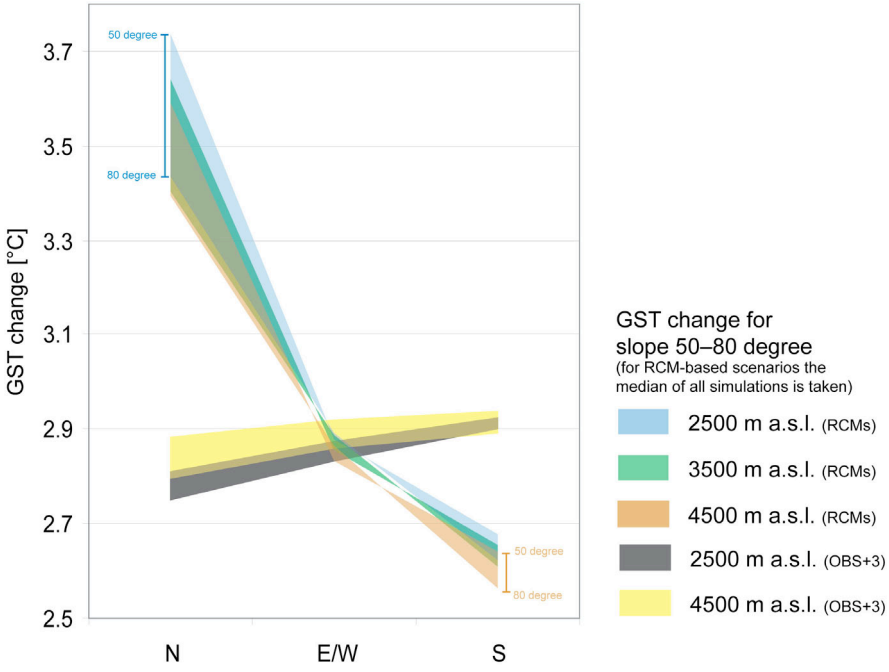

Figure 5. Median ΔGST for all scenario climate simulations, with separation between RCM-based and incremental scenarios (only OBS+3 is shown) and as a function of aspect (x axis), elevation (color), and slope (vertical extent).

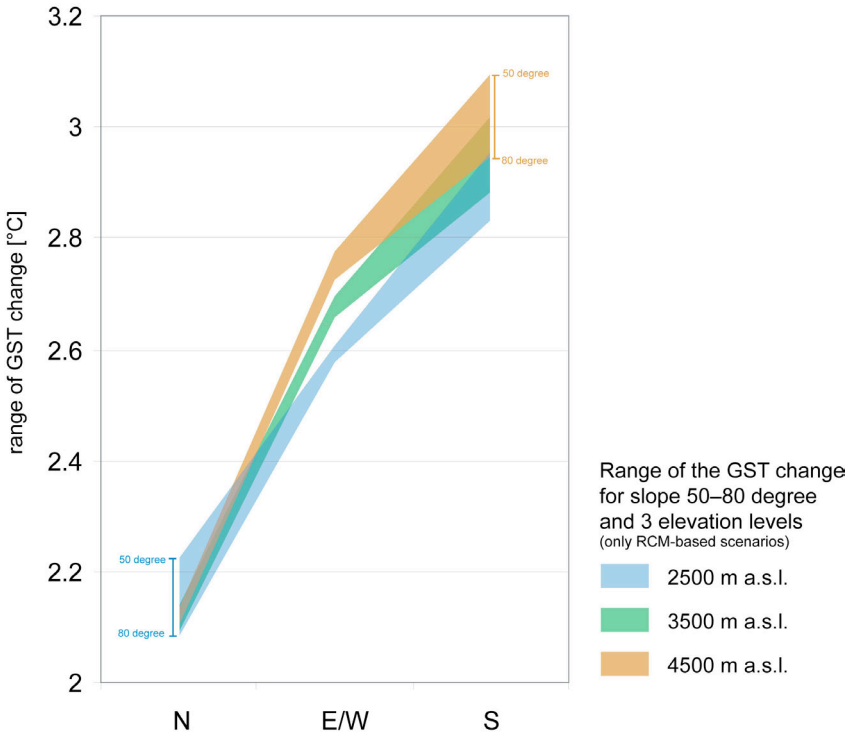

Figure 6. Range of ΔGST (RΔGST) including all scenario climate simulations (except incremental scenarios) as a function of aspect (x-axis), elevation (color), and slope (vertical extent).

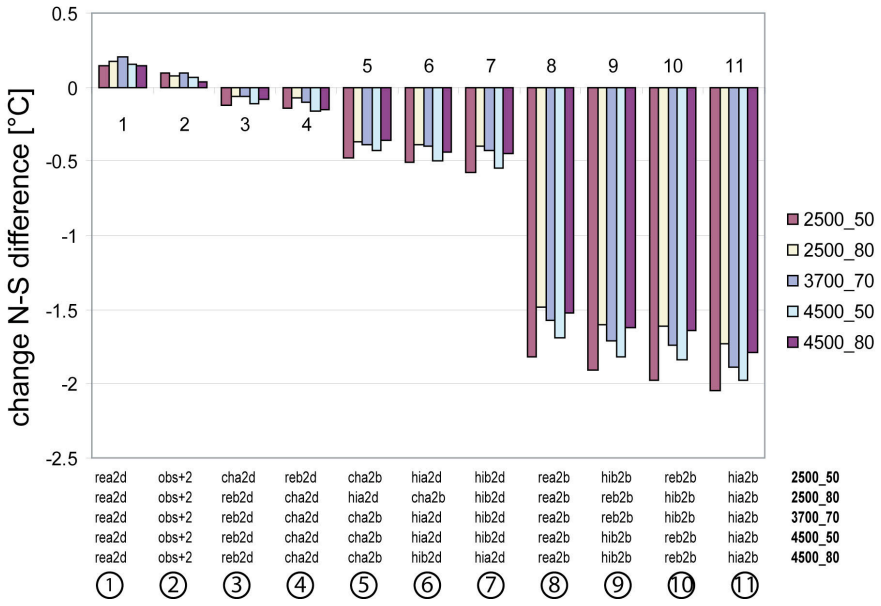

Figure 7. Change in the N-S difference for calculated GST for the scenario climate simulation (except OBS+3), shown as departure from observed climate time series.

Publication III

Transient Thermal Effects in Alpine Permafrost

This paper presents a systematic investigation of combined transient and topography effects in subsurface temperatures. Based on numerical experimentation with simplified mountain topography, we studied the effect of both past and projected variations in ground surface temperature (GST) on the distribution and thermal conditions of Alpine permafrost. Different GST histories, topographies, and subsurface characteristics were examined in sensitivity studies. In addition, the modeled transient three-dimensional subsurface temperature field in the Matterhorn, Switzerland, is presented.

Main Findings

- Paleoclimatic effects caused by past cold periods and the Holocene are small in the interior of high-mountain peaks, whereas recent and projected future warming lead to significant deviations from the steady state temperature field.
- Steep topography considerably accelerates the pace of a surface temperature signal intruding into the subsurface, making mountain permafrost particularly sensitive to degradation.
- Latent heat effects in low porosity rock can be neglected for model runs in time scales of millennia. Simulations over shorter timescales, in contrast, have to consider latent heat since it modifies the pattern and pace of permafrost degradation.
- Volume and vertical extent of warm permafrost significantly increase in the next centuries based on the scenario calculated.

Citation

Noetzli, J., and Gruber, S. in review. Transient thermal effects in Alpine permafrost. *The Cryosphere.*

Published discussion paper: Noetzli, J., and Gruber, S. 2008. Transient thermal effects in Alpine permafrost. *The Cryosphere Discussion,* 2, 185–224.

Transient Thermal Effects in Alpine Permafrost

Jeannette Noetzli and Stephan Gruber

Glaciology, Geomorphodynamics & Geochronology, Department of Geography, University of Zurich, Switzerland

Correspondence to:
Jeannette Noetzli, Glaciology, Geomorphodynamics & Geochronology, Department of Geography, University of Zurich, Winterthurerstrasse 190, CH-8057 Zurich
Email: jeannette.noetzli@geo.uzh.ch
Phone: +41 44 635 5224

Abstract

In high mountain areas, permafrost is important because it influences natural hazards and construction practices, and because it is an indicator of climate change. The modeling of its distribution and evolution over time is complicated by steep and complex topography, highly variable conditions at and below the surface, and varying climatic conditions. This paper presents a systematic investigation of effects of climate variability and topography that are important for subsurface temperatures in Alpine permafrost areas. The effects of both past and projected future ground surface temperature variations on the thermal state of Alpine permafrost are studied based on numerical experimentation with simplified mountain topography. For this purpose, we use a surface energy balance model together with a subsurface heat conduction scheme. The past climate variations that essentially influence the present-day permafrost temperatures at depth are the last glacial period and the major fluctuations in the past millennium. The influence of projected future warming was assessed to cause even larger transient effects in the subsurface thermal field because warming occurs on shorter time scales. Results further demonstrate the accelerating influence of multi-lateral warming in Alpine topography for a temperature signal entering the subsurface. The effects of thermal properties, porosity, and freezing characteristics were examined in sensitivity studies. A considerable influence of latent heat due to water in low-porosity bedrock was only shown for simulations over shorter time periods (i.e., decades to centuries). Finally, as an example of a real and complex topography, the modeled transient three-dimensional temperature distribution in the Matterhorn (Switzerland) is given for today and in 200 years.

Keywords subsurface temperatures, mountain permafrost, topography, numerical modeling, initial conditions, Matterhorn

1 Introduction

In alpine environments, permafrost is a widespread thermal subsurface phenomenon. Its warming and degradation in connection with climate change is regarded as a decisive factor influencing the stability of steep rock faces (Haeberli et al., 1997; Davies et al., 2001; Noetzli et al., 2003; Gruber and Haeberli, 2007). Assessing the impact of climate change on mountain permafrost is therefore important for the understanding of natural hazards and for construction practices (Haeberli, 1992; Harris et al., 2001; Romanovsky et al., 2007), especially in densely populated areas such as the European Alps. Further, permafrost degradation influences Alpine landscape evolution, hydrology, and it is monitored in the scope of climate observing systems (e.g., Global Terrestrial Network for Permafrost, GTN-P, within the Global Climate Observing System, GCOS). The quantification of temperature changes and the discernment of zones that are prone to permafrost degradation require knowledge of the spatial distribution of subsurface temperatures and of their evolution over time. Even though measured temperature profiles in boreholes enable an initial assessment of temperature changes (e.g., Isaksen et al., 2007; PERMOS, 2007), in complex mountain terrain they are only representative of isolated local spots and are of limited use for an extrapolation in space and time. The understanding of three-dimensional and transient subsurface temperature fields below steep topography can be improved by numerical modeling (e.g., Kohl et al., 2001; Noetzli et al., 2007b).

The simulation of ground temperatures below steep topography needs to account for two- and three-dimensional effects since geometry and variable surface temperatures induce strong lateral components of heat fluxes (Safanda, 1999; Kohl et al., 2001; Gruber et al., 2004c). Noetzli et al. (2007b) have shown that ground surface temperatures (GST) alone do not sufficiently indicate the thermal conditions at depth (when speaking of 'at depth' in this paper, we refer to the depth of the zero annual amplitude and deeper). Permafrost can occur at locations with clearly positive GST even if conditions are stationary. Stationary conditions, however, do not describe the situation found in nature and transient effects of past climate periods influence the subsurface temperature field. In the Swiss Alps, permafrost thickness ranges from a few metres up to several hundreds of metres below the highest peaks, such as the Monte Rosa massif (Luethi and Funk, 2001), and time scales involved in deep permafrost changes can be in the range of millennia, even without the retarding effect of latent heat (Lunardini, 1996; Kukkonen and Safanda, 2001; Mottaghy and Rath, 2006). Consequently, the influence of past cold periods such as the last Ice Age is likely to persist in permafrost temperatures in the interior of high mountains (Kohl, 1999; Kohl and Gruber, 2003). The recent and much smaller 20th century warming (Haeberli and Beniston, 1998; Beniston, 2005) currently affects ground temperatures mostly in the upper decameters. For a realistic simulation of today's thermal state of mountain permafrost it is therefore necessary to go back in time for model initialization. In addition, modeling of transient temperature fields is essential to assess permafrost temperatures in the coming decades and centuries.

Only sparse information is available on how steep topography influences transient subsurface temperature fields and how large the paleoclimatic effect is in the interior of Alpine peaks. A systematic study on combined transient and topography effects on the subsurface thermal field in high-mountain areas does not exist so far and is provided in this paper: We fist analyze past climate conditions and how they influence the present-day thermal state of mountain permafrost. Secondly, we consider a scenario of future climate change. Owing to the complex and highly variable conditions found in nature, our study is based on numerical experimentation with simplified topography and typical values of surface and subsurface conditions. The results so obtained are easier to interpret and a step towards assessing natural and more complex situations. As an example in real topography, we further present the modeled transient and three-dimensional permafrost distribution in the Matterhorn (Switzerland) for both, current and future climatic conditions. Results of this study will contribute to our understanding of the three-dimensional distribution of mountain permafrost, its thermal state today, and its possible evolution in the future. In addition, results will be useful to decide on the initialization procedure required for modeling of permafrost temperatures in high-mountains.

2 Background and Approach

Many studies point to significant temperature depression at depth that are caused by past climate conditions (e.g., Safanda and Rajver, 2001; Kohl and Gruber, 2003). The depth to which a surface temperature variation is perceivable is determined by its amplitude and duration, as well as by the thermo-physical properties of the subsurface. As a first approach, temperature depressions can be assessed by superposition of stepwise temperature changes using analytical heat transfer solutions (Birch, 1948; Carslaw and Jaeger, 1959). Based on this technique, an assumed 10 °C cooler surface temperature during the last Pleistocene Ice Age (ca. 70–100 ky BP) still causes a temperature depression of more than 4 °C at a depth of 1000 m (Kohl, 1999). Haeberli et al. (1984) have estimated a ground temperature depression from the last cold period of 5 °C at a depth of about 1000 to 1500 m for the Swiss Plateau. In modeling studies, transient effects are usually computed as deviations of actual thermal conditions from equilibrium conditions (e.g., Pollak and Huang, 2000; Beltrami et al., 2005). A large number of studies exist that use measured temperatures in deep boreholes to reconstruct past climatic conditions (e.g., Lachenbruch and Marshall, 1986; Pollak et al., 1998; Huang et al., 2000; Beltrami, 2001; Kukkonen and Safanda, 2001). Based on such studies, periods with climate variations that have an influence on current subsurface temperatures can be identified. However, climate reconstruction studies are typically based on data measured in boreholes that are drilled in flat areas and include one-dimensional vertical heat transfer. Only a few recent studies deal with the effect of past temperatures together with two- or three-dimensional topography. Kohl (1999) demonstrated that the transient temperature signal can be modified by topography even at depths of more than 1000 m. Case studies in permafrost areas in the Swiss Alps (Wegmann

et al., 1998; Luethi and Funk, 2001; Kohl and Gruber, 2003) indicate that the long term climate history has to be taken into account to realistically reproduce measured temperature profiles and warming rates at depth. GST histories considered reach back in time for 1200 years for local case studies (Wegmann et al., 1998) and more than 10,000 years for entire mountain massifs (Kohl et al., 2001).

The modeling of subsurface temperatures in high-mountains is complex because they are governed by (i) spatially variable ground surface temperatures, (ii) spatially variable thermophysical properties of the subsurface, (iii) three-dimensional effects caused by complex terrain geometry, and (iv) the evolution of the GST in the past. In this study, we used and further developed the approach described by Noetzli et al. (2007a; 2007b), which has been designed and tested for use in complex topography: A surface energy balance model and a heat-conduction model are coupled for forward simulation of a subsurface temperature field (Fig. 1). The TEBAL model (Gruber, 2005) calculates present mean ground surface temperatures (MGST). So calculated MGST then serve as upper boundary condition in the heat conduction scheme, which we solve within the modeling package COMSOL. To account for the evolution of the GST in the past, we compiled and simplified different GST histories, based on published changes in air temperatures and the assumption that GST follow these changes closely. Temporal variations of GST penetrate downward with amplitudes diminishing exponentially with depth. In this study, we ignore seasonal temperature variations, which may penetrate down to about 12 m in bedrock (Gruber et al., 2004a), and only consider long-term variations of time scales of decades to millennia. Such long-term GST variations still occur on much shorter timescales than the geological processes that determine the geothermal heat flow. The past climatologic variations are therefore only treated as transient effects of the upper boundaries in our model, and the lower basal heat flow boundary condition is kept constant (c.f. Pollak and Huang, 2000). The lack of information concerning the three-dimensional distribution of subsurface characteristics (thermophysical properties, porosity, freezing characteristics, etc.) is approached by using model assumptions based on sensitivity studies.

We performed the basic simulations for a simplified ridge, the most common feature comprising alpine topography. A ridge of 1000 m height was set to an elevation of 3500 m a.s.l. and east-west orientation. Hence, it has a warm south-facing and a cold north-facing slope, which induces a subsurface temperature field with near vertical isotherms in the uppermost part. The slope angle was set to 50°, a typical value for rock slopes that do not accumulate a thick snow cover. To study the influence of terrain geometry, we varied the topographic factors (i.e., elevation and slope angle) of the two-dimensional ridge. Finally, we compared the results of the two-dimensional ridge topography to those for a flat and one-dimensional plain and a three-dimensional pyramid geometry representing a simplified mountain peak.

3 Temperature Modeling

3.1 Energy Balance and Rock Surface Temperature

The TEBAL model (Topography and Energy BALance, Gruber, 2005) simulates hourly time series of surface energy fluxes based on observed climate time series, topography, and surface and subsurface information. The model is designed and validated for the calculation of near-surface temperatures in steep rock slopes in the Alps and was successfully applied in previous studies on bedrock permafrost (e.g., Gruber et al., 2004a; Noetzli et al., 2007b; Salzmann et al., 2007). MGSTs are computed with gridded digital elevation models (DEMs) of the topographies with a spatial resolution of 25 m and with hourly climate time series from the high elevation meteo station Corvatsch (3315 m a.s.l.), Upper Engadine (Data source: MeteoSwiss) for the period 1990–1999 AD. We further reference this period as 'today' or 'present'. Surface and subsurface properties for bedrock were set according to Noetzli et al. (2007b). The simulation of the snow cover was neglected in this study, because we focus on steep rock slopes that do not accumulate thick snow during winter (i.e., slopes angles of 50° and more).

3.2 Heat Conduction and Subsurface Temperature

In bedrock permafrost, heat transfer is mainly conductive and driven by the temperature variations at the surface and the heat flow from the earth's interior. Further processes such as the effects of fluid flow can, as a first approximation, be neglected (Kukkonen and Safanda, 2001). Accordingly, we considered a conductive transient thermal field (Carslaw and Jaeger, 1959) in an isotropic and homogeneous medium under complex topography. The thermo-physical properties were set based on literature: thermal conductivity is 2.5 W K^{-1} m^{-1} and volumetric heat capacity 2.0 x 10^6 J m^{-3} K^{-1} (Cermák and Rybach, 1982; Wegmann et al., 1998; Safanda, 1999).

Ice contained in the pore space and crevices delays the response to surface warming by the consumption of latent heat, which may influence the time and depth scales of permafrost degradation by orders of magnitude even in low porosity rock (Wegmann et al., 1998; Romanovsky and Osterkamp, 2000; Kukkonen and Safanda, 2001). This effect can be handled in heat transfer models by introducing an apparent heat capacity. We used the approach by Mottaghy and Rath (2006): The apparent heat capacity substitutes the heat capacity in the heat transfer equation within the freezing interval w, where phase transition takes place, and which relates to the steepness of the unfrozen water content curve. The parameter w makes it possible to account for a variety of ground conditions: Values typically range from 0.5 for material such as sand to 2 for material such as bentonite (Anderson and Tice, 1972; Williams and Smith, 1989), but information on bedrock material is sparse. Wegmann (1998) found that most of the interstitial ice in the rock of the Jungfrau East Ridge, Switzerland, freezes at –0.3 °C, which indicates a small freezing interval with a steep curve and a low value of w. A further controlling factor is the

porosity of the material, for which we assumed 3% (volume fraction, saturated conditions) to be a reasonable value to investigate the principal effects (Wegmann et al., 1998).

The finite-element (FE) modeling package COMSOL Multiphysics was used for forward modeling of subsurface rock temperatures (Noetzli et al., 2007a). The FE mesh was created with increasing vertical refinement from 250 m at depth to 10 m for elements closest to the surface. In order to avoid effects from the model boundaries, a rectangle of 2000 m height and thermal insulation at its sides was added below. The so created FE mesh consisted of about 1500 elements for a ridge, and of about 25,000 elements for a pyramid. The lower boundary condition was set to a uniform heat flux of 80 mW m^2 (Medici and Rybach, 1995), and for the upper boundary conditions the modeled MGSTs were given. The model was run with time-steps of 1 year for simulations over a period of more than 1000 years, and with time steps of 10 days for shorter periods. Sensitivity runs with higher refinement of the FE mesh as well as changing to smaller time steps did not considerably change any of the results (the maximum absolute difference in modeled temperatures was below 0.1 °C).

3.3 Evolution of Surface Temperature

A wealth of literature exists on temperature reconstructions from proxy data for global (Pollak et al., 1998; Huang et al., 2000; Jones and Mann, 2004), hemispheric (Jones et al., 1998; Petit et al., 1999;), and regional scale (Patzelt, 1987; Isaksen et al., 2000; Casty et al., 2005) over the past centuries and millennia. For the European Alps, temperature variations are generally more pronounced with larger amplitudes compared to those averaged globally or for the Northern Hemisphere (Beniston et al., 1997; Pfister, 1999; Luterbacher et al., 2004). In the uppermost kilometers of the Earth's crust, mainly the thermal effects of two events are prominent today (Haeberli et al., 1984): the temperature depression during the Pleistocene Ice Age and the sharp rise in temperatures between the time of maximum glaciation (around 18 ky BP) and the beginning of the thermally more stable Holocene (around 10 ky BP). For the Holocene, the Climatic Optimum (HCO, ca. 5–6 ky BP), the Medieval Warmth (MW, ca. 800–1300 AD), the Little Ice Age (LIA, ca. 1300–1850 AD), and the subsequent warming are typically resolved in temperature reconstructions (Dahl-Jensen et al., 1998). With increasing spatial and temporal refinement, climate variations become more complex and reconstructions more detailed, particularly towards the present time. This meets our needs since a temperature signal entering into the subsurface is dampened with depth, that is, the temporal resolution of the surface temperature variations affecting subsurface temperatures decreases with depth.

In this study, we analyze the influence of the above-mentioned periods (Fig. 2) on the present-day subsurface temperature field below steep mountains. The effects of temperature variations further back in time or of smaller amplitude are considered negligible. For a detailed description of the most recent temperature fluctuations we used measured variations in mean annual air temperatures (MAAT) from a high alpine station (Jungfraujoch, Switzerland, 3576

m a.s.l.), where air temperature data is available back to 1933 AD (Data Source: MeteoSchweiz). The difference in mean temperatures between the periods 1990–1999 AD and 1933–1950 AD amounts to +1 °C for this station. Additionally, we assumed a difference in air temperature of +0.5 °C between the end of the LIA and the start of the data recordings, resulting in a total increase of +1.5 °C since 1850 AD (c.f. Boehm et al., 2001).

Based on these considerations, we analyzed the effect of the following temperature variations (Fig. 2):

- The Pleistocene Ice Age (1/2; numbers in brackets correspond to Fig. 2): Temperature depressions are assumed –10 °C colder compared to present-day temperatures (Patzelt, 1987), followed by a linear increase from the time of maximum glaciation (18 ky BP) to the beginning of the Holocene (10 ky BP). For the Holocene no temperature variations were considered. To assess the effect of colder estimates, we additionally used a value of –15 °C (Haeberli et al., 1984).
- HCO (3): During the Holocene Climate Optimum summer temperatures were approx. 1.5–3 °C warmer than today (Burga, 1991). Mean annual temperatures probably were not as high, but to test the influence of this period we assumed +2 °C.
- Last millennium (4): In contrast to e.g., von Rudloff (1980), newer studies conclude that air temperatures in Europe during the MW were probably not warmer than or comparable to today (Hughes and Diaz, 1994; Crowley and Lowery, 2000; Goosse et al., 2006). Yet, to estimate its possible influence we used 0.5 °C higher surface temperatures than at present. For the LIA, we assumed temperatures 1.5 °C lower (Boehm et al., 2001).
- Recent warming: We used a linear temperature increase following the LIA (5) and, in addition, annual MAAT variations taken from meteodata (6).

In addition, we used a linear warming of the rock surface of +3 °C/100y for the next 200 years (Salzmann et al., 2007) to simulate a future subsurface temperature field.

4 Transient Temperature Fields Below Idealized Topography

4.1 Effects of Past Climatic Conditions

If not indicated otherwise, results are discussed and visualized for a ridge cross section of 1000 m height with a maximum elevation of 3500 m a.s.l., and a slope angle of 50°. The subsurface material is assumed homogenous and isotropic, and no latent heat is considered. Variations from these basic settings are mentioned in the text and indicated in the figures with checkboxes and corresponding abbreviations (i.e., *ini* for initialized, *lh* for latent heat considered, and *iso* for isotropic subsurface conditions).

In general, the subsurface temperature pattern of a ridge does not vary greatly for different GST histories and is characterized by the stationary temperature field. Initialized temperatures,

255 however, are lower for the entire thermal field and all GST histories. In Fig. 3, 0 °C and –3 °C-isotherms of computed temperature fields initialized with different GST histories are compared to current GST stationary conditions. The 0 °C isotherm represents the permafrost boundary, whereas the –3 °C isotherm gives the temperature distribution inside the permafrost body. The temperature depression from the last Ice Age (1) is in the range of –0.5 °C for the upper half of
260 the geometry, and in the range of –2.5 °C for the lower part. When assuming colder GST in the last Ice Age (2) these values amount to –1 °C and –4 °C, respectively. Simulating the GST variations during the Holocene (4) results in additionally lower temperatures: On the one hand, the LIA (5) is perceivable down to about 250 m depth. On the other hand, deeper parts are modeled colder because (1) and (2) do not consider that present-day GST are somewhat higher
265 than Holocene average. The effect of the HCO (3) on the temperatures is below 0.1 °C for the entire geometry, and results are therefore not displayed in Fig. 3. Results for GST history (6) do not notably differ from (5) and are not shown, either. Based on the results for (1) to (6), we compiled GST history (7), which takes into account the main GST variations that influence the subsurface thermal field in a high mountain ridge. That is, the cold temperatures during the last
270 Ice Age (1) and the major fluctuations in the past millennium (4). GST history (7) is used for all subsequent calculations and is referred to as 'initialized' or 'transient'.

Figure 4 depicts the isotherms of the initialized temperature pattern together with the stationary field for current GST. The initialized temperature field is colder and in the uppermost 100 m the recent warming since the LIA is clearly visible. In the middle part of the warmer side
275 of the ridge, the inclination of the isotherms is reversed. In this part of the geometry, we identify the biggest differences compared to stationary conditions. The absolute temperature difference of a transient to a stationary thermal field for present-day GST is plotted in Fig. 5. Maximum calculated temperature depressions in the innermost parts of the geometry are –3 °C, whereas the temperature depression does not exceed 1 °C in the upper half of the geometry. The MW and
280 the fact that the LIA has not yet penetrated to great depth cause the warmer area visible in the top center of the ridge (Fig. 5).

4.1.1 Topography

For simulations based on conduction only, the elevation of the geometry changes the absolute temperature field but not its pattern. The temperature depressions given above are thus valid for
285 ridge-topographies of any elevation, but the position of the 0 °C isotherm (or permafrost boundary) varies (Fig. 5). The difference in permafrost thickness (which we consider vertical to the surface) between stationary and transient results is bigger for higher mountains with deeper permafrost occurrence. For the highest example shown in Fig. 5 (i.e., 4500 m a.s.l.), the difference amounts to more than 100 m. For the lowest example (i.e., 3000 m a.s.l.) it is still in the di-
290 mension of decameters.

Convex topography accelerates the reaction of the subsurface temperature to changing surface conditions. Firstly and more obviously, the distance that a signal has to penetrate by conduction to reach the permafrost base in the interior of the mountain is shorter than in flat terrain. The steeper the topography, the shorter is this distance. In addition to this effect, the warming signal reaches the interior from more than one side, that is, from two sides in the case of a ridge, and from four sides in a pyramid-like situation. To demonstrate this effect of multi-lateral warming, we compare the temperature depressions in T(z)-profiles in a flat one-dimensional plain, a two-dimensional ridge, and a three-dimensional pyramid (Fig. 6). For the two- and three-dimensional geometry, the profiles are extracted vertically from the top of the geometry. The resulting temperature depression, however, was not plotted versus the length of the profile, but versus the shortest distance of the profile to the surface (c.f. small schematic plots in Fig. 6). In this way, multi-lateral warming causes the effect shown, and not the fact that the distance to the surface is shorter than the depth of the profile. For the two mountain geometries the modeled temperature depression is roughly half of that for a flat plain in the 200 m closest to the surface. For the deeper parts (i.e., 300 m and more), the difference increases and ca. –3 °C for flat terrain contrast with ca. –1 °C for mountain topography. The effect of three-dimensional compared to two-dimensional geometry is small for the long time scale of the simulation and the depth range shown. This is due to the fact that the major part of the temperature signal has reached the depths shown in both mountain geometries (cf. also section 4.2 and Fig. 9).

4.1.2 Subsurface Properties

Information about subsurface properties (e.g., porosity, freezing characteristics) of bedrock is sparse for natural conditions in high mountains. In order to gain confidence in the modeling results, we tested their possible influence in sensitivity studies.

In low porosity material and for time scales of millennia, energy consumption due to latent heat is of minor importance (Fig. 5): Subsurface temperatures are slightly colder, but differences to simulations without latent heat do not exceed 0.2 °C at depth. This is in accordance with calculations by Haeberli et al. (1984) or model experiments by Mottaghy and Rath (2006). The effect of latent heat only becomes important for transient simulations over shorter time periods (see below) or for considerably higher porosities. In mountain permafrost areas, high ice contents may be present in the near surface layer, where porosity is often increased due to weathering and fracturing. For example, the ice content of the Schilthorn crest, Switzerland, is estimated to be 10–20% in the upper meters and around 5% in the deeper parts (Hauck et al., 2008). We tested if this has an influence on the transient temperature field by adding a 15 m thick layer with 20% porosity as a surface layer to the ridge geometry. Yet, no considerable difference to the simulations with homogenous porosity for the entire ridge resulted.

Thermal conductivities of bedrock often show large variations due to anisotropy (e.g., in gneiss). Values for the anisotropy factor of crystalline rocks are typically between 1.2 and 2 (Schoen, 1983; Kukkonen and Safanda, 2001). In order to investigate the anisotropy effect on

the initialized temperature field we performed model runs with thermal conductivity increased both horizontally and vertically (i.e., 3 W K^{-1} m^{-1} and 2 W K^{-1} m^{-1} in the perpendicular direction). An increased horizontal thermal conductivity supports lateral heat fluxes and the effect of steep topography, whereas an increased vertical component reduces it. The latter has a bigger effect on the modeled temperatures at depth: Differences to isotropic conditions amount up to –2 °C for increased vertical thermal conductivity, and 0.5 °C for increased horizontal thermal conductivity.

The heat capacity of bedrock typically ranges from about 1.8 to 3 x 10^6 J kg^{-1} K^{-1} (Cermák and Rybach, 1982). Test runs with these values result in a maximum difference of less than 1 °C for the innermost part of the geometry.

The geothermal heat flux has only little effect on the stationary subsurface temperature field inside steep mountain peaks (Noetzli et al., 2007b). This is also true for transient calculations: Resulting temperature depressions from simulations with a zero heat flux lower boundary condition were assessed to differ less than 0.2 °C. Moreover, we tested the influence of radiogenetic heat production. Values for rock are given between 0.5 and 6 μW m^{-3} (Kohl, 1999). We used a medium value of 3 μW m^{-3} for a test run. Maximum differences to results without heat production were assessed to be below 0.5 °C for the entire ridge, and below 0.1 °C for the upper half.

4.2 Effects of Future Warming

The effect of an assumed linear temperature rise of +3 °C/100 y during 200 years has been shown by Noetzli et al. (2007b). The warming has penetrated to a depth of approximately 250 m, but only about 50% of the temperature change has reached a depth of more than 100 m. Temperatures at greater depth still remain unchanged. Further, a retarding influence of latent heat was demonstrated. In this study, we analyzed the effect of elevation, geometry, and subsurface conditions on future transient thermal fields in high-mountains.

4.2.1 Topography

The state of the permafrost body inside ridges of different elevations in 200 years is displayed schematically in Fig. 8. The position of the 0 °C isotherm 250 m or less below the surface changes drastically and is bent towards the top. On the warmer side of the ridge, the isotherms first change to lie more or less parallel to the surface and then move rather uniformly towards the colder side. For all elevations modeled, no permafrost remains at the surface on the southern slope. Nevertheless, a significant permafrost occurrence remains below the surface for a long time, especially for higher elevations. For lower topographies relict permafrost remains on the colder side.

The above-described effect of multi-lateral warming is also significant for shorter time periods. Figure 9 displays the percentage of a surface temperature signal that has reached a certain depth after 100 and 200 years, respectively. For example, 50% of the temperature signal has

reached a depth of ca. 60 m after 200 years in a one-dimensional vertical simulation. In the two-dimensional situation, it has already penetrated to about 90 m, and in the three-dimensional situation to about 115 m. In the same way as in Fig. 6, values for the two- and three-dimensional geometries are plotted versus the shortest distance to the surface, rather than versus the length of the extracted profile.

4.2.2 Subsurface Conditions

The effect of latent heat on future temperature fields is illustrated in Fig. 10. With varying freezing range (parameter w) the size of the modeled permafrost body does not change much, but the temperature distribution inside changes. A smaller value of w (i.e., a smaller freezing range and a steeper unfrozen water content curve) keeps the thermal field in the temperature range little below the melting point for a longer time period. This leads to more homogeneous temperature fields in warming permafrost than when modeled with a larger value of w. In terms of T(z)-profiles from boreholes this results in steeper profiles and smaller temperature gradients with depth (Fig. 11). For example, this effect can be observed in the temperature profiles of the two 100 m deep boreholes on the Schilthorn crest (Switzerland), which are entirely in the range of –2 to 0 °C. This points to a small freezing interval and a low value of w (Noetzli et al., 2008). The observed high ice-content in the near-surface layer (c.f. section 4.1.2) can act as a buffer to temperature changes at the surface and further delay the short-term reaction of the subsurface temperature field (Fig. 11).

5 Permafrost Distribution and Evolution in the Matterhorn

The Matterhorn (4478 m a.s.l.) in Switzerland is probably the most prominent mountain peak in the European Alps. Its distinctive topography resembles a pyramid of about 1500 m height and faces exposed to all four main orientations. Slope angles are >45 °C for the most parts and only isolated and small patches of snow persist on the rock. With this extreme three-dimensional geometry, the Matterhorn constitutes a prime example for an application of the presented modeling approach to real topography.

A north-south cross section through the modeled subsurface temperature field of the Matterhorn for today and in 200 years is given in Fig. 12. Surface temperatures were modeled using climate time series from the Corvatsch (data source: MeteoSwiss), which is located in a central Alpine climate similar to the Matterhorn area (c.f. Gruber et al., 2004b). Surface properties were used according to the previous simulations and Noetzli et al. (2007b). The topography was taken from the 25 m DEM Level 2 by Swisstopo and the FE mesh contained nearly 55,000 elements. The lithology of the Matterhorn mainly consists of gneiss and granite of the east Alpine Dent-Blanche nappe. We set a thermal conductivity of 2.5 W m^{-1} K^{-1}, a volumetric heat capacity of 2.2 x 10^6 J m^{-3} K^{-1}, a porosity of 3%, and w=2. Boundary conditions and time steps were the same as in the simulations presented above, and anisotropy was not considered.

The extreme geometry of the Matterhorn leads to a strongly three-dimensional subsurface temperature field, which is characterized by steeply inclined isotherms, a strong heat flux from the south to the north face, and a smaller heat flux from the east to the west face. For current conditions, the entire mountain is within permafrost, except for the lowest parts of the southern side. For the calculated scenario, in contrast, no permafrost remains at the surface on the southern side after 200 years. On the northern side, the permafrost boundary at the surface has risen to an elevation of about 3500 m a.s.l. However, both on the south and the north side, substantial permafrost remains a few decameters below the surface. Temperatures of the remaining permafrost body are warming and the extent of so-called warm permafrost (i.e., about –2 to 0 °C) is significantly increasing in volume as well as in vertical extent (Fig. 13).

6 Discussion

With the experiments conducted in this study we analyzed the influence of combined transient and three-dimensional topography effects on the subsurface temperature field in mountain permafrost. For the correct interpretation of the results, a number of uncertainties and limitations of the modeling approach are important, which are discussed in the following.

Instrumental records of climate parameters are typically available for the past ca. 100 years. Reconstructions of pre-industrial climate rely on proxy data and are subject to a great number of uncertainties, which may be even larger than the influence a certain time period has on the subsurface temperatures. In general, climate reconstruction studies agree well on the shape of the climate fluctuations, whereas the absolute amplitude of the temperature variations ranges signifycantly (Esper et al., 2005). Further, we assumed that changes in GST closely follow air temperatures. Salzmann et al. (2007) demonstrated a considerable influence of topography on the reaction of surface temperatures in steep rock to changing atmospheric conditions. The dimensions of the GST changes, however, are not influenced, and in view of the above-mentioned uncertainties of the reconstructed amplitudes of temperature variations, we consider this effect to be less important for this study.

For the scenario calculations we assumed a linear temperature rise of +3 °C in 100 y. An exponential temperature rise as generally proposed for climate change scenarios may slow down the temperature changes calculated. Contrastingly, the temperature increase assumed represents a mean change in GST of bedrock in Alpine terrain for different climate scenarios (Salzmann et al., 2007) and is at the lower range of the scenarios presented for air temperature change by IPCC (2007), where a double temperature raise is not considered unrealistic or extreme for the Alps.

Variations of the surface conditions such as glacier coverage were neglected in this study. Haeberli (1983) points to higher temperatures at a glacier base than for rock exposed directly to the atmosphere during the past cold periods and, hence, paleoclimatic effects below previously glacier-covered areas are smaller. This may be important, for example, for the lower parts of the Matterhorn. Further, snow that may remains in steep bedrock can have a cooling effect on steep

slopes even in summer (Gruber and Haeberli, 2007). This cooling effect, however, has not yet been quantified.

In terms of subsurface characteristics, errors induced by uncertain assumptions of thermal conductivity, heat capacity, and heat production increase with depth and length of the simulation, whereas errors caused by uncertainties in subsurface ice decrease. Information on the amount and freezing characteristics of subsurface ice in bedrock is required to improve realistic modeling, but is still scarce. The joint interpretation of numerical model results with data from geophysical monitoring (e.g., electrical resistivity tomography, ERT) has been successfully realized for a first case study of the Schilthorn crest in the Swiss Alps (Noetzli et al., 2008), and information gained in this way can improve the representation of the subsurface in the model.

Neglecting water circulation along the joint systems of bedrock is an important limitation of the approach used. For example, advective heat transfer along clefts can contribute to subsurface heat transfer and lead to thaw corridors in permafrost, which substantially modify a purely conductive system (Gruber et al., 2004a; Gruber and Haeberli, 2007). First applications of geophysical monitoring in solid rock walls recently identified thawed cleft systems influenced by moving water (Krautblatter and Hauck, 2007). Process understanding of advective heat transfer processes in steep bedrock permafrost, however, is limited.

Because of its temperature range, the acceleration of subsurface temperature changes through multi-lateral warming, and the virtual decoupling of the mountain from the geothermal heat flux, bedrock permafrost in high mountains is particularly sensitive to climate change. Simulations of possible future subsurface temperatures illustrate the long lasting and deep-reaching changes in the subsurface thermal field, and point to hardly any remaining permafrost at the surface on south-facing Alpine slopes in 200 years. Permafrost boundaries are about to lie surface-parallel in the top parts of the mountains and then move rather uniformly towards the colder side. In terms of temperature-related instabilities such a thawing and horizontally migrating permafrost table may be delicate: rock volumes with temperatures close to the melting point, possibly containing critical ice-water-rock mixtures, increase and may extend over large vertical distances up to entire mountain flanks. For the Matterhorn, for example, warm permafrost exists today in the middle of the southern side, where rock fall events actually have been observed in recent years (2003 and 2006). In the calculated scenario, the warm permafrost zone extends over the entire south face and, in addition, over large parts of the north face.

7 Conclusions and Perspectives

The results of the simulations performed in this study lead to the following conclusions:

- The main variations in surface temperatures that influence present-day subsurface temperatures in Alpine permafrost are the last glacial period and the major temperature variations in the past millennium.

- Transient paleothermal effects caused by past climate variations exist in the interior of high-mountain peaks. Modeled temperature depressions at a distance of 500 m from the surface are in the range of –3 °C compared stationary conditions from present-day GST.
- For temperature fields influenced by future warming, transient effects are more important. Scenarios point to temperature fields that are characterized by long-term and deep reaching perturbations and by temperature patterns that strongly deviate from stationary conditions.
- Two- and three-dimensional topography significantly accelerates the pace of a surface temperature signal entering into the subsurface. Together with the fast and unfiltered reaction of its surface to changes in atmospheric conditions and the low ice content, this makes bedrock permafrost in high mountains particularly sensitive to degradation.
- In low porosity rock, the influence of latent heat on the temperature depressions caused by past GST variations is too small to be important and can be neglected. In connection with probable future warming, however, latent heat effects modify the pace of permafrost degradation considerably.
- Temperatures of the permafrost body are warming in the calculated scenario, and the extent of warm permafrost is significantly increasing in volume as well as in vertical extent.
- The distribution and extent of temperatures little below the melting point in warming permafrost is determined by the freezing characteristics of the subsurface material. A small freezing range leads to more homogenous temperature fields and T(z) profiles with small temperature gradients.

The investigation of mountain permafrost by transient three-dimensional modeling has only been used for a few case studies of real mountain topography so far. It bears potential for various applications that require knowledge of current and future thermal conditions of mountain permafrost, for instance, the reanalysis of the thermal conditions in rock fall starting zones located in permafrost areas, the improved interpretation of T(z) profiles measured in boreholes, and the assessment of thermal conditions and their evolution in rock below infrastructure. The limitations and uncertainties discussed above call for improved knowledge of subsurface properties in bedrock permafrost, as well as for enhanced validation and modeling practices. A promising approach may be the combination of numerical modeling together with measurements and interpretation of field data. For example, the representation of the subsurface physical properties in the model can be improved by incorporating subsurface information (e.g., geological structures, water/ice content) detected by geophysical surveys. Further, process understanding and incorporation of advective heat transfer and snow remaining in steep rock will be important for realistic modeling of subsurface temperature field.

Acknowledgements. This study was supported by the Swiss National Science Foundation, as part of the NF 20-10796./1 project 'Frozen rock walls and climate change: transient 3-dimensional investigation of permafrost degradation'. Special thanks go to Sven Friedel for support with the COMSOL software and for providing an import routine for DEMs. Fruitful discussions with W. Haeberli and M. Hoelzle contributed to the development of this study.

References

Anderson, D. M., and Tice, A. R.: Predicting unfrozen water contents in frozen soils from surface area measurements, Highway Research Record, 393, 12–18, 1972.

Beltrami, H.: On the relationship between ground temperature histories and meteorological records: A report on the Pomquet Station, Global Planet. Change, 29, 327–348, 2001.

Beltrami, H., Ferguson, G., and Harris, R. N.: Long-term tracking of climate change by underground temperatures, Geophys. Res. Lett., 32, doi:10.1029/2005GL023714, 2005.

Beniston, M., Diaz, H. F., and Bradley, R. S.: Climatic change at high elevation sites: An overview, Climatic Change, 36, 233-251, 1997.

Beniston, M.: Mountain climates and climate change: An overview of processes focusing on the European Alps, Pure Appl. Geophys., 162, 1587-1606, 2005.

Birch, F.: The effects of Pleistocene climatic variations upon geothermal gradients, Am. J. Sci., 246, 729-760, 1948.

Boehm, R., Auer, I., Brunetti, M., Maugeri, M., Nanni, T., and Schoener, W.: Regional temperature variability in the European Alps: 1760-1998 from homogenized instrumental time series, Int. J. Climatol., 21, 1779-1801, 2001.

Burga, C.: Vegetation history and paleoclimatology of the middle Holocene: Pollen analysis of Alpine peat bog sediments, covered formerly by the Rutor Glacier, 2510 m (Aosta Valley, Italy), Global Ecol. Biogeogr., 1, 143-150, 1991.

Carslaw, H. S., and Jaeger, J. C.: Conduction of heat in solids, Oxford science publications, Clarendon Press, Oxford, 510 pp., 1959.

Casty, C., Wanner, H., Luterbacher, L., Esper, J., and Boehm, R.: Temperature and precipitation variability in the European Alps since 1500, Int. J. Climatol., 25, 1855-1880, 2005.

Cermák, V., and Rybach, L.: Thermal conductivity and specific heat of minerals and rocks, in: Landolt-börnstein Zahlenwerte und Funktionen aus Naturwissenschaften und Technik, neue Serie, physikalische Eigenschaften der Gesteine (v/1a), edited by: Angeneister, G., Springer, Berlin, 305-343, 1982.

Crowley, T. J., and Lowery, T. S.: How warm was the Medieval Warm Period? Ambio, 29, 51-54, 2000.

Dahl-Jensen, D., Modegaard, K., Gundestrup, N., Clow, G. D., Johnsen, S. J., Hansen, A. W., and Balling, N.: Past temperatures directly from the Greenland Ice Sheet, Science, 282, 268-271, 1998.

Davies, M. C. R., Hamza, O., and Harris, C.: The effect of rise in mean annual temperature on the stability of rock slopes containing ice-filled discontinuities, Permafrost Periglac., 12, 137–144, 2001.

Esper, J., Wilson, R. J. S., Frank, D. C., Moberg, A., Wanner, H., and Luterbacher, J.: Climate: Past ranges and future changes, Quarternary Sci. Rev., 24, 2164-2166, 2005.

Goosse, H., Arzel, O., Luterbacher, J., Mann, M. E., Renssen, H., Riedwyl, N., Timmermann, A., Xoplaxi, E., and Wanner, H.: The origin of the European 'Medieval Warm Period', Climate of the Past, 2, 99-113, 2006.

Gruber, S., Hoelzle, M., and Haeberli, W.: Permafrost thaw and destabilization of Alpine rock walls in the hot summer of 2003, Geophys. Res. Lett., 31, doi:10.1029/2004GL0250051, 2004a.

Gruber, S., Hoelzle, M., and Haeberli, W.: Rock wall temperatures in the Alps: Modeling their topographic distribution and regional differences, Permafrost Periglac., 15, 299-307, 2004b.

Gruber, S., King, L., Kohl, T., Herz, T., Haeberli, W., and Hoelzle, M.: Interpretation of geothermal profiles perturbed by topography: The Alpine permafrost boreholes at Stockhorn Plateau, Switzerland, Permafrost Periglac., 15, 349-357, 2004c.

Gruber, S.: Mountain permafrost: Transient spatial modelling, model verification and the use of remote sensing, Department of Geography, University of Zurich, Zurich, 2005.

Gruber, S., and Haeberli, W.: Permafrost in steep bedrock slopes and its temperature-related destabilization following climate change, J. Geophys. Res., 112, doi:10.1029/2006JF000547, 2007.

Haeberli, W.: Permafrost-glacier relationships in the Swiss Alps – today and in the past, 4th International Conference on Permafrost. Proceedings, Fairbanks, Alaska, 1983, 415–420,

Haeberli, W., Rellstab, W., and Harrison, W. D.: Geothermal effects of 18 ka BP ice conditions in the Swiss Plateau, Ann. Glaciol., 5, 56–60, 1984.

Haeberli, W.: Construction, environmental problems and natural hazards in periglacial mountain belts, Permafrost Periglac., 3, 111–124, 1992.

Haeberli, W., Wegmann, M., and Vonder Mühll, D.: Slope stability problems related to glacier shrinkage and permafrost degradation in the Alps, Eclogae Geol. Helv., 90, 407–414, 1997.

Haeberli, W., and Beniston, M.: Climate change and its impacts on glaciers and permafrost in the Alps, in: Ambio - a journal of the human environment, edited by: Rapp, A., and Kessler, E., 4, The Royal Swedish Academy of Sciences, 258–265, 1998.

Harris, C., Davies, M. C. R., and Etzelmüller, B.: The assessment of potential geotechnical hazards associated with mountain permafrost in a warming global climate, Permafrost Periglac., 12, 145–156, 2001.

Hauck, C., Bach, M., and Hilbich, C.: A 4-phase model to quantify subsurface ice and water content in permafrost regions based on geophyiscal datasets, 9th International Conference on Permafrost, Fairbanks, US, 2008,

Huang, S., Pollak, H. N., and Shen, P. Y.: Temperature trends over the last five centuries reconstructed from borehole temperatures, Nature, 403, 756-758, 2000.

Hughes, M. K., and Diaz, H. F.: Was there a 'Medieval Warm Period', and if so, where and when? Climatic Change, 26, 109-142, 1994.

IPCC: Climate change 2007: The physical science basis. Contribution of working group I to the fourth assessment report of the Intergovernmental Panel on Climate Change, edited by: Solomon, S., Qin, D., Manning, M., Chen, Z., Marquis, M., Averyt, K. B., Tignor, M., and Miller, H. L., Cambridge University Press, Cambridge, United Kingdom and New York, 996, 2007.

Isaksen, K., Vonder Mühll, D., Gubler, H., Kohl, T., and Sollid, J. L.: Ground surface temperature reconstruction based on data from a deep borehole in permafrost at Janssonhaugen, Svalbard, Ann. Glaciol., 31, 287–294, 2000.

Isaksen, K., Sollid, J. L., Holmlund, P., and Harris, C.: Recent warming of mountain permafrost in Svalbard and Scandinavia, J. Geophys. Res., F02S04, doi:10.1029/2006JF000522, 2007.

Jones, P. D., Briffa, K. R., Barnett, T. P., and Tett, S. F. B.: High-resolution paleoclimatic records for the last millennium: Interpretation, integration, and comparison with general circulation model control-run temperatures, Holocene, 8, 455-471, 1998.

Jones, P. D., and Mann, M. E.: Climate over past millennia, Rev. Geophys., 42, RG2002:doi:2010.1025/2003RG000143, 2004.

Kohl, T.: Transient thermal effects at complex topographies, Tectonophysics, 306, 311-324, 1999.

Kohl, T., Signorelli, S., and Rybach, L.: Three-dimensional (3-D) thermal investigation below high Alpine topography, Phys. Earth Planet. In., 126, 195-210, 2001.

Kohl, T., and Gruber, S.: Evidence of paleaotemperature signals in mountain permafrost areas, 8th International Conference on Permafrost, Extended Abstracts, Zürich, 2003, 83–84,

Krautblatter, M., and Hauck, C.: Electrical resistivity tomography monitoring of permafrost in solid rock walls, J. Geophys. Res., 112, doi:10.1029/2006JF000546, 2007.

Kukkonen, I. T., and Safanda, J.: Numerical modelling of permafrost in bedrock in northern Fennoscandia during the Holocene, Glob. Planet. Change, 29, 259–273, 2001.

Lachenbruch, A. H., and Marshall, B. V.: Changing climate: Geothermal evidence from permafrost in the alaskan arctic, Science, 234, 689–696, 1986.

Luethi, M., and Funk., M.: Modelling heat flow in a cold, high-altitude glacier: Interpretation of measurements from Colle Gnifetti, Swiss Alps, J. Glaciol., 47, 314-324, 2001.

Lunardini, V. J.: Climatic warming and the degradation of warm permafrost, Permafrost Periglac., 7, 311–320, 1996.

Luterbacher, J., Dietrich, D., Xoplaxi, E., Grosjean, M., and Wanner, H.: European seasonal and annual temperature variability, trends and extremes since 1500, Science, 303, 1499-1503, 2004.

Medici, F., and Rybach, L.: Geothermal map of Switzerland 1995 (heat flow density), Géophysique 30, Schweizerische Geophysikalische Kommission, 1995.

Mottaghy, D., and Rath, V.: Latent heat effects in subsurface heat transport modeling and their impact on paleotemperature reconstructions, Geophys. J. Int., 164, 236-245, 2006.

Noetzli, J., Hoelzle, M., and Haeberli, W.: Mountain permafrost and recent Alpine rock-fall events: A GIS-based approach to determine critical factors, 8th International Conference on Permafrost, Proceedings, Zürich, 2003, 827–832,

Noetzli, J., Gruber, S., and Friedel, S.: Modeling transient permafrost temperatures below steep alpine topography, COMSOL User Conference, Grenoble, 2007a, 139-143,

Noetzli, J., Gruber, S., Kohl, T., Salzmann, N., and Haeberli, W.: Three-dimensional distribution and evolution of permafrost temperatures in idealized high-mountain topography, J. Geophys. Res., 112, doi:10.1029/ 2006JF000545, 2007b.

Noetzli, J., Hilbich, C., Hauck, C., Hoelzle, M., and Gruber, S.: Comparison of simulated 2D temperature profiles with time-lapse electrical resistivity data at the Schilthorn crest, Switzerland., 9th International Conference on Permafrost, Fairbanks, US, 2008,

Patzelt, G.: Neue Ergebnisse der Spät- und Postglazialforschuung in Tirol, in: Jahresbericht, Österreichische Geographische Gesellschaft, Zweigverein Innsbruck, 11-18, 1987.

PERMOS: Permafrost in Switzerland 2002/2003 and 2003/2004, Glaciological report (Permafrost) no. 4/5 of the Cryospheric Commission of the Swiss Academy of Sciences (SCNAT) and Department of Geography, University of Zurich, edited by: Vonder Muehll, D., Noetzli, J., Roer, I., Makowski, K., and. Delaloye, R., 104 pp., 2007.

Petit, J. R., Jouzel, J., Raynnaud, D., Barkov, N. I., Barnola, J.-M., Basile, I., Bender, M., Chappellaz, J., Davis, M., Delaygue, G., Delmotte, M., Kotlyakov, V. M., Legrand, M., Lipenkov, V. Y., Lorius, C., Pépin, L., Ritz, C., Saltzman, E., and Stievenard, M.: Climate and atmospheric history of the past 420,000 years from the Vostok ice core, Antarctica, Nature, 399, 429-436, 1999.

Pfister, C.: Wetternachhersage, Haupt, Bern, 304 pp., 1999.

Pollak, H. N., Huang, S., and Shen, P. Y.: Climate change record in subsurface temperatures: A global perspective, Science, 282, 279281, 1998.

Pollak, H. N., and Huang, J.: Climate reconstruction from subsurface temperatures, Ann. Rev. Earth Planet. Sci., 28, 339-365, 2000.

Romanovsky, V. E., and Osterkamp, T. E.: Effects of unfrozen water on heat and mass transport processes in the active layer and permafrost, Permafrost Periglac., 11, 219–239, 2000.

Romanovsky, V. E., Gruber, S., Instanes, A., Jin, H., Marchenko, S. S., Smith, S. L., Trombotto, D., and Walter, K. M.: Frozen ground, in: Global outlook for ice and snow, edited by: UNEP, UNEP/GRID-Arendal, Norway, 182-200, 2007.

Safanda, J.: Ground surface temperature as a function of slope angle and slope orientation and its effect on the subsurface temperature field, Tectonophysics, 306, 367-375, 1999.

Safanda, J., and Rajver, D.: Signature of the last ice age in the present subsurface temperatures in the Czech Republic and Slovenia, Glob. Planet. Change, 29, 241-257, 2001.

Salzmann, N., Noetzli, J., Gruber, S., Hauck, C., and Haeberli, W.: RCM-based ground temperature scenarios in high-mountain topography and their uncertainty ranges, J. Geophys. Res., 112, doi:10.1029/2006JF000527, 2007.

Schoen, J.: Petrophysik, Ferdinand Enke, Stuttgart, 1983.

Von Rudloff, H.: Das Klima – Entwicklung in den letzten Jahrhunderten im mitteleuropäischen Raume (mit einem Rückblick auf die postglaziale Periode), in: Das Klima – Analysen und Modelle, Geschichte und Zukunft, edited by: Oeschger, H., Messerli, B., and Silvar, M., Springer, Berlin, 125-148, 1980.

Wegmann, M.: Frostdynamik in hochalpinen Felswänden am Beispiel der Region Jungfraujoch-Aletsch, 161, Versuchsanstalt für Wasserbau, Hydrologie und Glaziologie der ETH Zürich, ETH Zürich, Zürich, 143 pp., 1998.

Wegmann, M., Gudmundsson, G. H., and Haeberli, W.: Permafrost changes in rock walls and the retreat of alpine glaciers: A thermal modelling approach, Permafrost Periglac., 9, 23-33, 1998.

Williams, P. J., and Smith, M. W.: The frozen earth, 1 ed., Studies in polar research, Cambridge University Press, Cambridge, 306 pp., 1989.

Figures

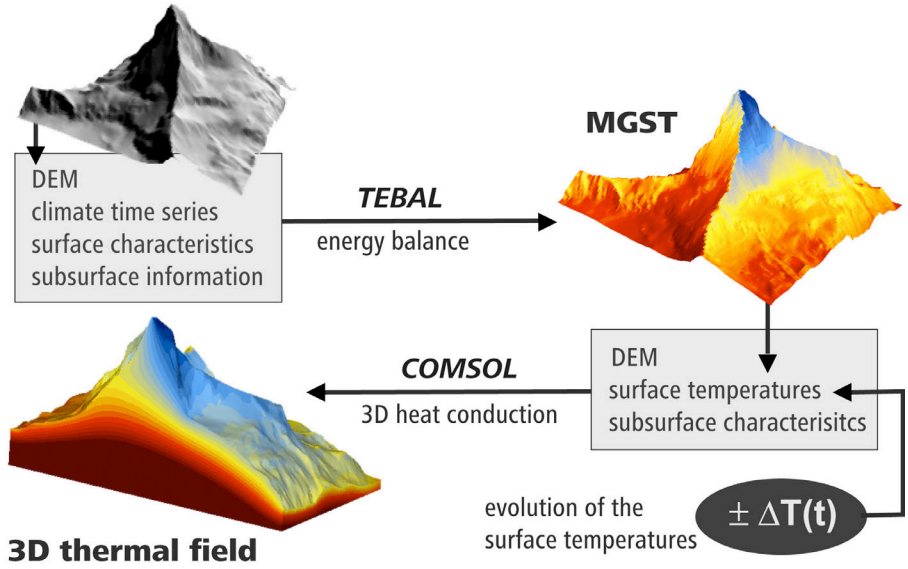

Figure 1. Mean ground surface temperatures (MGST) are modeled based on a surface energy balance model (TEBAL). They are used as upper boundary condition in a three-dimensional finite element heat conduction scheme (within COMSOL) to compute the subsurface temperature field. For transient simulations the evolution of the surface temperatures is prescribed.

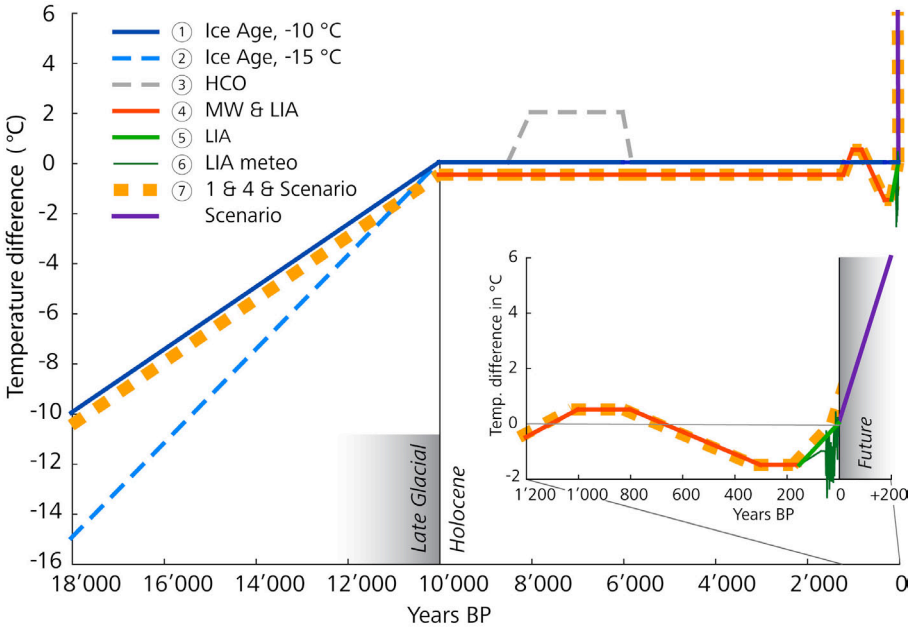

Figure 2. For the initialization runs, surface temperature histories of diverse lengths and temporal resolutions were used. Based on the results obtained, an initialization curve for further simulations was compiled (thick dashed orange line). Scenarios were calculated assuming a uniform linear warming of +3 °C/100 y. MW = Medieval Warmth, HCO = Holocene Climate Optimum, LIA = Little Ice Age.

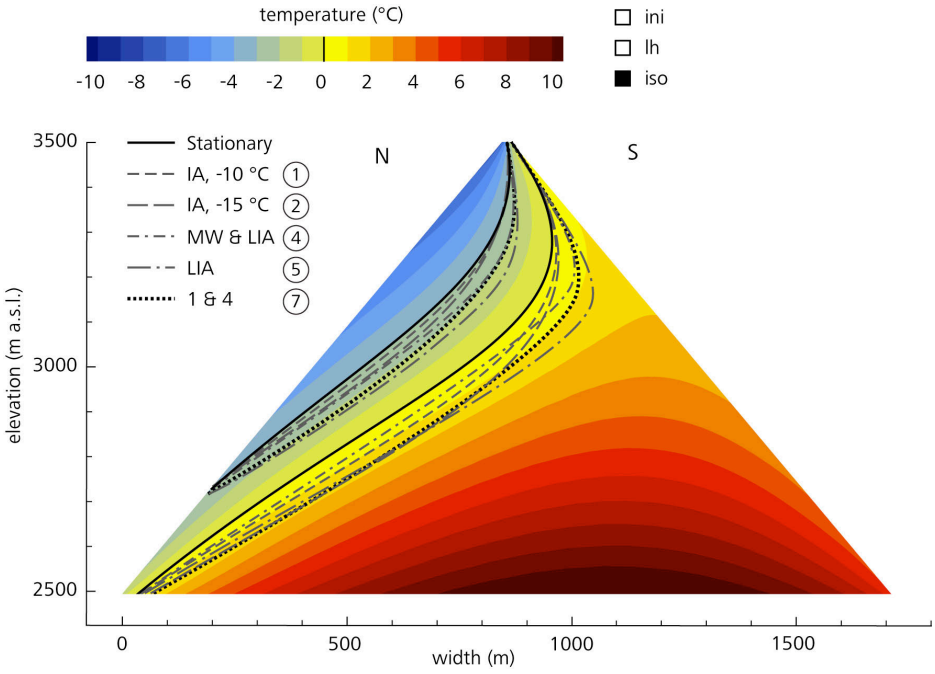

Figure 3. Difference in the subsurface temperature field for a stationary simulation compared to model runs using different surface temperature histories: The 0 °C and –3 °C isotherms for the different model runs are plotted over the stationary solution depicted in color.

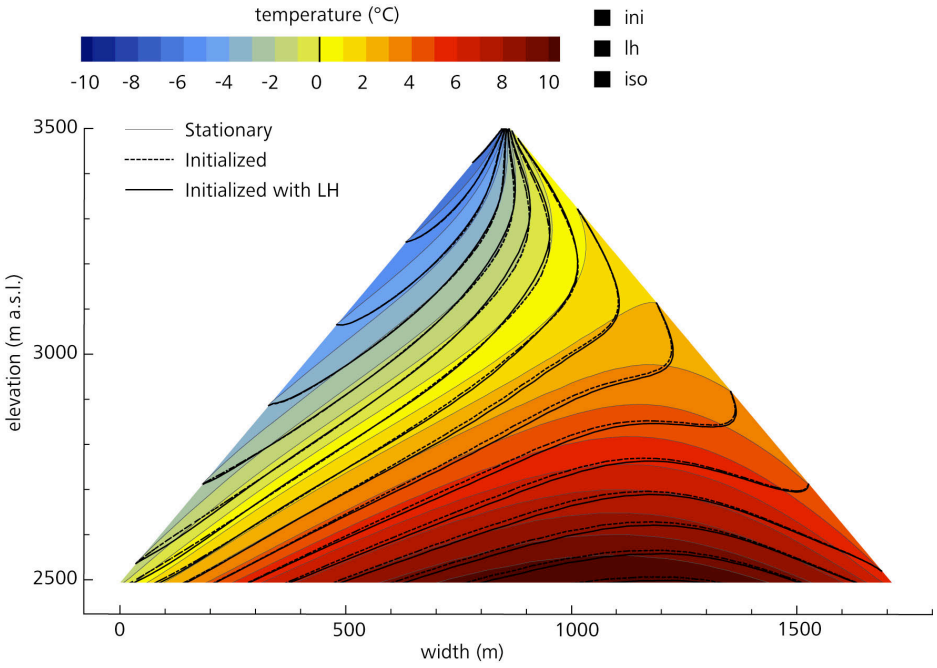

Figure 4. The isotherms of a stationary temperature field (thin grey lines and background colors) compared to an initialized one (temperature history (7) from Fig. 2). The transient temperature field is shown for simulations both with (solid line) and without (dotted line) considering the effects of latent heat. The porosity was set to 3%.

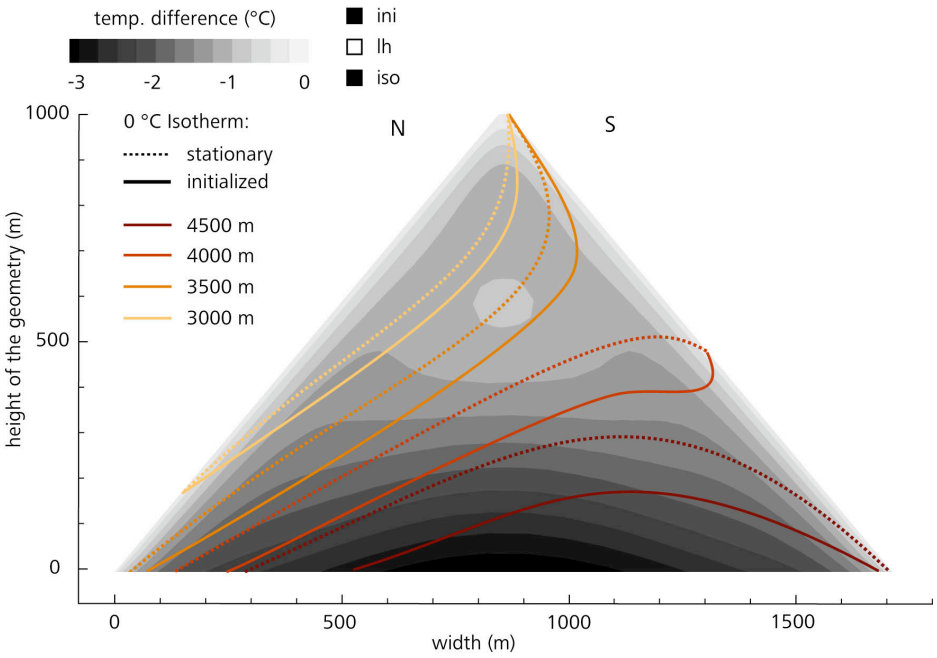

Figure 5. The difference of the stationary solution to an initialized one (temperature history (7) from Fig. 2) is shown in gray colors. The lines indicate the permafrost boundary for the stationary (dotted line) and the transient (solid line) simulation, respectively, for four different maximum elevations of a ridge ranging from 3000 to 4500 m a.s.l. Colors indicate different elevations.

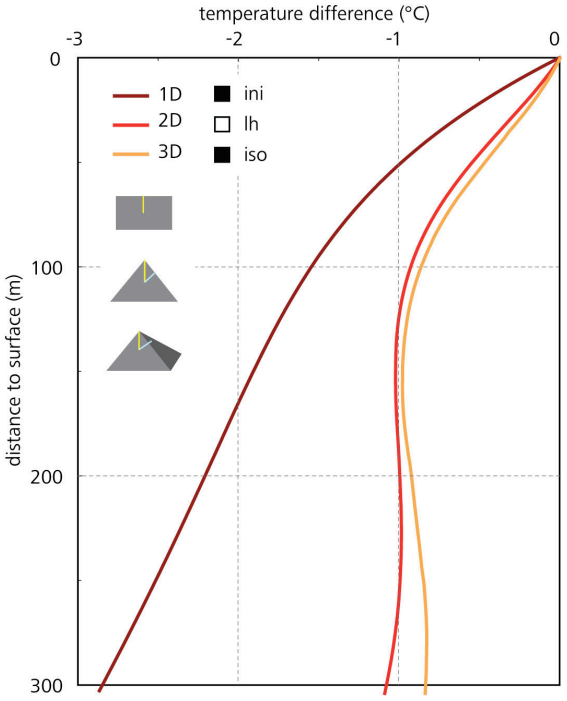

Figure 6. Temperature depression in the subsurface thermal field of today caused by colder past surface temperatures for one- (flat terrain), two- (ridge), and three-dimensional (pyramid) situations. In the two- and three-dimensional situations, profiles are extracted vertically from the top of the geometry. Temperature differences are plotted versus the shortest distance to the surface, i.e., the distance the temperature signal penetrated.

Figure 7.

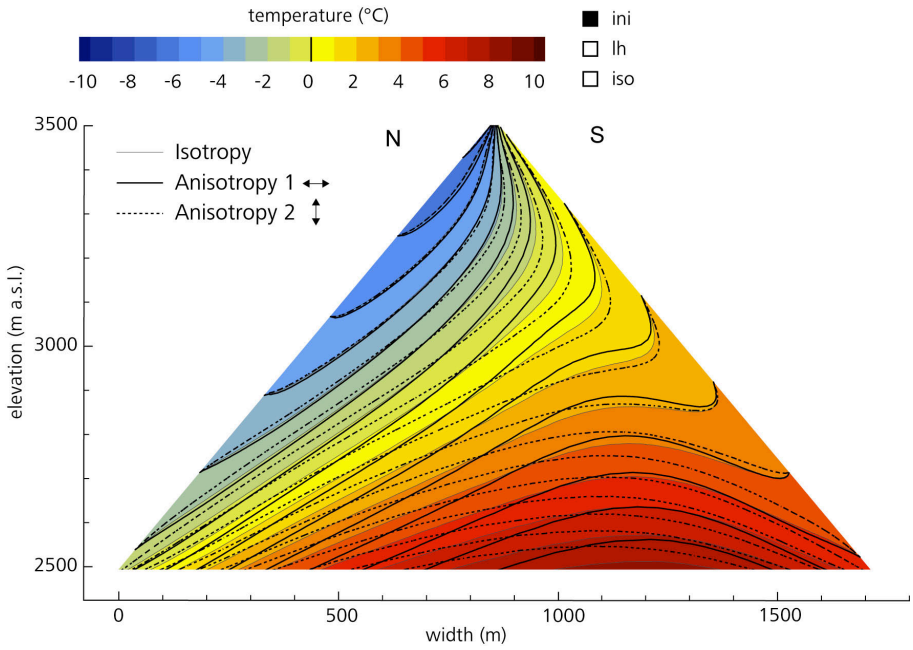

Figure 7. Transient temperature field of an isotropic medium (background colors, gray lines) compared to anisotropic mediums with increased horizontal (anisotropy 1, solid lines) and vertical (anisotropy 2, dotted lines) thermal conductivity, respectively.

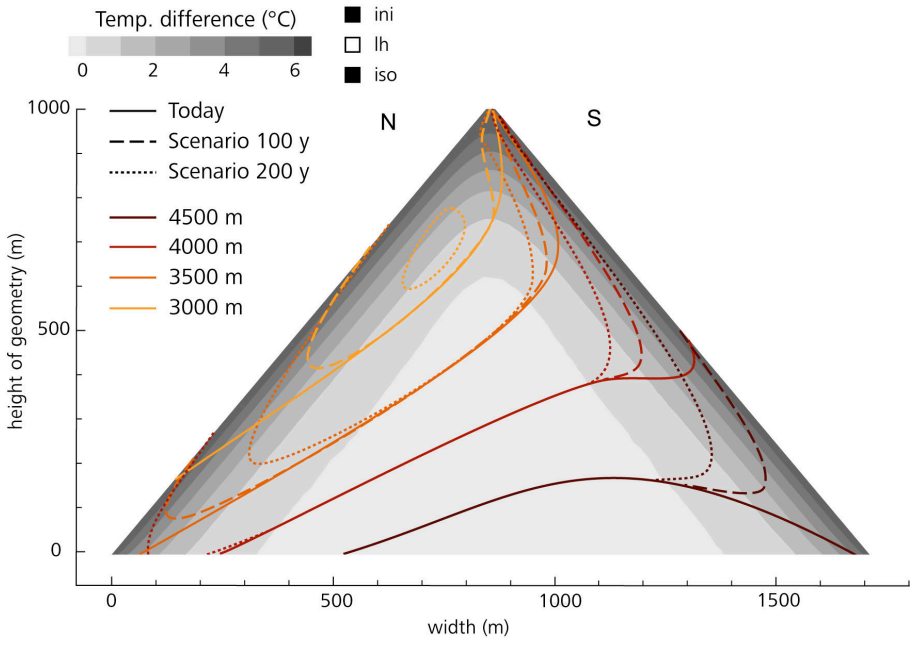

Figure 8. The temperature difference between the current transient temperature field and a 200-year scenario simulation is displayed in gray shadings. The warming has penetrated to ca. 250 m depth. The evolution of the 0 °C isotherms for a 200-year scenario is plotted for different elevations of the ridge. Colors indicate different elevations, whereas the dotted patterns represent the situation today (solid lines), in 100 years (dashed lines), and in 200 years (dotted lines).

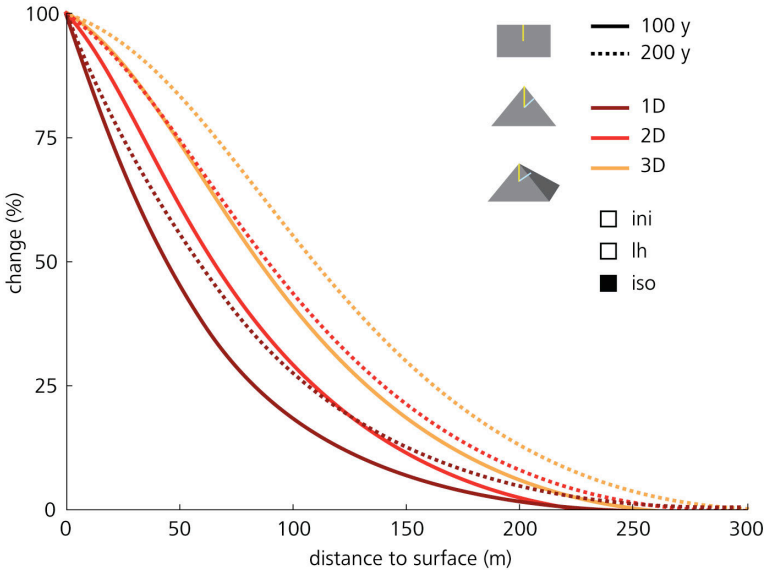

Figure 9. Percent of a temperature signal at the surface that has penetrated to depth: This effect is shown for a one- (flat terrain), two- (ridge), and three-dimensional (pyramid) situation after 100 (solid lines) and 200 years (dotted lines), respectively. In the two- and three-dimensional situations values are plotted versus the shortest distance to the surface.

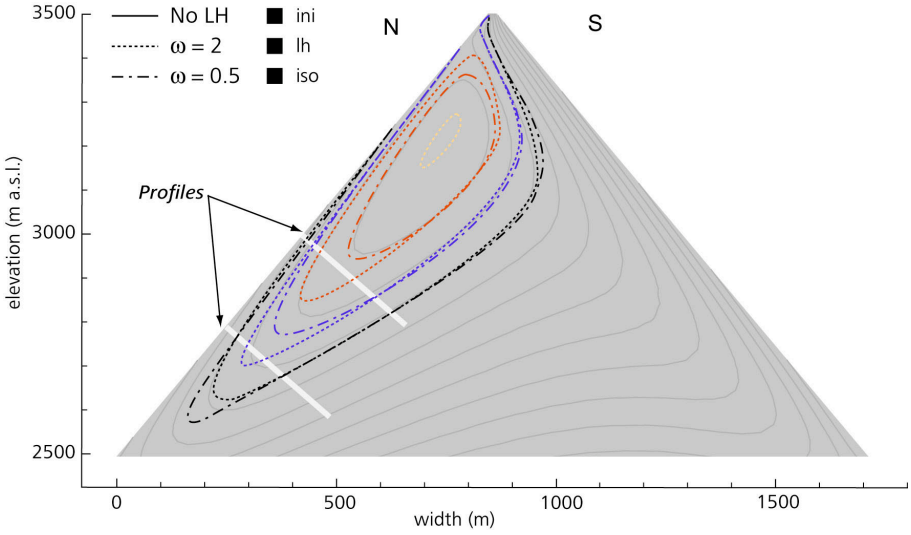

Figure 10. The permafrost body in a ridge calculated for a 200-year scenario is displayed for simulations with and without considering the effects of latent heat and a porosity of 3%. Additionally, different values of the parameter *w*, which describes the unfrozen water content curve, have been considered. Black lines represent the modeled 0 °C isotherm, i.e., the remaining permafrost body; blue, red, and yellow lines the -1, -2, and -3 °C isotherms.

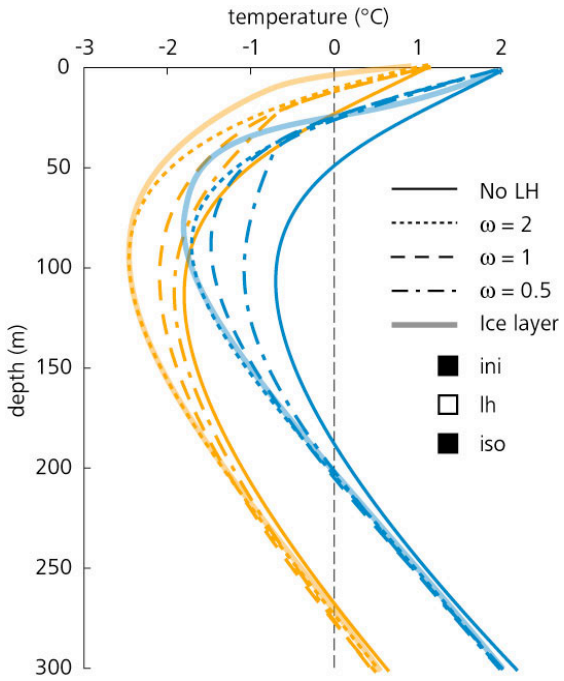

Figure 11. T(z)-profiles of two synthetic boreholes vertical to the slope in the middle and the lower part of the northern side of a ridge (cf. Fig. 8) illustrate the effect of latent heat and the freezing range w.. In addition, the profile of a simulation with a 20 m ice-rich layer at the surface is displayed by thick, brighter lines.

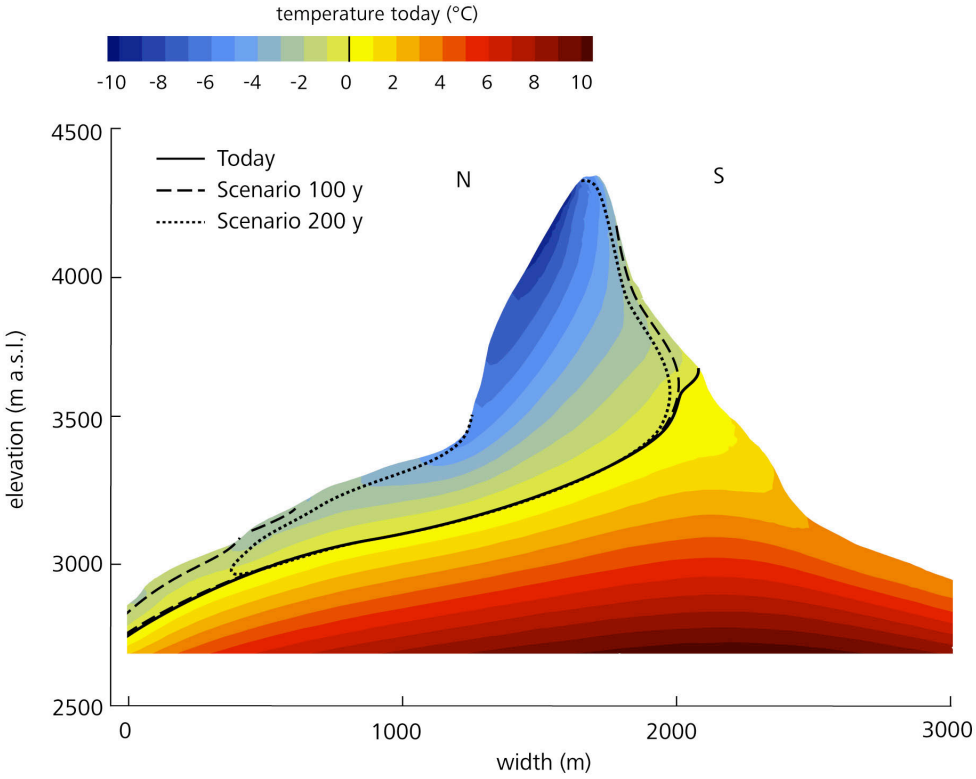

Figure 12. North-south cross section of the Matterhorn (4478 m a.s.l.) and modeled subsurface temperature field for today (i.e., the mean of the period 1990–1999 AD). The temperature field was computed transient, three-dimensional, isotropic, and with 3% subsurface ice in the frozen parts. The black lines represent the 0 °C isotherms for today (solid line), in 100 years (dashed line), and in 200 years (dotted line). We assumed a linear warming scenario of +3 °C/100 y.

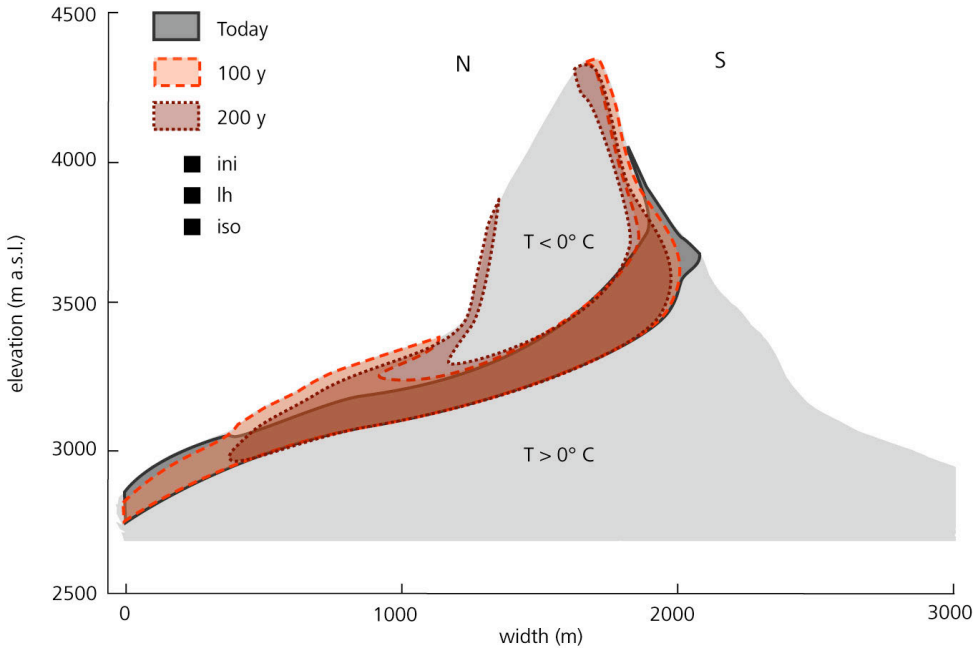

715 Figure 13. Modeled temperature range of -2 to 0 °C in a north-south cross section of the Matterhorn for today (gray), in 100 years (light red), and in 200 years (red). We assumed a linear warming scenario of +3 °C/100 y.

Publication IV

Comparison of Simulated 2D Temperature Profiles with Time-Lapse Electrical Resistivity Data at the Schilthorn Crest, Switzerland

In this paper, we are interested in the thermal conditions below the Schilthorn Crest, Swiss Alps. To investigate the subsurface thermal field, we combine ground temperature measurements at the surface and in boreholes, electric resistivity tomography (ERT) monitoring, and transient numerical modeling. This approach further allows for a qualitative validation of the modeling results.

Main Findings

- Topography and transient effects predominantly influence the subsurface thermal regime in the Schilthorn Crest. Both modeled and measured mean annual ground temperatures are above -3 °C for the entire crest.
- The thermal regime of the profile can be characterized by a cold zone below the upper part of the northern slope, permafrost occurrence little below the surface on the southern slope and in the lower part of the northern slope, and rather homogeneous thermal conditions at and below the area of the boreholes.
- The modeled temperature field agrees well with the results from ERT monitoring. Cross validation of results from the two complementary approaches enables a more sound and reliable interpretation than based on only one of the two. The combination used bears potential to improve modeling and validation strategies.

Citation

Noetzli, J., Hilbich, C., Hauck, C., Hoelzle, M., and Gruber S. 2008. Comparison of simulated 2D temperature profiles with time-lapse electrical resistivity data at the Schilthorn crest, Switzerland. Proceedings of the 9th International Conference on Permafrost, Fairbanks, US, 1293–1298.

Comparison of Simulated 2D Temperature Profiles with Time-Lapse Electrical Resistivity Data at the Schilthorn Crest, Switzerland

Jeannette Noetzli
Glaciology, Geomorphodynamics, Geochronology, Geography Department, University of Zurich, Switzerland
Christin Hilbich
Department of Geography, University of Jena, Germany
Christian Hauck
Institute for Meteorology and Climate Research, University of Karlsruhe/Forschungszentrum, Karlsruhe, Germany
Martin Hoelzle
Glaciology, Geomorphodynamics, Geochronology, Geography Department, University of Zurich, Switzerland
Stephan Gruber
Glaciology, Geomorphodynamics, Geochronology, Geography Department, University of Zurich, Switzerland

Abstract

The Schilthorn crest in the Bernese Alps, Switzerland, is a prominent permafrost research site. Topographic and transient effects influence the temperature field below the east-west oriented crest. Measured T(z)-profiles in boreholes, however, do not provide sufficient information for a comprehensive description of the subsurface temperature distribution. We combine ground temperature measurements, electric resistivity tomography (ERT) monitoring, and numerical modeling to investigate the 3-dimensional thermal regime below the crest. The modeled temperature field of a north-south oriented cross section agrees well with ERT results along the same profile. The simulated thermal regime below the Schilthorn is characterized by generally warm permafrost, with the coldest zone below the upper part of the north-facing slope, and permafrost a little below the surface on the south-facing slope. The combination of temperature modeling and measurements and geophysical monitoring bears potential to improve simulation and validation strategies.

Keywords: Alpine permafrost distribution; thermal modeling; electrical resistivity tomography monitoring; transient and topographical temperature effects

Introduction

Permafrost was first found on Schilthorn summit, Switzerland, when the facilities for the cable car were built between 1965 and 1967. During the construction of the buildings several ice lenses with a thickness of up to 1 m were encountered. Since then, extensive research has taken place on Schilthorn (e.g., Imhof 2000, Vonder Muehll et al. 2000, Hauck 2001, Mittaz et al. 2002, Hilbich et al. 2008), making it to one of the most intensively investigated permafrost sites in the European Alps. Three boreholes in perennially frozen ground were drilled within the PACE-project between 1998 and 2001 (Harris 2001). These boreholes provide the basis for monitoring and quantification of changes in the permafrost thermal regime.

In mountain areas the interpretation of T(z)-profiles measured in boreholes with respect to climate signals is complicated by topographic effects (Gruber et al. 2004). The Schilthorn represents an east-west oriented ridge with a warm south-facing and a colder north-facing slope. Even though measured temperature profiles in boreholes enable an initial assessment of topography related and transient effects, they are only representative of isolated local spots. A comprehensive analysis of permafrost distribution and evolution below the crest can only be achieved by integrating additional subsurface data.

In this paper, we combine measurements of surface and subsurface temperatures, electric resistivity tomography (ERT), and numerical modeling of a subsurface thermal field for a 2-dimensional investigation of permafrost conditions below the Schilthorn crest. A 2D heat transfer model is forced by measured near-surface temperatures at the upper boundary to simulate the thermal field of a north-south cross section of the ridge. An ERT monitoring system was installed across the same profile, which provides additional information on subsurface conditions, and enables comparison of modeling results for a qualitative validation.

The Field Site

The Schilthorn (2970 m asl., 46.56° N/7.83° E, Figs. 1, 2) is located in the Bernese Oberland in the Northern Swiss

Figure 1. View of the Schilthorn Crest in the Bernese Alps looking eastward. The ERT-Profile starts just below the meteo station in the northern slope and reaches across the crest approximately to the southern border of the photo.

Alps. The three boreholes are located on a small plateau on the north-facing slope approximately 60 m below the summit. Air temperatures recorded at the meteo station close to the boreholes indicate an annual mean of -2.8 °C for the years 1999–2007 (Hoelzle and Gruber 2008). The annual precipitation is estimated to 2700 mm and about 90% of it falls as snow (Imhof 2000). As the precipitation maximum occurs during summer and due to additional snow input through wind transport, the snow cover on the northern slope usually persists from October until June or even July (Hauck 2001). The average snow depth since the beginning of measurements at the meteo station in 1999 is around 80 cm. The Schilthorn consists of dark micaceous shales that weather to form a fine-grained debris layer of up to several meters in thickness covering the entire summit region. The ice content of the subsurface material is assumed to be generally low (around 5-10% in the upper meters, as reported from direct observations, Imhof et al. 2000, Vonder Mühll et al. 2000).

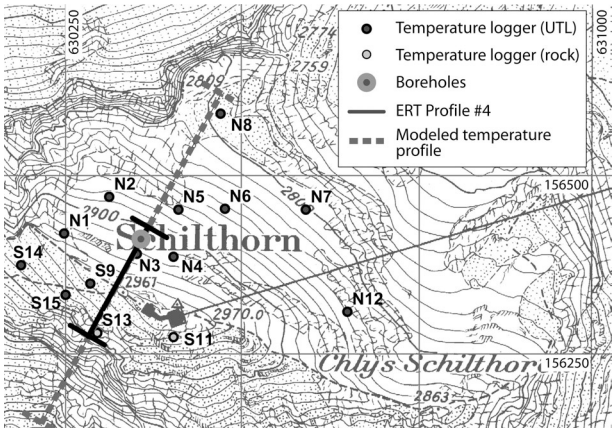

Figure 2. Overview of the field site Schilthorn Crest showing the locations of the near-surface temperature loggers, the boreholes, the measured ERT profile, and the modeled north-south cross section. Map: Swisstopo.

Temperature Measurements

Boreholes

In the scope of the PACE project, a 14 m borehole was drilled in 1998 and complemented by two 101 m boreholes in 2000. Today, these boreholes are part of the Permafrost Monitoring Switzerland (PERMOS). The deeper boreholes were drilled vertical and with an angle of 60° to the vertical in order to account for topography related effects. Temperatures measured in these boreholes point to warm permafrost conditions with temperature values between -1 and 0 °C below depth of the zero annual amplitude (ZAA) at approximately 20 m, and to a very small temperature gradient with depth (Fig. 3, left). The temperature gradient in the oblique borehole is slightly greater than in the vertical borehole. Ground temperatures are considerably higher compared to other sites at similar altitude and exposition, which is probably due to the low bedrock albedo, thick snow cover, and low ice content at the site (Hauck 2001).

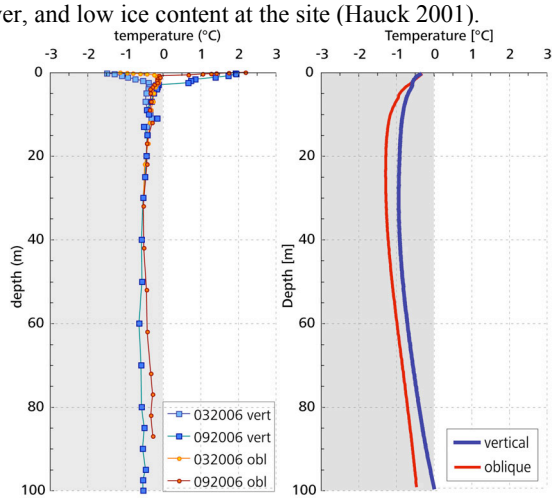

Figure 3. T(z)-profiles for the 101 m vertical (vert, blue) and oblique (obl, red) boreholes on the Schilthorn for spring and autumn 2006 (left). Modeled T(z)-profiles extracted from the temperature field in Fig. 4 at the locations of the two boreholes (right).

Ground surface temperatures

In addition to the borehole measurements, 14 temperature loggers were distributed on both sides of the crest in summer 2005 and 2006 to measure near surface-temperatures (see Fig. 2). The loggers were installed at a depth of 30 cm (UTL mini loggers) and 10 cm (rock temperature loggers), respectively, and temperatures are recorded every 2 hours. The accuracy of the temperature loggers is given as ±0.25 °C and ±0.1 °C, respectively. As the lower parts of the steep southern slope are difficult to access, loggers were only placed in the upper part of the slope. These near-surface temperature measurements provide the upper boundary condition for the numerical heat transfer model presented in the following section. In addition, they can be used to constrain the interpretation of the geophysical results concerning the subsurface thermal regime.

Numerical Modeling of Subsurface Temperatures

General approach

We considered a purely conductive transient thermal field under variable topography in an isotropic and homogeneous medium according to Carslaw and Jaeger (1959). In steep topography, heat transfer at depth mainly results from conduction, driven by the temperature variations at the surface. Processes such as fluid flow are not included in this first step. Subsurface temperatures are calculated for conditions in the hydrological year 2006/2007 (i.e., 1 Oct to 30 Sep) based on mean annual conditions at the surface. That is, seasonal variations at the surface are not included, and temperature variations above the ZAA are not simulated.

Ice contained in the pore space and crevices delays the response to surface warming by the uptake of latent heat during warming. This is addressed in our finite-element heat

transport model by apparent heat capacity, which substitutes the volumetric heat capacity in the heat transfer equation and includes energy consumed during phase change. We used the approach described by Mottaghy & Rath (2006).

The resulting temperature pattern is expected to be similar for any north-south oriented cross crest profile. Hence, simulations are conducted for a 2D section across the crest and the borehole site on the northern slope. The assumption of symmetry in east-west direction is supported by first results of a quasi-3D geoelectrical investigation including four parallel and two orthogonal ERT-profiles in the Schilthorn summit area (Krauer, 2008). The selected profile was extracted from a digital elevation model (DEM) with 10 m horizontal resolution (Data Source: Swissphoto). The finite element (FE) mesh was generated for this geometry with corresponding 10 m resolution at the surface, and lower resolution at greater depth. The mesh consists of 1468 elements. The software package COMSOL Multiphysics was used for forward modeling of subsurface temperatures.

Boundary conditions

For all near-surface temperature loggers the mean annual temperature for the hydrological year 2006/2007 was calculated and set as upper boundary condition at the corresponding elevation and side of the modeled profile. The measured thermal offset between the ground surface and TTOP is small at Schilthorn (about 0.3 °C; cf. Hoelzle & Gruber 2008) and is, hence, neglected in the simulations.

The years 2006 and 2007 were very warm and clearly above the long term average. Therefore, measured near-surface temperatures are not representative for the thermal conditions at the surface during the past decades and century. Transient effects are likely to occur and, therefore, initialization of the heat conduction model is required in order to perform a realistic simulation of the current subsurface temperature field. Based on the assumption that surface temperature fluctuations mainly follow air temperatures, we used mean annual air temperatures (MAAT) from the meteo station on Jungfraujoch (3576 m asl, Data source: MeteoSwiss) some 10 km east of Schilthorn to describe the evolution of the upper boundary. For Jungfraujoch, air temperature data is available back to 1933. The total difference in MAAT between 2006 and the mean of the period 1933–1950 is +1.52 °C. We additionally assumed a difference in air temperature of +0.5 °C between the start of the data recordings and the Little Ice Age (ca. 1850). The model initialization was started in 1850, and daily time steps were taken. A uniform lower boundary heat flux of 0.08 W m^{-2} was set at sea level, and thermal insulation was assumed for the lateral boundaries of the geometry.

Subsurface properties

Subsurface material properties were assigned on the generated FE mesh. In purely diffusive and transient simulations, thermal conductivity, volumetric heat capacity, and the ice/water content are the petrophysical parameters of importance. However, only little is known on the subsurface characteristics below steep topography and the parameters were set based on published values: Thermal conductivity was assumed as 2.5 W K^{-1} m^{-1}, and heat capacity to 2.0 x 10^6 J m^{-3} K^{-1} for the bulk material (Cermák & Rybach 1982).

Based on estimations from geophysical measurements (cf. Hauck et al. 2008) for the upper layers, a uniform ice content of 5% for the entire profile was assumed in the model simulations. The unfrozen water content is described by an exponential function and the steepness factor was set to 0.2 (cf., Mottaghy & Rath 2006).

Modeling results

The resulting temperature field for the Schilthorn profile is depicted in Figure 4. Maximum permafrost thickness amounts to roughly 100 m below the northern slope and the top of the crest. Isotherms are steeply inclined in the top part and a lateral heat flow exists from the warm south to the colder north face. Simulated permafrost temperatures are higher than -2 °C for the entire profile.

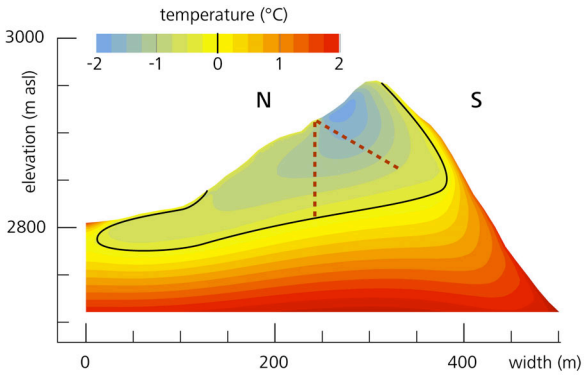

Figure 4. Modeled subsurface temperature field for a north-south cross section of the Schilthorn crest. The 0 °C isotherm is depicted in black, and the dashed red lines indicate the boreholes.

The coldest temperatures exist below the northern and central part of the ridge. The reason is that coldest surface temperatures are found in the steep part of the northern slope (mainly due to reduced solar radiation and longer snow cover duration), and that surface temperatures are higher on the small plateau where the boreholes are located as well as on the southern side. The southern slope is mainly permafrost-free at the surface. However, due to the cold northern slope permafrost can be found below the surface. In addition, this is caused by the fact that 20th century warming has not yet penetrated to greater depth in the model, which lowers the temperatures a few tens of meters below the surface compared to present-day steady-state conditions. Similarly, permafrost remains below the surface at the foot of the northern slope. These results point to the importance of transient 2D/3D modeling, as such transient and topography related effects could not be detected using steady state 1D models.

In contrast to ERT profiles (c.f., next section), which mainly allow for a qualitative validation of the general pattern of temperature distribution, comparison with extracted T(z)-profiles at the locations of the boreholes shows the accuracy of the modeled temperature values (Fig. 3). In general, the modeled profiles correspond to the

measured data in Figure 3 as temperatures are below -1.5 °C for the entire profile and temperature gradients with depth are small. For both measured and modeled profiles the oblique borehole shows a slightly more curved profile. However, temperatures of the modeled profile average about 0.2 °C colder than the measured values, but range up to 1 °C in the upper half of the profile. Further, in the lower parts the oblique profile is warmer than the vertical profile, which could not be reproduced in the simulation. The results are encouraging given the model error sources, which include: (1) subsurface properties (i.e., ice content, thermal conductivity) are assumed as homogenous for the entire profile and are hardly known at depth; (2) the temperature evolution at the surface may be influenced by effects of solar radiation and snow cover, and, hence, not exactly follow air temperature. In addition, the higher ice-content in the limestone scree in the upper meters can slow down the reaction of the subsurface to changing surface temperatures by the uptake of latent heat; (3) small scale variability at the site may cause random errors in logger measurements, and (4) processes such as heat transport by convection are not taken into account.

Geophysical Measurements

Electrical Resistivity Tomography (ERT)

In 1999 a semi-automatic ERT monitoring system was installed on a 60 m line close to the three boreholes in the north facing slope to observe subsurface resistivity changes with respect to ground ice and water content (Hauck 2001, Hilbich et al. 2008). In summer 2005, a second ERT monitoring line (188 m) was installed across the crest, complemented by a quasi-3D ERT survey along four transects across the crest in 2006. Datasets across the crest can be used to analyze the 3D permafrost distribution.

The measured signal is sensitive to temporally variable properties such as temperature, via the unfrozen water, and ice content, as well as unchanging material characteristics, such as lithology and porosity. Repeated ERT measurements, therefore, yield information on the changes occurring in the physical properties of the ground with changing temperature and time (Fortier et al. 1994).

ERT monitoring data of the cross-crest profile (Fig. 2) are available on different time scales: (a) annual measurements in late summer (August/September) for 2005, 2006, and 2007, and (b) seasonal-scale measurements between August and December 2006. Whereas the annual resolution provides inter-annual resistivity changes between 2005 and 2007, the seasonal scale helps to identify zones with pronounced resistivity changes to delineate ice-free from ice-rich regions. ERT data were processed with the software RES2DINV (Loke & Barker 1995). Besides a qualitative comparison of individual tomograms, a so-called time-lapse inversion of time series of ERT data allows for a quantitative assessment of the resistivity changes.

Results

Figure 5 shows the results of the ERT monitoring across the Schilthorn crest. In general, measured resistivities are quite low compared to other permafrost sites and do not exceed 4000 Ωm. This is mainly due to the thick fine-grained debris layer covering the summit region. Outcrops of the underlying bedrock also indicate strongly weathered conditions of the micaceous shales with crevices, where water can percolate. In addition to the comparably conductive host material, the low ice content is in accordance with the low resistivity values.

A number of features can be observed in all tomograms (cf. Fig. 6): (A) a relatively homogeneous zone with resistivities between 700 and 1600 Ωm in the lower part of the northern slope, (B) a high resistive zone (> 3000 Ωm) in the upper part of the northern slope, (C) a homogeneous intermediary zone in the southern slope with resistivities from 1200 to 1700 Ωm, and (D) a very low resistive anomaly (< 500 Ωm) with an underlying high resistive anomaly (> 2300 Ωm) at the summit.

The high resistive anomaly in the northern slope (B) may indicate the presence of ground ice and/or firm bedrock.

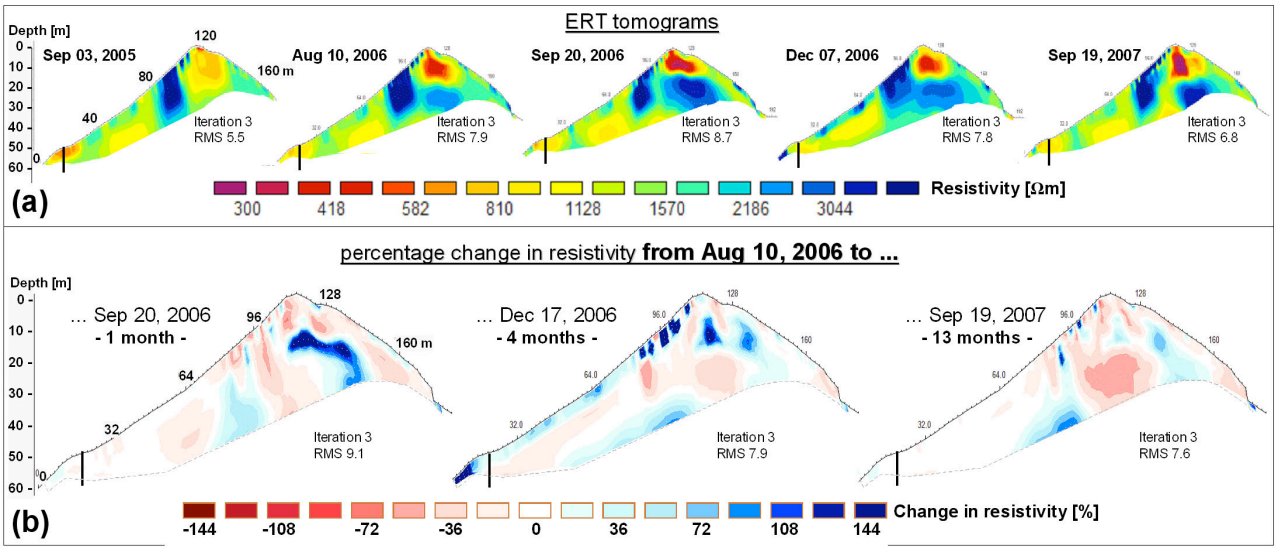

Figure 5. ERT monitoring data illustrated as individual resistivity tomograms for subsequent measurement dates (a), and as calculated change in resistivity based on the reference profile from August 10, 2006 over one, four, and 13 months (b).

Both possibilities would result in increased resistivity values compared to regions with lower ice contents or more weathered bedrock occurrences, respectively. The low resistive anomaly at the crest (D) is difficult to interpret. In comparable terrain, such low resistivity values are normally associated with very high amounts of unfrozen water or conductive man made structures (e.g., cables). The presence of such a large amount of water is very unlikely since the crest consists of firm bedrock without a superficial debris cover, whereas metallic remnants from the construction of the summit station (e.g., anchors) are found all over the crest. A man-made low resistive anomaly can therefore not be excluded. The high resistive anomaly directly below this feature is believed to be an inversion artifact, which is often generated during inversion below a zone of anomalously high or low resistivity values (Rings et al. 2007).

Apart from the high and low resistive anomalies close to the crest, the characteristics of the northern (A) and southern (B) slope seem to be similar. From the qualitative analysis of the individual tomograms no clear indication of differences in permafrost occurrence and ice content between the two slopes is apparent. Calculating the percentage change of resistivities between subsequent measurements (Fig. 6) the tomograms can be transferred into information on seasonally changing properties. From this, zone (A) in the northern slope can be seen as a region with little changes in the deeper parts but with pronounced resistivity changes within the upper 4-5 m. This clearly indicates the presence of permafrost with active layer freezing in winter. The deeper parts tend to exhibit slightly lower resistivities in winter, which we interpret as delayed advance of the summer heating (increasing unfrozen water content and therefore decreasing resistivities) into the ground. Zone (B) only yields systematic resistivity changes near the surface, that can be attributed to thawing (decreasing resistivities) between August and September and freezing (increasing resistivities) processes until December. Both processes are similar to the features in zone (A) but seem to be more pronounced. Zone (C) is characterized by a homogeneous resistivity decrease during summer, but shows almost no changes between August and December, i.e., no active layer freezing can be observed. In contrast to the very similar absolute resistivity values, seasonal changes are different in the northern and southern slope. This can be related to differences in subsurface material properties, i.e. permafrost or ice content.

Discussion

In both the modeled temperature field and the ERT profiles, three zones in the investigated cross section of the Schilthorn crest can be distinguished that are particularly interesting (Fig. 6). Cross validation of the results of the two complementary approaches enables an interpretation as follows.

(A) In the lower part of the northern slope a zone of homogeneous temperatures and resistivities exits. The small variations in temperature in this area may be explained by the fact that temperature values are only little below the melting point and the energy input of the recent warming is consumed by latent heat. Also the results from ERT monitoring suggest high amounts of unfrozen water and only little ice content (Hauck et al. 2008).

(B) In the upper part of the northern slope a zone of cold temperatures exists. The corresponding zone of high resistivity in the ERT profile is, hence, probably caused by higher ice content rather than by geological characteristics. This is also supported by the larger seasonal resistivity changes pointing to higher contents of ice and unfrozen water than in the lower part of the northern slope.

(C) The permafrost boundary on the southern slope is likely situated only little below the surface, an effect that can be mainly attributed to surface warming of the past century that has not yet affected greater depths. Seasonal resistivity changes support the hypothesis that there is no permafrost near the surface in the southern slope.

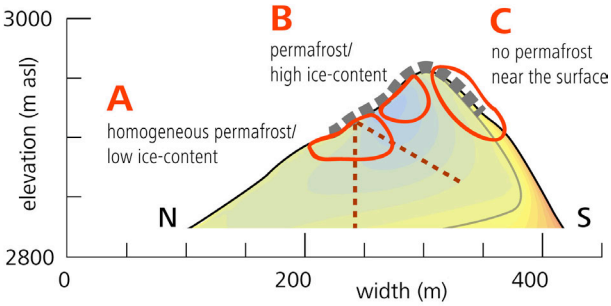

Figure 6. Three features that are addressed in the discussion section are highlighted by red circles: (A) A homogeneous permafrost zone in the lower northern slope with low ice-content, (B) a cold zone in the north slope with a high ice-content, and (C) no permafrost near the surface on the southern slope. Additionally, red dashed lines indicate the boreholes, and the gray dashed line the extent of the ERT profile.

The results of this qualitative validation corroborate the assumption that the general pattern of the subsurface temperature field can be modeled using diffusive and transient 2D and 3D simulations. Using such an approach enables the simulation of temperature fields at greater depths that cannot be reached by geophysical measurements or direct measurements in boreholes. Additionally, the numerical model can be used to calculate scenarios of the evolution of subsurface temperatures and of future permafrost occurrence below the Schilthorn crest by prescribing the evolution of the upper boundary condition or by coupling the model to a surface energy balance model and/or using regional climate model output (cf., Noetzli et al. 2007).

Conclusions and Perspectives

The subsurface thermal field of a 2D-section across the Schilthorn was modeled assuming a purely conductive and homogenous underground in a first approach. Comparison with measured ground temperatures and ERT profiles leads to the following conclusions:

- The subsurface thermal regime of the Schilthorn crest is predominantly influenced by both topography and

transient effects. The cold northern slope and the recent 20th century warming induce permafrost on the southern side of the crest only little below the surface.
- The thermal regime of the profile can be characterized by a cold zone below the upper part of the northern slope, permafrost occurrence only little below the surface on the southern slope and in the lowest part of the northern slope, and rather homogeneous conditions at and below the area of the boreholes.
- The modeled temperature field agrees with the results from ERT monitoring. The three zones mentioned above can be distinguished in the results of both methods.

ERT monitoring on Schilthorn is being continued in the scope of PERMOS. The combination of thermal modeling, temperature measurements in boreholes and geophysical surveys bears potential to further improve modeling and validation strategies. These may include (1) quantitative comparison of numerical results and measured data to estimate model performance, (2) extending single point temperature data to larger scales using 2D or 3D resistivity values, and (3) improving the representation of the subsurface physical properties in the model by incorporating subsurface information (e.g., geological structures, water/ice content) detected by geophysical surveys.

Acknowledgments

We are indebted to Michael Krauer for making us available the ERT data measured within his MSc thesis. Further, we like to thank the motivated students that helped us in the field and the Schilthornbahnen AG for generous logistic support. Part of this study (JN) was financed by the Swiss National Science Foundation as part of the NF 20-10796./1 project, and geophysical fieldwork (CH) was partly financed by PERMOS.

References

Carslaw, H.S. & Jaeger, J.C. 1959. *Conduction of heat in solids*, in Oxford Science Publications, edited, p. 510, Clarendon Press, Oxford.

Cermák, V. & Rybach, L. 1982. *Thermal conductivity and specific heat of minerals and rocks*, in Landolt-Börnstein Zahlenwerte und Funktionen aus Naturwissenschaften und Technik, Neue Serie, Physikalische Eigenschaften der Gesteine (V/1a), edited by Angeneister, G., pp. 305-343, Springer, Berlin.

Gruber, S., King, L., Kohl, T., Herz, T., Haeberli, W. & Hoelzle, M. 2004. Interpretation of geothermal profiles perturbed by topography: The Alpine permafrost boreholes at Stockhorn Plateau, Switzerland, *Permafrost and Periglacial Processes*, 15 (4): 349-357.

Fortier, R., Allard, M. & Seguin, M.K. 1994. Effect of physical properties of frozen ground on electrical resistivity logging. *Cold Regions Science and Technology* 22: 361-384.

Harris, C., Haeberli, W., Vonder Muehll, D., and King, L. 2001. Permafrost monitoring in the high mountains of Europe: The PACE project in its global context, *Permafrost and Periglacial Processes*, 12, 3-11.

Hauck, C. 2001. *Geophysical methods for detecting permafrost in high mountains*, PhD thesis, ETH-Zürich, Zürich, 204 pp.

Hauck, C., Bach, M. & Hilbich, C. 2008. A 4-phase model to quantify subsurface ice and water content in permafrost regions based on geophysical datasets. *This proceedings.*

Hilbich, C., Hauck, C., Hoelzle, M., Scherler, M., Schudel, L., Völksch, I., Vonder Mühll, D. & Mäusbacher, R. 2007. Monitoring of mountain permafrost evolution using electrical resistivity tomography: A seven-year study of seasonal, annual and long-term variations at Schilthorn, Swiss Alps. *Journal of Geophysical Research,* 113: F01S90, doi:10.1029/2007JF000799.

Hilbich, C., Hauck, C., Delaloye, R. & Hoelzle, M. 2008. A geoelectric monitoring network and resistivity-temperature relationships of different mountain permafrost sites in the Swiss Alps. *This proceedings.*

Hoezle, M & Gruber, S. 2008. Borhole measurements and ground surface temperatures and their relationship to meteorological conditions in the Swiss Alps. *This proceedings*.

Imhof, M. 2000. Permafrost investigation in the Schilthorn massif, Bernese Alps, Switzerland, *Permafrost and Periglacial Processes*, 11 (3): 189–206.

Krauer, M. 2008. Versuch einer 3-dimensionalen Erfassung des Peramfrosts in der Gipfelregion des Schltohrns mittels Geoelektrik, MSc Thesis, University of Zurich, 112 p.

Loke, M.H. & Barker, R.D. 1995. Least-squares deconvolution of apparent resistivity. *Geophysics* 60: 1682-1690.

Mottaghy, D. & Rath. V. 2006. Latent heat effects in subsurface heat transport modeling and their impact on paleotemperature reconstructions, *Geophysical Journal International*, 164: 236-245.

Noetzli, J., Gruber, S., Kohl, T., Salzmann, N. & Haeberli, W. 2007. Three-dimensional distribution and evolution of permafrost temperatures in idealized high-mountain topography, *Journal of Geophysical Research*, 112: doi:10.1029/ 2006JF000545.

Rings, J., Preko, K., Scheuermann, A. & Hauck, C. 2007. Soil water content monitoring on a dike model using electrical resistivity tomography. *Near Surface Geophysics* (in press).

Stocker-Mittaz, C. 2002. *Permafrost distribution modeling based on energy balance data*, PhD thesis, University of Zurich, Zurich, 122 p.

Vonder Mühll, D., Hauck, C. & Lehmann, F. 2000. Verification of geophysical models in Alpine permafrost by borehole information, *Annals of Glaciology*, 31: 300–306.

Appendix

Personal Bibliography

Publications by Jeannette Noetzli

The papers that form this thesis are marked with an asterisk (*); cf. *Table of Contents* and *Part II – Publications*. Publications are listed chronologically.

Peer-reviewed Publications

(*) **Noetzli, J.**, and Gruber, S. in review. Transient thermal effects in Alpine permafrost. *The Cryosphere. (*Published discussion paper: Noetzli, J., and Gruber, S. 2008. Transient thermal effects in Alpine permafrost. *The Cryosphere Discussion,* 2, 185–224.*)*

Harris, C., Arenson, L.U., Christiansen, H.H., Etzelmueller, B., Frauenfelder, R., Gruber, S., Haeberli, W., Hauck, C., Hoelzle, M., Humlum, O., Isaksen, K., Kääb, A., Lehning, M., Luetschg, M.A., Matsuoka, N., Murton, J.B., **Noetzli, J.**, Phillips, M., Ross, N., Seppälä, M., Springman, S.M., and Vonder Muehll, D. in review. Permafrost and climate in Europe: geomorphological impacts, hazard assessment, and geotechnical response. *Earth Science Reviews.*

(*) **Noetzli, J.**, Hilbich, C., Hauck, C., Hoelzle, M., and Gruber, S. 2008. Comparison of transient 2D temperature fields with time-lapse electrical resistivity data at the Schilthorn crest, Switzerland. Proceedings of the 9th International Conference on Permafrost, Fairbanks, US, 1293-1298.

Vonder Muehll, D., **Noetzli, J.**, and Roer, I. 2008. PERMOS – A comprehensive monitoring network of mountain permafrost in the Swiss Alps. Proceedings of the 9th International Conference on Permafrost, Fairbanks, US, 1869–1874.

(*) **Noetzli, J.**, Gruber, S., Kohl, T., Salzmann, N., and Haeberli, W. 2007. Three-dimensional distribution and evolution of permafrost temperatures in idealized high-mountain topography. *Journal of Geophysical Research*, 112, F02S13, doi:10.1029/ 2006JF000545.

(*) Salzmann, N., **Noetzli, J.**, Hauck, C., Gruber, S., Hoelzle, M., and Haeberli, W. 2007. RCM-based ground temperature scenarios in high-mountain topography and their uncertainty ranges. *Journal of Geophysical Research*, 112, F02S12, doi:10.1029/2006JF000527.

Fischer, L., Kääb, A., Huggel, C., and **Noetzli, J.** 2006. Geology, Glacier Changes, permafrost, and related slope instabilities in a high-mountain rock wall: Monte Rosa east face, Italian Alps. *Natural Hazards and Earth System Sciences*, 6, 761–772.

Noetzli, J., Huggel, C., Hoelzle, M., and Haeberli, W. 2006. GIS-based modeling of rock/ice avalanches from Alpine permafrost areas. *Computational Geosciences*, 10, 161–178.

Noetzli, J., Hoelzle, M., and Haeberli, W. 2003. Mountain permafrost and recent Alpine rock fall events: a GIS-based approach to determine critical factors. Proceedings of the 8th International Conference on Permafrost, Zurich, Switzerland, 1, 827–832.

Publications without Peer Review

PERMOS 2007. Permafrost in Switzerland 2002/2003 and 2003/2004. Vonder Muehll, D., **Noetzli, J.**, Roer, I., Makowski, K., and Delaloye, R. (eds), Glaciological Report (Permafrost) No. 4/5 of the Expert Commission on Cryosphere (CC) of the Swiss Academy of Sciences (SCNAT) and the Department of Geography, University of Zurich, 107 pp.

Noetzli, J., Gruber, S., and Friedel, S. 2007. Modeling transient permafrost temperatures below steep alpine topography. Proceedings of the COMSOL Conference 2007, Grenoble, France, 1, 139–143.

Noetzli, J., Roer, I., and Vonder Muehll, D. 2007. Permafrost in der Schweiz – Bedeutung und Beobachtung. *Bündnerwald*, 3, 27–34.

Noetzli, J., Vonder Muehll, D., Roer, I., Delaloye, R., Frei, C., Gruber, S., Haeberli, W., Hoelzle, M., and Phillips, M. 2007. Permafrost in den Schweizer Alpen 2004/05 und 2005/06. *Die Alpen*, 9, 10–17.

Noetzli, J., Gruber, S., and Haeberli, W. 2006. 3D-Modellierung der thermischen Bedingungen im Bereich des Gipfelgrates der Zugspitze. Report to the Bavarian State Ministry of the Environment. Glaciology and Geomorphodynamics Group, Department of Geography, University of Zurich, Unpublished Report, 21 pp.

IUGG(CCS)/UNEP/UNESCO 2005. Glacier Mass Balance Bulletin No. 8 (2002-2003). Haeberli, W., **Noetzli, J.,** Zemp, M., Baumann, S. Frauenfelder, R., and Hoelzle, M. (eds.), World Glacier Monitoring Service, University of Zurich, 100 pp.

Noetzli, J., and Gruber, S. 2005. Alpiner Permafrost – ein Überblick. In: Lintzmeyer, K. (Ed.), Jahrbuch des Vereins zum Schutz der Bergwelt, Selbstverlag, Munich, 111–121.

Huggel, C., **Noetzli, J.**, Kääb, A., and Haeberli, W. 2004. Permafrost Modeling Studies for the Monte Rosa East Face, Macugnaga. Report to Regione Piemonte. Glaciology and Geomorphodynamics Group, Department of Geography, University of Zurich, Unpublished Report, 25 pp.

Noetzli, J., Gruber, S., and Hoelzle, M. 2004. Permafrost und Felsstürze im Hitzesommer 2003. GEOforum actuel, 20, 11–14.

PERMOS 2004. Permafrost in Switzerland 2000/2001 and 2001/2002. Vonder Muehll, D., **Noetzli, J.,** Makowski, K., and Delaloye, R. (eds.), Glaciological Report (Permafrost) No. 2/3 of the Glaciological Commission (GC) of the Swiss Academy of Sciences (SAS) and Department of Geography, University of Zurich, 86 pp.

Noetzli, J. 2003. Felsstürze aus Permafrost über Gletscher – Ansätze zur GIS-basierten Modellierung. MSc Thesis, Department of Geography, University of Zurich, 122 pp.

Curriculum Vitae

Jeannette Noetzli

Date of birth: 3 January 1977; Place of origin: Pfäffikon, ZH and Oetwil an der Limmat, ZH; Nationality: Swiss.

Education

Department of Geography, University of Zurich, Zurich
PhD Dissertation | 2005–2008
Thesis: «Modeling Transient 3-dimensional Temperature Fields in Mountain Permafrost»

Department of Geography, University of Zurich, Zurich
Diploma (Master) in geography | 1997–2003
Studied subjects: geography, glaciology, and computer science
Thesis: «GIS-basierte Modellierung von Felsstürzen über Gletscher»

Kantonsschule Zürcher Unterland, Bülach
Matura Typus B | 1990–1997

Employment

Department of Geography, University of Zurich, Zurich
PhD student / research associate, Physical Geography Division | May 2005–May 2008

Permafrost Monitoring Switzerland (PERMOS), University of Zurich, Zurich
Research associate, member of the coordination office | Since Jan 2007
Co-editor of the biannual Glaciological Reports (Permafrost) | Jan 2004–Dec 2006

World Glacier Monitoring Service (WGMS), University of Zurich, Zurich
Research associate, webmaster | Dec 2003–Mar 2005

Swiss Reinsurance Company, Zurich
Part-time assistant to the GEO Services Team / Cat Perils Group | Aug 2001–Dec 2006

Athena Data Engineering and Consulting, Zurich
Temporary assistant for java programming | Aug 2000–Sep 2000

Move and Dance, Freienstein
Dance instructor | Aug 1996–Mar 2005

Erismann Feueremail, Glattbrugg
Industrial and administrative activities, part time work | 1992–1999

Acknowledgements

I am very grateful for the immense support I received from my advisors, colleagues, students, friends, and family whilst researching and writing up this dissertation. I would especially like to express my gratitude to the following people:

First and foremost, I like to thank Stephan Gruber, who was a fantastic supervisor and friend and guided and motivated me firmly through the course of my dissertation. His doors have always been wide open and I am very grateful for the countless times he helped me with sound advice on smaller and bigger problems of all kind and in terrain of all steepness.

My gratitude also goes to Wilfried Haeberli, who sparked my enthusiasm for high mountain research, for his continuous motivation and trust, and for helping me not to lose sight of the forest for the trees (or rather the mountain for the rocks). He always managed to find time for interesting discussions or reading drafts. Martin Hoelzle's scientific input was at all times valuable and I could benefit from numerous intense discussions about glaciology, but also science in general. I appreciate the willingness of Vladimir Romanovsky and Charles Harris to contribute an external expertise of the work.

Further, I thank Thomas Kohl and his team at Geowatt AG for letting me use the FRACTure simulator and for assistance in getting started with heat conduction modeling. I am obliged to Sven Friedel for the generous support for handling the COMSOL software and for providing an import routine for DEMs. The collaboration with all the co–authors of the papers, which are the main part of my thesis, was a great experience and contributed essentially to this work. I also like to acknowledge field assistance of colleagues and students as well as generous logistic support from the Schilthornbahnen AG.

I like to say thank you to my office mates and the 3G-Group for the stimulating and most enjoyable working atmosphere, scientific discussions, field assistance and adventures, as well as for funny coffee and lunch breaks. Many thanks go to Roland Lüthi for editing the English of the thesis. And I am especially grateful to David Caduff for valuable technical and scientific input, but also for moral support, mainly in the final phase.

Last, but certainly not least, a big merci viilmol to my family and friends for their support; to my family for giving me the best support and encouragement I could imagine, to my friends for sharing life in- and outside the ivory tower, in the snow, on the rock, on evenings out, or at home, and for not tiring of my frosty business but keeping me laughing.

This dissertation was financed by a grant from the Swiss National Science Foundation (project 20-10796./1) entitled «Frozen rock walls and climate change: transient 3-dimensional investigation of permafrost degradation».